Hydrol. Earth Syst. Sci., 29, 5791–5833, 2025 https://doi.org/10.5194/hess-29-5791-2025 © Author(s) 2025. This work is distributed under the Creative Commons Attribution 4.0 License.





Catchment Attributes and MEteorology for Large-Sample SPATially distributed analysis (CAMELS-SPAT): streamflow observations, forcing data and geospatial data for hydrologic studies across North America

Wouter J. M. Knoben¹, Cyril Thébault¹, Kasra Keshavarz¹, Laura Torres-Rojas², Nathaniel W. Chaney³, Alain Pietroniro¹, and Martyn P. Clark¹

Correspondence: Wouter J. M. Knoben (wouter.knoben@ucalgary.ca)

Received: 25 February 2025 – Discussion started: 12 March 2025

Revised: 9 June 2025 - Accepted: 5 August 2025 - Published: 28 October 2025

Abstract. We build on the existing Catchment Attributes and MEteorology for Large-sample Studies (CAMELS) dataset to present a new dataset aimed at hydrologic studies across North America, with a particular focus on facilitating spatially distributed studies. The dataset includes basin outlines, streamflow observations, meteorological data and geospatial data for 1426 basins in the US and Canada. To facilitate a wide variety of studies, we provide the basin outlines at a lumped and semi-distributed resolution; streamflow observations at daily and hourly time steps; variables suitable for running a wide range of models obtained and derived from different meteorological datasets at daily (one dataset) and hourly (three datasets) time steps; and geospatial data and derived attributes from 11 different datasets that broadly cover climatic conditions, vegetation properties, land use and subsurface characteristics. Forcing data are provided at their original gridded resolution, as well as averaged at the basin and sub-basin level. Geospatial data are provided as maps per basin, as well as summarized as catchment attributes at the basin and sub-basin level with various statistics. Attributes are further complemented with statistics derived from the forcing data and streamflow and focus on quantifying the variability of natural processes and catchment characteristics in space and time. Our goal with this dataset is to build upon existing large-sample datasets and provide the means for a more detailed investigation of hydrologic behaviour across large geographical scales. In particular, we hope that this dataset provides others with the data needed to implement a wide range of modelling approaches and to investigate the impact of basin heterogeneity on hydrologic behaviour and similarity. The CAMELS-SPAT (Catchment Attributes and MEteorology for Large-Sample SPATially distributed analysis) dataset is available at https://doi.org/10.20383/103.01306 (Knoben et al., 2025).

1 Introduction

Increases in geospatial data availability and computing power have enabled rapid advances in large-domain and large-sample hydrology (Cloke and Hannah, 2011; Addor et al., 2020). A key difference between these fields is the spatial continuity of the study area. Where large-domain studies concern themselves with obtaining predictions across continuous areas, large-sample studies tend to select separate basins in a given area of interest. The large-sample approach strikes a balance between spatial variability and ease of use. Large-sample studies can be representative of larger spatial regions at a fraction of the computational effort needed to run a large-domain study over the same geographical region.

Building upon the foundations laid by the MOPEX dataset (Schaake et al., 2006), a driving force behind the large-sample movement has been the "CAMELS" family of

¹Schulich School of Engineering, Department of Civil Engineering, University of Calgary, Calgary, Alberta, Canada

²Atmospheric & Oceanic Sciences, Princeton University, Princeton, New Jersey, US

³Civil and Environmental Engineering, Duke University, Durham, North Carolina, US

datasets. The original Catchment Attributes and MEteorology for Large-sample Studies (CAMELS) dataset was developed as a two-part initiative. First, basin-averaged meteorological time series were provided for several hundreds of basins across the contiguous US (Newman et al., 2015). Second, statistical descriptors (referred to as catchment attributes) of each catchment's hydroclimatic conditions were made available (Addor et al., 2017a). This combined dataset has proven useful for various purposes, mainly within the overarching themes of understanding, quantifying and modelling hydrologic processes across a diverse range of catchments (e.g. Kratzert et al., 2019; Knoben et al., 2020; Stein et al., 2021) and quantifying hydrologic predictability (e.g. Wood et al., 2016; Newman et al., 2017). The success of the CAMELS dataset has motivated the development of multiple (typically national) variants (see Table 1 for a summary of these), as well as the aggregated cloud-based CARAVAN collection (Kratzert et al., 2023, see also Färber et al., 2024).

Table 1 provides a brief overview of the main characteristics of various CAMELS(-like) datasets. Because our interest is in hydrologic modelling, we limit this overview to datasets that include meteorologic time series that could serve as input to hydrologic models. A commonality between most of these datasets is a focus on aggregated data: meteorologic forcing data and catchment attributes are typically provided as basin-averaged values, and the temporal resolution of provided forcing data is almost always at daily time steps. Similarly, most datasets provide a specific selection of forcing variables: precipitation (P) and temperature (T) are always included, as well as a potential evapotranspiration (PET) time series or the variables necessary to calculate PET. In modelling terms, these datasets focus strongly on catchment modelling with lumped conceptual models. Such models treat catchments as single (i.e. lumped) entities, are typically run at daily time resolutions and generally require only time series of P, T and PET to function. Commonly known examples of such models are SAC-SMA (National Weather Service, 2005), HBV (Lindström et al., 1997) and GR4J (Perrin et al., 2003). These models are computationally cheap but are often criticized for their somewhat empirical and spatially lumped nature and their lack of explicit energy balance calculations.

Spatially distributed process-based models, such as VIC (Liang et al., 1994) and SUMMA (Clark et al., 2015a, b), address these concerns but come with the trade-off of increased computational cost and face their own challenges. Notable challenges include the definition of appropriate parameter values and questions about the scale-dependency of their constitutive functions (Hrachowitz and Clark, 2017). Investigating these models in large-sample studies could provide helpful insights, but running such models is not easily possible with most of the datasets listed in Table 1. The clearest exception to this are the LamaH-CE (Klingler et al., 2021) and LamaH-Ice datasets (Helgason and Nijssen, 2024), which cover the Upper Danube River basin in Central

Europe and interior Iceland, respectively. Both datasets provide data in a semi-distributed spatially continuous fashion and provide a collection of forcing variables generally associated with process-based modelling approaches. However, the spatially continuous nature of these datasets means they are somewhat constrained geographically, covering an area of only 170 000 km² (roughly 600 by 300 km) in Central Europe and an area of 46 000 km² (roughly 300 by 150 km) in interior Iceland, respectively. Both datasets also still aggregate data at the sub-basin level, prohibiting the use of gridbased models. There is a clear gap in the current collection of large-sample hydrologic datasets that (1) enables the use of spatially distributed process-based models across a wide range of hydroclimatic conditions and (2) enables studies aimed at investigating spatial heterogeneity at a resolution made possible by the geospatial datasets that underpin the current generation of large-sample hydrology datasets.

In this paper, we introduce the CAMELS-SPAT dataset ("Catchment Attributes and MEteorology for Large-Sample SPATially distributed analysis"). We expand on the original CAMELS dataset (Newman et al., 2015; Addor et al., 2017a) in various ways. First, we provide the CAMELS-SPAT data at three spatial resolutions: (1) at its original gridded resolution, (2) spatially averaged at the sub-basin level (defined as smaller areas that subdivide the area upstream of each gauge to facilitate semi-distributed modelling) and (3) spatially averaged at the basin level (equivalent to how catchments are treated as lumped entities in the original CAMELS dataset). Second, we extend the geographical domain of the dataset to include Canada, which includes various types of hydrologically challenging landscapes not included in the original CAMELS dataset (e.g. glaciated basins, regions with extensive permafrost, arctic deserts). Third, we provide a wider range of forcing variables at a temporal resolution (i.e. hourly) suitable for process-based modelling, in addition to a commonly used daily dataset. Fourth, to facilitate sub-daily analyses, we provide streamflow data at both daily and hourly resolutions. Fifth, we provide a wider range of catchment attributes, with the specific goal of quantifying the attributes' ranges in time and space rather than providing mean values only. Compared to LamaH-CE and LamaH-Ice, our main contributions can be found in the wider range of hydroclimatic conditions found across the US and Canada and the inclusion of forcing and geospatial data at their original (non-aggregated) resolution. Compared to HYSETS, another large-sample dataset focused on North America, our main contributions can be found in the wider range of forcing variables, a higher temporal and spatial resolution of forcing data, the inclusion of forcing and geospatial data at their original (non-aggregated) spatial resolution and the inclusion of streamflow data at an hourly time step.

This paper is structured as follows. Section 2 starts by outlining our design considerations for this dataset, followed by five longer subsections that describe the methods and outcomes of our basin selection (Sect. 2.1), basin

delineation (Sect. 2.2), streamflow observation processing (Sect. 2.3), forcing data processing (Sect. 2.4) and geospatial data-processing procedures (Sect. 2.5). Section 3 then provides details on how we used the geospatial data to derive over 1100 statistical descriptors, also known as catchment attributes, for each basin. Section 4 has various recommendations for data providers based on our experiences with constructing the CAMELS-SPAT dataset (Sect. 4.1), as well as various recommendations for data users based on our expectations of how the CAMELS-SPAT data might be used (Sect. 4.2). Section 4 also contains some thoughts about the extension of the dataset to new regions (Sect. 4.3) and notes on the dataset structure and size (Sect. 4.4). A summary and conclusions are given in Sect. 5.

2 Design considerations and outcomes

Our goal with this dataset is to enable studies that investigate spatial heterogeneity across a wide variety of catchments, with a specific focus on spatially distributed process-based modelling. We also envision this dataset to be used to compare the performance of these models to their more empirical counterparts and for analyses not directly based on hydrologic models. Consequently, we processed a variety of data sources at various levels. We provide further detail about these requirements in the following subsections, as needed. Our general methodology for creating CAMELS-SPAT is as follows:

- 1. Define an initial set of basins of potential interest, covering the US and Canada;
- 2. Create consistent basin delineations for all basins identified under (1);
- 3. Obtain and process streamflow observations for the basins identified under (1), removing those basins for which no streamflow data can be found;
- 4. Obtain and process meteorological forcing data for the basins identified under (3);
- Obtain and process geospatial datasets (e.g. data describing each basin's climate, vegetation, land use, topography, soil and geology) for the basins identified under (3);
- Remove a number of very large basins from the basins identified under (3) and divide the remaining basins into various sub-datasets, based on disk space considerations;
- 7. Calculate catchment attributes using the data processed under (3), (4) and (5).

Figure 1 shows a visual summary of the main steps and decision points in this process, and each step is explained in more

detail in the following subsections. For the reader's benefit, we present combined descriptions of the methods and results for each of these steps in the following seven subsections, instead of splitting these into dedicated Methods and Results sections. The code used to generate this dataset is available online (see the "Code and data availability" statement).

2.1 Basin pre-selection

2.1.1 Context

We impose two initial constraints on the basins we will consider including in this dataset. First, we have chosen to focus this dataset on (near-)natural basins. Human impacts on the earth system are critically important but substantially complicate hydrologic behaviour and are typically difficult to quantify and thus difficult to account for during analyses. Such impacts include but are not limited to (i) the construction of water management structures such as dams and drainage ditches at the local level, of which the location and size are difficult to ascertain and usually unreported in the continental-scale datasets that CAMELS-SPAT relies on; (ii) the construction of large water management infrastructure such as diversions and reservoirs, which may appear in continental-scale datasets but for which operating procedures are typically unknown; and (iii) surface and groundwater abstractions (e.g. agricultural and industrial use), for which abstraction and return volumes are typically unknown. That said, it is almost unavoidable that any selected basin includes at least some human impacts (tourism/recreation, drainage, forest management, etc.). We rely on existing classifications to select basins that are closer to the natural end of this continuum. Second, we require the availability of at least some streamflow observations at a sub-daily resolution. Process-based models are typically run at sub-daily time steps to more accurately simulate diurnal variation in processes such as evaporation, transpiration, sublimation and snow melt. In certain basins, such diurnal variability is visible in the streamflow record, and sub-daily observations are necessary to evaluate the appropriateness of process-based model equations. Daily data are by definition too coarse to distinguish such patterns.

2.1.2 Methods and outcomes

For basins in the US, we rely on the basin selection made by Newman et al. (2015) that was used for the CAMELS dataset (Addor et al., 2017a). This ensures that some level of comparison between outcomes of studies using either CAMELS or CAMELS-SPAT is possible. We refer the reader to Sect. 2.1 in Newman et al. (2015) for a description of the criteria used to create this selection of 671 basins, and note that, despite meeting these criteria, no basins in Alaska, Hawaii or Puerto Rico were included in the original CAMELS dataset due to limited spatial coverage of the

Table 1. Overview of large-sample datasets aimed at hydrologic modelling. Datasets are listed chronologically.

Dataset	Temporal coverage	Region	#basins	Tempor resolution	Temporal Spatial resolution resolution	Forcing data # products	Forcing variables
MOPEX ^{a,b}	1948–2003	Contiguous US	438	Daily	Basin-averaged	Station observations in basins	Precipitation, climatic potential evaporation, maximum air temperature, minimum air temperature
CANOPEX ^a	Varies per basin	Canada	698	Daily	Basin-averaged	2 (1 station, 1 gridded)	Precipitation, maximum temperature, minimum temperature
CAMELS ^a	Varies per forcing dataset	Contiguous US	671	Daily	Basin-averaged; per elevation band	3	Precipitation, maximum temperature, minimum temperature, shortwave downward radiation, day length, vapour pressure
CAMELS-CL ^a	Varies per basin	Chile	516	Daily	Basin-averaged	Multiple, depending on variable	Precipitation, maximum temperature, mean temperature, minimum temperature, potential evapotranspiration
HYSETS ^a	Varies per basin	North America	14 425	Daily	Basin-averaged	7	Precipitation, maximum air temperature, minimum air temperature
CAMELS-BR ^a	1981–2018	Brazil	897	Daily	Basin-averaged	Multiple, depending on variable	Precipitation, maximum temperature, average temperature, minimum temperature, potential evapotranspiration, actual evapotranspiration
CAMELS-GB ^a	1970–2015	Great Britain	671	Daily	Basin-averaged	_	Precipitation, average temperature, potential evapotranspiration, potential evapotranspiration with interception correction, wind speed, specific humidity, downward shortwave radiation, longwave radiation
CABra ^a	1980–2010	Brazil	785	Daily	Basin-averaged	3	Precipitation, maximum temperature, minimum temperature, solar radiation, 2 m wind speed, potential evapotranspiration (three estimates), actual evapotranspiration
CAMELS-AUS ^a	Varies per forcing dataset and variable	Australia	222 (v2: 561)	Daily	Basin-averaged	Multiple, depending on variable	Precipitation, maximum temperature, minimum temperature, potential evapotranspiration (four estimates), actual evapotranspiration, solar radiation, vapour pressure, vapour pressure deficit, relative humidity at time of minimum temperature, mean sea level pressure
LamaH-CE ^{a, c}	1981–2019	Central Europe	859	Daily, hourly	Basin-averaged at three basin levels	-	Precipitation, 2 m air temperature, 10 m wind in U direction, 10 m wind in V direction, net solar radiation at the surface, net thermal radiation at the surface, surface pressure, total evapotranspiration
CCAM ^a	1990–2020	China	4911	Daily	Basin-averaged	1	Precipitation, 2 m mean temperature, ground surface temperature, potential evapotranspiration, measured evaporation, ground pressure, relative humidity, 2 m wind speed, sunshine duration
CAMELS-CH ^{a, d}	1981–2020	Switzerland and surrounding areas	331	Daily	Basin-averaged	1 (used to derive extra variables)	Precipitation, maximum temperature, mean temperature, minimum temperature, relative sunshine duration
CAMELS-SE ^a	1961–2020	Sweden, with small parts of Norway	50	Daily	Basin-averaged	1	Precipitation, temperature
LamaH-Ice ^{a,c}	Varies per basin	Iceland	107	Daily, hourly	Basin-averaged at three basin levels	3	Precipitation, 2 m air & dew point temperature, surface net solar & thermal radiation, surface pressure, specific humidity, complemented with various outputs from a land surface model such as soil water content, total evaporation and snow water equivalent
CAMELS-FR ^a	1970–2021	France	654	Daily	Basin-averaged	1	Solid precipitation, liquid precipitation, minimum & maximum air temperature, wind speed, specific humidity, atmospheric & visible radiation, three potential evapotranspiration estimates, as well as soil moisture and snow water equivalent estimates from a land surface model
CAMELS-DE ^a	Varies per basin	Germany	1582	Daily	Basin-averaged	1	Precipitation, minimum/mean/maximum temperature, humidity, radiation, potential evapotranspiration
CAMELS-DK ^a	Varies per basin	Denmark	3330e	Daily	Basin-averaged	_	Precipitation, temperature, potential evapotranspiration, complemented with various outputs from a land surface model
CAMELS-IND ^a	1980–2020	India	472e	Daily	Basin-averaged	Multiple, depending on variable	Precipitation, minimum/mean/maximum temperature, downward longwave radiation, downward shortwave radiation, wind speed in U,V and average direction, relative humidity, two potential evapotranspiration estimates, complemented with various outputs from a land surface model

^a References: MOPEX (Schaale et al., 2006), CANOPEX (Assenault et al., 2016), CAMELS-GI (Newman et al., 2017a), CAMELS-CI (Abraez-Garreton et al., 2018), HYSETS (Assenault et al., 2020), CAMELS-BI (Chagas et al., 2020), CAMELS-BI (Chagas et al., 2020), CAMELS-BI (Chagas et al., 2020), CAMELS-DE (Loriz et al., 2021), CAMELS-BI (Chagas et al., 2024), CAMELS-BI (Chagas et al., 2024), CAMELS-DE (Loriz et al., 2024), CAMELS-BI (Chagas et al., 2024), CAMELS-DE (Loriz et al., 2024), CAMELS-DE (Loriz et al., 2025), b MOPEX variables as described in the "basic requirements" in Duan et al. (2006).

c Lamalt-CE and Lamalt-lee basins are spatially connected.
d CAMELS-CH (Chagas et al., 2024), CAMELS-DE (Loriz et al., 2024), CAMELS-DE (Loriz et al., 2025), connected from the core forcing include precipitation, mean temperature, global radiation, sunshine duration, wind speed, relative humidity, potential evapotranspiration, actual evapotranspiration and intercepted evapotranspiration.

Hydrol. Earth Syst. Sci., 29, 5791–5833, 2025

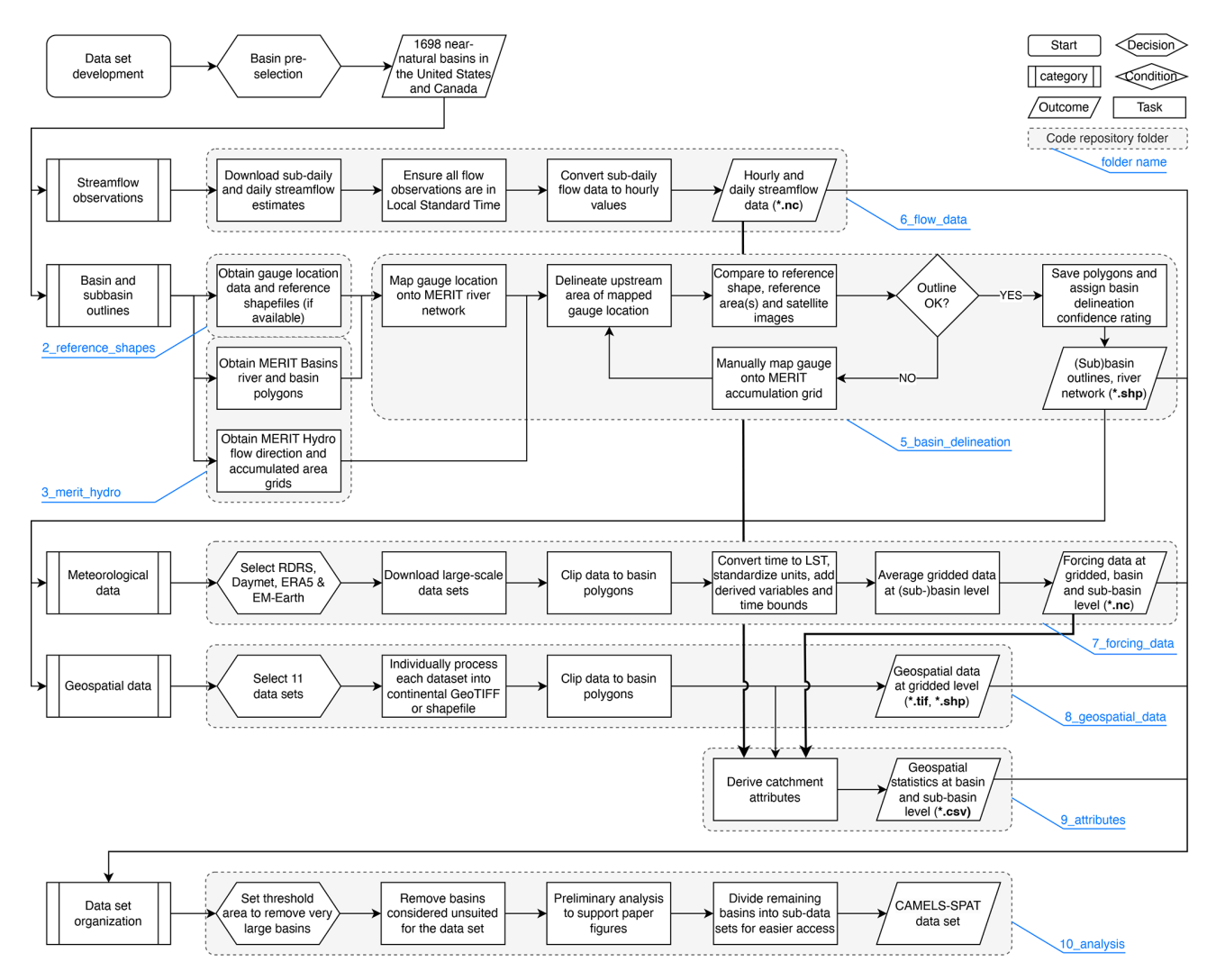


Figure 1. Overview of the CAMELS-SPAT workflow. Grey boxes and light-blue call-outs indicate specific folders on the GitHub repository, where the necessary code to reproduce these steps can be found. Note that the repository folder 4_data_structure_prep is not listed in this figure because it contains no methodological choices.

Daymet data at the time. Our primary forcing dataset (see Sect. 2.4) does not have the coverage to include basins in Hawaii or Puerto Rico, but cold region processes as may be found in Alaska are covered by our selection of Canadian basins.

For basins in Canada, we start with the list of 1027 gauges included in the "Reference Hydrometric Basin Network" (RHBN; Environment and Climate Change Canada, 2020a, retrieved: 18 August 2022). These gauges have a minimum data availability of 20 years and minimal anthropogenic impacts as quantified by the presence of agriculture, built-up areas and water management infrastructure, as well as population and road density. These criteria are comparable to those described in Newman et al. (2015). Note that agriculture presence in the Canadian prairie provinces (Alberta, Saskatchewan, Manitoba) and southern Ontario is substantial and above the 10% area threshold used for the other

provinces and territories (Pellerin and Nzokou Tanekou, 2020, p. 7). Excluding these basins would severely reduce the number of Canadian gauges we could include in the dataset, and we thus retain these gauges but include various data products in CAMELS-SPAT that can be used to quantify or filter by the presence of agriculture.

Our initial basin selection included 1698 basins across the US and Canada. Various basins had to be removed due a lack of streamflow estimates or sub-daily data (see Sect. 2.3). We further removed several of the largest basins from the dataset, under the assumption that any new insights that could be gained from these extremely large basins are minimal (especially given that these basins are severely under-gauged for their size) and do not outweigh the extra disk space needed to store the data for these basins (see Sect. S3 in the Supplement for details). Our final selection consists of 1426 basins, with an approximately even spread between the US and Canada.

For clarity, any outcomes shown in Sects. 2.2 to 4.4 only show the final 1426 basins we have made publicly available, rather than the 1698 basins that are the outcome of this basin pre-selection step.

2.2 Basin delineation

2.2.1 Context

Hydrologic datasets such as this are conditional on having accurate basin outlines. Basin outlines are used to estimate a drainage basin's area, to crop meteorological and geospatial data to the area of interest and to define the spatial extent of model configurations. Basin area estimates are also often used to convert the units of fluxes from volume-per-time to depth-per-time or vice versa (e.g. from m³ s⁻¹ to mm s⁻¹). Using incorrect basin area estimates can lead to large conversion errors that propagate into any further analysis (McMillan et al., 2023).

The basin polygons provided as part of the CAMELS data (Newman et al., 2014; Addor et al., 2017b) are administrative boundaries. These polygons are not based on gauge locations, and the polygons thus tend to overestimate the basins' drainage areas. Estimated area errors (derived from a comparison of reported upstream area for each gauge and actual area of the basin polygon) are typically in the order of some percent (below 2% for approximately 70% of basins) but can be substantial (above 10% for approximately 8.5% of basins, with individual cases well above 100%). Additionally, openly available polygons for the Canadian gauges did at the time of project initialization not fully cover all 1027 basins listed in the Reference Hydrometric Basin Network (RHBN) (Environment and Climate Change Canada, 2020b, retrieved: 31 January 2022).

To address both concerns, we delineated new basin outlines for all basins identified as potential candidates in Sect. 2.1. Our specific goals were to (1) identify the upstream area of each gauge and (2) divide this upstream area into subbasin polygons of roughly equal size.

2.2.2 Method and outcomes

We obtained gauge metadata (location, name, reference areas, etc.), as well as reference basin outline polygons if these were available, for all gauges identified in the first step. For the US gauges, metadata and polygons showing each basin's outline were obtained from the CAMELS dataset (Newman et al., 2014; Addor et al., 2017b). For the Canadian gauges, an initial download of the RHBN metadata was used to identify which gauges are included in the RHBN version released in 2020. Further metadata (location, name) were then extracted from the HYDAT database (Environment and Climate Change Canada, 2010). Two different sets of reference polygons were available (Environment and Climate Change Canada, 2020b; Government of Canada, 2022, ac-

cessed: 23 August 2022, 18 August 2022, respectively), of which we preferentially used the newer polygons if these were available for our basins of interest.

To divide larger basins into smaller sub-basins, we used the MERIT Basins dataset (Lin et al., 2019). This dataset contains vectorized river basins and river networks, derived from the MERIT Hydro data (Yamazaki et al., 2019). The mean sub-basin size in the MERIT Basins data is 45.6 km² (median: 36.8 km²). We refer the reader to Lin et al. (2019) for further details. We also obtained the MERIT Hydro flow direction and accumulation grids (Yamazaki et al., 2019). The MERIT Hydro data are provided as gridded data in a regular longitude/latitude coordinate system (EPSG:4326). This is a common format (most of the meteorological data, and many of the geospatial datasets we discuss in Sect. 2.4 and 2.5 are also only available in EPSG:4326). We adopt this as the standard in CAMELS-SPAT to the extent feasible. The one exception is the RDRS meteorological dataset, which is originally provided on a custom rotated latitude/longitude grid. Any area calculations and certain shapefile intersection operations are performed in the North America Albers Equal Area Conic projection (ESRI:102008).

The MERIT Basin network was derived independently from gauges, and the sub-basins in this dataset therefore do not align with gauge locations as reported by the U.S. Geological Survey and the Water Survey of Canada. For a given basin, we thus needed to clip the most downstream sub-basin polygon to the gauge. We therefore first mapped the gauge locations onto the MERIT Hydro river network using automated techniques. This mapping is intended to guarantee that the delineation of the upstream area of a given gauge starts from a pixel in the flow direction grid that is part of the main river (rather than the most downhill pixel of a single hillslope). However, there are various scenarios where automatic mapping is inaccurate and manual intervention is needed. We identified those cases through a combination of accuracy metrics (area comparison between new basin delineation and reported reference area(s) as well as percentage overlap between new basin delineation and reference polygon if any were available) and visual inspection of the new basin delineation, reference polygon, underlying MERIT Hydro data grids and satellite images. If necessary, we manually defined a better outlet location to delineate the basin from and tracked this intervention in the CAMELS-SPAT metadata. We also assigned confidence ratings to our new basin polygons based on these quality assurance checks. As the final step, we identified all cases of nested gauges where a larger basin includes a smaller one. In such cases, we split the sub-basin polygon that contains the nested gauge and assigned unique identifiers to the upstream and downstream parts of the sub-basin and river segment.

Figure 2 shows the resulting polygons for the 1426 basins that form the final CAMELS-SPAT dataset, with colours indicating the confidence ratings we assigned based on the checks listed previously (i.e. automated overlap and area

checks, as well as manual inspection of polygons and satellite images). "Unknown" refers to cases where no confidence rating could be assigned, mainly due to lacking reference polygons. "Low" ratings are assigned when evidence suggests that our basin delineations are inaccurate, and we were unable to manually find a better outlet location that would lead to improved basin outlines. "Medium" ratings indicate that there are substantial differences between our new delineations and existing ones and/or reference areas but that it is difficult to decide whether our new delineation or the reference(s) are more accurate. "High" ratings are assigned when there is a clear match between our new polygons and the reference(s) or when evidence suggests our new delineations are more accurate than the reference(s). Detailed reasons for these ratings are tracked as part of the CAMELS-SPAT metadata. Medium and low confidence ratings occur primarily in regions with flat topography where finding the true outline of any drainage basin is difficult.

2.3 Streamflow observations

2.3.1 Context

Streamflow is a key variable for many hydrologic studies. Streamflow estimates are typically provided as either instantaneous values (i.e. valid at a given point in time) or as averages over a given time interval. It is critical to know what type of values (instantaneous or time averages) are available, as well as the time zones that the data are provided in.

The U.S. Geological Survey (USGS) typically collects instantaneous streamflow observations at 15 or 60 min intervals. USGS also provides daily average values, computed from the instantaneous data from 00:00 to 24:00 local standard time (LST; USGS, personal communication, 20 June 2023). Both instantaneous values and daily averages are publicly available.

The Water Survey of Canada (WSC) typically collects instantaneous streamflow observations at 5 min intervals and from these calculates daily averages that are reported in LST through the HYDAT database (WSC, personal communication, 4 July 2023). However, when instantaneous values are extracted through the WSC API, the time series are converted to coordinated universal time (UTC) before being given to the user (Government of Canada, 2023). Instantaneous streamflow observations are available through this API for the period between the present and minus 18 months. Recently, WSC has also released sub-daily data going back to 2011 (last access: 2 June 2025, Water Survey of Canada, 2025), although this cannot be accessed through the standard API. To expand the hourly data availability for Canadian basins, we included this data source in our processing. Daily average values are available for the full time period for which a gauge has been active.

Our goal with this project is to provide data that are useful for running and evaluating process-based hydrological

models. We therefore include daily average streamflow values as available through USGS and WSC. We also include hourly average streamflow values to match the temporal resolution of our selected meteorological datasets. Hourly average flow data are computed from the sub-daily instantaneous data available through both agencies. All flow data, as well as meteorological forcing data, are included in the CAMELS-SPAT dataset in local standard time. The time zone of each gauge is tracked as part of the metadata.

2.3.2 Method and outcomes

For the gauges in the US, daily average streamflow data and instantaneous (sub-daily) data can both be extracted through API requests (https://nwis.waterservices. usgs.gov/nwis/dv/ and https://nwis.waterservices.usgs.gov/ nwis/iv/, respectively; last access: 16 June 2023). For the Canadian gauges, sub-daily data were extracted from the Environment and Climate Change Canada FTP server (https://collaboration.cmc.ec.gc.ca/cmc/hydrometrics/ www/UnitValueData/, last access: 31 May 2025). Daily data were extracted from the HYDAT database, version 20230505. We excluded four gauges in the US and 180 Canadian gauges from the original 1697 pre-selected stations because sub-daily data were not available for these stations. We removed a further 13 Canadian gauges for lacking daily discharge values. Manual checks of these gauges through the WSC website (https://wateroffice.ec.gc.ca/search/historical e.html, last access: 6 February 2025) indicate that these stations measure water levels in lakes.

Daily average values for both countries are provided in LST. We updated the time indices for the sub-daily instantaneous values to match. For the gauges in the US, this meant shifting the time series by 1 h for time steps that were provided in local daylight saving time for gauges in states where daylight saving time is observed. For the Canadian gauges, this meant shifting the entire time series for each gauge by the offset needed to convert UTC to LST. We then set any negative streamflow values to zero and used a massconserving averaging approach to turn instantaneous flow data into hourly averages (see Sect. S1 in the Supplement for more details about the averaging procedure). We specified the condition that every hourly average must be based on at least one observation during that time window. Hours for which no data observations were available were set to not-a-number (NaN).

Note the critical assumption that we calculated the average hourly flows as the value at the top of the hour (e.g. 12:00) using a forward-looking window (in this case, the value at 12:00 is the average during the time window 12:00–13:00). This matches the daily flows, which are provided under the same assumption by USGS and WSC (e.g. the 1 January 2000 value is calculated from data between 00:00, 1 January and 24:00, 1 January; USGS, personal communication, 20 June 2023; WSC, personal communication

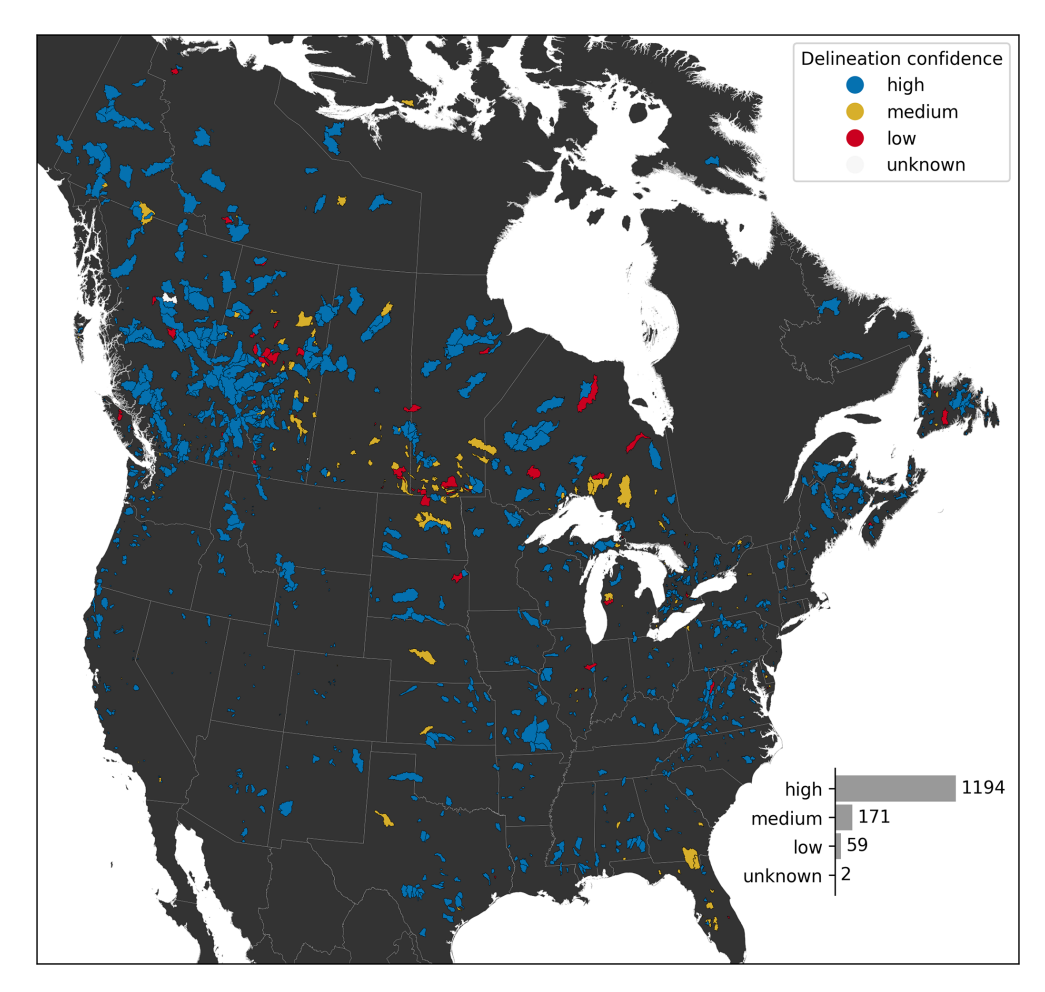


Figure 2. Location and delineation confidence of 1426 CAMELS-SPAT basins. Political boundaries by the Commission for Environmental Cooperation (2022, last access: 20 December 2023).

tion, 26 June 2023). This information is also stored in the *time_bnds* (time bounds) variable available in the provided NetCDF files.

Daily and sub-daily observations were originally provided in text-based formats. We converted these to NetCDF4 formats to ensure consistency between gauges in the two countries and to track metadata in a more accessible way (compared to storing the metadata in separate files or headers in text files). For both USGS and WSC data, we retained the quality flags that accompany the data and stored these in the same NetCDF files that contain the streamflow observations. These quality flags indicate conditions that may adversely affect the observations (e.g. gauge malfunction, ice conditions) and whether data have been formally approved or are still considered provisional.

Figure 3 shows aggregated flow data availability for the 1426 catchments included in the CAMELS-SPAT dataset, with the total record length in blue (number of years between first and last available streamflow observation) and missing values in red (number of years in the record length for which no observations are available). Hourly flow data come

in two distinct categories: records for the Canadian gauges are around a decade in length, while sub-daily records for gauges in the US are typically two to three times longer. This is a consequence of the Water Survey of Canada's policy to make high-resolution gauge data publicly available for only a relatively short historical period. Missing data for these shorter records are, however, typically low (see also Fig. A1). For approximately 60 % of gauges, missing hourly observations account for up to 10% of the record length. Data may be missing for up to 40 % of the record for most remaining gauges, with a handful of gauges having extremely large data gaps. Daily data record lengths are similar for Canadian and US gauges. Missing values are relatively rare (< 1 % for up to 849 out of our 1426 gauges and < 10% for 1070 out of 1426 gauges), although this can be substantial (up to approximately 60 %; see Fig. A1). The period with the greatest overlap of data records is 1990-2020; hourly observations are available for only a handful of gauges before this time. Some further statistics on the streamflow regimes available in CAMELS-SPAT are discussed in Sect. 3.5.

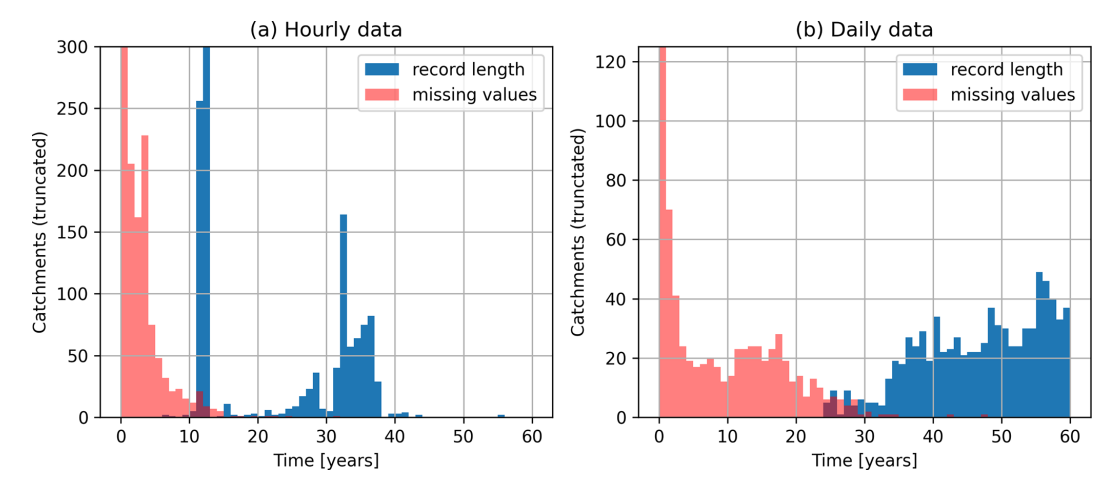


Figure 3. Flow data availability for gauges included in CAMELS-SPAT. Record length refers to the period between the first publicly available flow record for a given station and its last. Missing values occur in this record period and are given here in the same units as the record length itself. Note that both *y* axes are truncated: in **(a)**, there are 556 cases where the number of *missing values* falls between 0 and 1 years of total (although note that these missing values are not necessarily consecutive and in fact in many cases are caused by seasonally active gauges). Also truncated is the *record length* bar showing the 498 cases where the length of the hourly data record is between 12 and 13 years. In **(b)**, *missing values* has a count of 898 for *time* between 0 and 1 years. **(a, b)** Note that the colours are partly transparent and that overlaps between the *record length* and *missing values* bars will appear as dark red.

2.4 Forcing data

2.4.1 Context

Meteorological forcing data in existing datasets are typically provided as catchment-averaged (lumped) daily data and tends to be limited to precipitation, temperature and potential evapotranspiration variables (Table 1). While a large number of the more conceptual models can be run with only precipitation, temperature and potential evapotranspiration inputs (see e.g. Knoben et al., 2019; Trotter et al., 2022), more complex hydrologic models typically require a wider array of inputs at a higher temporal resolution. Table 2 shows a brief overview of the meteorological data requirements for a selection of process-based hydrological models. Typical variables include (1) precipitation, (2) air temperature, (3) radiation (often distinguishing between shortwave and longwave radiation), (4) air pressure, (5) humidity and (6) wind speed.

It is clear from Table 2 that it is impossible to define a small set of forcing variables that would allow the use of a large number of process-based hydrologic models. We therefore decided to include a broad selection of meteorological variables, accepting that this comes at the cost of extra disk space. We provide these variables at hourly time steps, at their original gridded resolution as well as averaged at the sub-basin level. To facilitate the use of the broadest range of modelling tools, we also include time series of potential evaporation (see footnote in Table 3) and forcing variables aggregated at the lumped basin level.

2.4.2 Methods and outcomes

CAMELS-SPAT includes four forcing datasets, each with a specific focus:

- 1. First, we primarily use the high-resolution RDRS v2.1 dataset (Gasset et al., 2021, available at 10 km or approximately 0.09° resolution). RDRS covers the North American continent and provides those variables needed to run process-based models directly and derive most other variables listed in Table 2. A key advantage of RDRS is that it assimilates precipitation observations, which should improve the accuracy of its precipitation field.
- 2. Second, for continuity with the original CAMELS dataset, we include the Daymet v4 R1 dataset (Thornton et al., 2021, available at a 1 km or approximately 0.009° resolution). Daymet is based on weather station observations and gridded terrain data and is available at a daily resolution between 1980 and 2023 on a 365 d calendar (during leap years, 31 December is missing). The dataset does not include all the forcing variables needed to run process-based models but, if combined with an appropriate estimate of potential evapotranspiration (PET), provides sufficient information to run more conceptual and data-driven models. We infill the missing day in leap years as a linearly interpolated value between the preceding and following days. Following Newman et al. (2015), we add a Priestley-Taylor PET estimate (Priestley and Taylor, 1972, further details available in Sect. S2.5 in the Supplement).

Table 2. Meteorological data needs for CATFLOW (Maurer and Zehe, 2007), CHM (Marsh et al., 2020), CHRM (Pomeroy et al., 2007), ESCROC (Lafaysse et al., 2017), HYPE (SMHI, 2022), MESH (Mekonnen and Brauner, 2020), Noah-LSM (Mitchell et al., 2005), PARFLOW (Maxwell et al., 2019), MM-PIHM (PIHM team, 2007; Yuning Shi, 2018), SUMMA (Clark et al., 2015a, b; Nijssen, 2017), VIC (Liang et al., 1994; Hamman et al., 2018) and WaSIM (Schulla, 2021). Models are listed alphabetically. Optional inputs indicated with *. t indicates an arbitrary time unit.

Variable	CATFLOW	СНМ	CHRM	ES-CROC	НҮРЕ	MESH
Precipitation	$[mt^{-1}]$	$[mmt^{-1}]$	$[mmt^{-1}]$	$[kg m^{-2} s^{-1}]$	$[mmt^{-1}]$	$[kg m^{-2} s^{-1}]$
Downward shortwave radiation	$[W m^{-2}]$	$[W m^{-2}]$		$[W m^{-2}]$	$[MJm^{-2}d^{-1}]*$	$[W m^{-2}]$
Downward longwave radiation		$[W m^{-2}]$		$[W m^{-2}]$		$[W m^{-2}]$
Air temperature	[°C]	[°C]	[°C]	[K]	[°C]	[K]
Air pressure				[Pa]		[Pa]
Specific humidity					1 .	$[kgkg^{-1}]$
Wind speed (U direction)					$[m s^{-1}]^*$	
Wind speed (V direction)					$[m s^{-1}]*$	
Sunshine duration			2-			
Reflected shortwave radiation	2-		$[W m^{-2}]$			
Net radiation	$[\mathrm{W}\mathrm{m}^{-2}]$		$[\mathrm{W}\mathrm{m}^{-2}]$			
Vapour pressure	[%]	[%]	r <i>o</i> / 1	[%]	г 1*	
Relative humidity	$[m s^{-1}]$	$[ms^{-1}]$	[%] [m s ⁻¹]	$[m s^{-1}]$	$[-]^*$ $[m s^{-1}]$	$[ms^{-1}]$
Wind speed (mean) Wind direction	[degrees]	[degrees]	[IIIS]	[IIIS]		[IIIS -]
Willia direction	[degrees]	[degrees]				
Variable	Noah-LSM	PARFLOW	MM-PIHM	SUMMA	VIC	WaSIM
Variable Precipitation	Noah-LSM [in. (30 min) ⁻¹]	PARFLOW [mm s ⁻¹]	$\frac{\text{MM-PIHM}}{[\text{kg m}^{-2} \text{s}^{-1}]}$	$\frac{\text{SUMMA}}{[\text{kg m}^{-2} \text{s}^{-1}]}$	VIC [mmt ⁻¹]	WaSIM [mm]
Precipitation	$[in. (30 min)^{-1}]$	[mm s ⁻¹]	$[kg m^{-2} s^{-1}]$	$[kg m^{-2} s^{-1}]$	$[mmt^{-1}]$	[mm]
Precipitation Downward shortwave radiation Downward longwave radiation Air temperature	[in. (30 min) ⁻¹] [W m ⁻²] [W m ⁻²] [°C]	$[mm s^{-1}]$ $[W m^{-2}]$	$[kg m^{-2} s^{-1}]$ $[W m^{-2}]$	[kg m ⁻² s ⁻¹] [W m ⁻²] [W m ⁻²] [K]	[mmt ⁻¹] [Wm ⁻²] [Wm ⁻²] [°C]	[mm]
Precipitation Downward shortwave radiation Downward longwave radiation Air temperature Air pressure	[in. (30 min) ⁻¹] [W m ⁻²] [W m ⁻²]	[mm s ⁻¹] [W m ⁻²] [W m ⁻²] [K] [Pa]		[kg m ⁻² s ⁻¹] [W m ⁻²] [W m ⁻²] [K] [Pa]	$[mmt^{-1}]$ $[Wm^{-2}]$ $[Wm^{-2}]$	[mm] [W h m ⁻²]
Precipitation Downward shortwave radiation Downward longwave radiation Air temperature Air pressure Specific humidity	[in. (30 min) ⁻¹] [W m ⁻²] [W m ⁻²] [°C]	[mm s ⁻¹] [W m ⁻²] [W m ⁻²] [K] [Pa] [kg kg ⁻¹]	[kg m ⁻² s ⁻¹] [W m ⁻²] [W m ⁻²] [K]	[kg m ⁻² s ⁻¹] [W m ⁻²] [W m ⁻²] [K]	[mmt ⁻¹] [Wm ⁻²] [Wm ⁻²] [°C]	[mm] [W h m ⁻²]
Precipitation Downward shortwave radiation Downward longwave radiation Air temperature Air pressure Specific humidity Wind speed (U direction)	[in. (30 min) ⁻¹] [W m ⁻²] [W m ⁻²] [°C]	[mms ⁻¹] [W m ⁻²] [W m ⁻²] [K] [Pa] [kg kg ⁻¹] [ms ⁻¹]	[kg m ⁻² s ⁻¹] [W m ⁻²] [W m ⁻²] [K]	[kg m ⁻² s ⁻¹] [W m ⁻²] [W m ⁻²] [K] [Pa]	[mmt ⁻¹] [Wm ⁻²] [Wm ⁻²] [°C]	[mm] [W h m ⁻²]
Precipitation Downward shortwave radiation Downward longwave radiation Air temperature Air pressure Specific humidity Wind speed (<i>U</i> direction) Wind speed (<i>V</i> direction)	[in. (30 min) ⁻¹] [W m ⁻²] [W m ⁻²] [°C]	[mm s ⁻¹] [W m ⁻²] [W m ⁻²] [K] [Pa] [kg kg ⁻¹]	[kg m ⁻² s ⁻¹] [W m ⁻²] [W m ⁻²] [K]	[kg m ⁻² s ⁻¹] [W m ⁻²] [W m ⁻²] [K] [Pa]	[mmt ⁻¹] [Wm ⁻²] [Wm ⁻²] [°C]	[mm] [Whm ⁻²] [°C]
Precipitation Downward shortwave radiation Downward longwave radiation Air temperature Air pressure Specific humidity Wind speed (<i>U</i> direction) Wind speed (<i>V</i> direction) Sunshine duration	[in. (30 min) ⁻¹] [W m ⁻²] [W m ⁻²] [°C]	[mms ⁻¹] [W m ⁻²] [W m ⁻²] [K] [Pa] [kg kg ⁻¹] [ms ⁻¹]	[kg m ⁻² s ⁻¹] [W m ⁻²] [W m ⁻²] [K]	[kg m ⁻² s ⁻¹] [W m ⁻²] [W m ⁻²] [K] [Pa]	[mmt ⁻¹] [Wm ⁻²] [Wm ⁻²] [°C]	[mm] [W h m ⁻²]
Precipitation Downward shortwave radiation Downward longwave radiation Air temperature Air pressure Specific humidity Wind speed (<i>U</i> direction) Wind speed (<i>V</i> direction) Sunshine duration Reflected shortwave radiation	[in. (30 min) ⁻¹] [W m ⁻²] [W m ⁻²] [°C]	[mms ⁻¹] [W m ⁻²] [W m ⁻²] [K] [Pa] [kg kg ⁻¹] [ms ⁻¹]	[kg m ⁻² s ⁻¹] [W m ⁻²] [W m ⁻²] [K]	[kg m ⁻² s ⁻¹] [W m ⁻²] [W m ⁻²] [K] [Pa]	[mmt ⁻¹] [Wm ⁻²] [Wm ⁻²] [°C]	[mm] [Whm ⁻²] [°C]
Precipitation Downward shortwave radiation Downward longwave radiation Air temperature Air pressure Specific humidity Wind speed (<i>U</i> direction) Wind speed (<i>V</i> direction) Sunshine duration Reflected shortwave radiation Net radiation	[in. (30 min) ⁻¹] [W m ⁻²] [W m ⁻²] [°C]	[mms ⁻¹] [W m ⁻²] [W m ⁻²] [K] [Pa] [kg kg ⁻¹] [ms ⁻¹]	[kg m ⁻² s ⁻¹] [W m ⁻²] [W m ⁻²] [K]	[kg m ⁻² s ⁻¹] [W m ⁻²] [W m ⁻²] [K] [Pa]	[mmt ⁻¹] [W m ⁻²] [W m ⁻²] [°C] [kPa]	[mm] [Whm ⁻²] [°C]
Precipitation Downward shortwave radiation Downward longwave radiation Air temperature Air pressure Specific humidity Wind speed (<i>U</i> direction) Wind speed (<i>V</i> direction) Sunshine duration Reflected shortwave radiation Net radiation Vapour pressure	[in. (30 min) ⁻¹] [W m ⁻²] [W m ⁻²] [°C] [mbar]	[mms ⁻¹] [W m ⁻²] [W m ⁻²] [K] [Pa] [kg kg ⁻¹] [ms ⁻¹]	[kg m ⁻² s ⁻¹] [W m ⁻²] [W m ⁻²] [K] [Pa]	[kg m ⁻² s ⁻¹] [W m ⁻²] [W m ⁻²] [K] [Pa]	[mmt ⁻¹] [Wm ⁻²] [Wm ⁻²] [°C]	[mm] [Whm ⁻²] [°C]
Precipitation Downward shortwave radiation Downward longwave radiation Air temperature Air pressure Specific humidity Wind speed (<i>U</i> direction) Wind speed (<i>V</i> direction) Sunshine duration Reflected shortwave radiation Net radiation	[in. (30 min) ⁻¹] [W m ⁻²] [W m ⁻²] [°C]	[mms ⁻¹] [W m ⁻²] [W m ⁻²] [K] [Pa] [kg kg ⁻¹] [ms ⁻¹]	[kg m ⁻² s ⁻¹] [W m ⁻²] [W m ⁻²] [K]	[kg m ⁻² s ⁻¹] [W m ⁻²] [W m ⁻²] [K] [Pa]	[mmt ⁻¹] [W m ⁻²] [W m ⁻²] [°C] [kPa]	[mm] [Whm ⁻²] [°C]
Precipitation Downward shortwave radiation Downward longwave radiation Air temperature Air pressure Specific humidity Wind speed (<i>U</i> direction) Wind speed (<i>V</i> direction) Sunshine duration Reflected shortwave radiation Net radiation Vapour pressure	[in. (30 min) ⁻¹] [W m ⁻²] [W m ⁻²] [°C] [mbar]	[mms ⁻¹] [W m ⁻²] [W m ⁻²] [K] [Pa] [kg kg ⁻¹] [ms ⁻¹]	[kg m ⁻² s ⁻¹] [W m ⁻²] [W m ⁻²] [K] [Pa]	[kg m ⁻² s ⁻¹] [W m ⁻²] [W m ⁻²] [K] [Pa]	[mmt ⁻¹] [W m ⁻²] [W m ⁻²] [°C] [kPa]	[mm] [Whm ⁻²] [°C]

- 3. Third, to facilitate possible extension of CAMELS-SPAT beyond North America, as well as provide hourly data for gauges with observations before 1980 (i.e. outside the time period covered by RDRS), we include the globally available ERA5 data (Hersbach et al., 2020, available at a 0.25° resolution). Like RDRS, ERA5 provides all variables needed to run process-based models directly and derive most other variables listed in Table 2. However, unlike the other datasets listed here, ERA5 is a reanalysis product and does not integrate station observations. Local accuracy may thus be lower for ERA5 data than for datasets that do use station observations.
- 4. Fourth, to partly address this weakness of ERA5 data, we include the high-resolution EM-Earth dataset (Tang

et al., 2022b, available at a 0.10° resolution). Previous work has shown that using station-based precipitation and temperature data from EM-Earth provides better modelling results for the North American continent than using ERA5 alone (Rakovec et al., 2023). However, note that EM-Earth has a fixed temporal coverage of 1950–2019, whereas our selected gauges have data beyond 2019.

Table 3 shows an overview of forcing variables available as time series in the CAMELS-SPAT dataset. Compared to Table 2, we provide net radiation terms at the surface separated into net shortwave and net longwave terms and do not provide a summed net radiation component or a reflected shortwave variable. Either can be easily derived from the pro-

vided net shortwave and longwave components (see Hogan, 2015, but also footnote b in Table 3). We also do not provide sunshine duration because this is not available in RDRS, Daymet and EM-Earth. While sunshine duration is available in ERA5, it is not an independent variable: it is derived directly from downward shortwave radiation using a threshold of 120 W m⁻² (Hogan, 2015). We complement the forcing datasets with various additional variables derived from the downloaded data in cases where we judged the processing to be too cumbersome to pass down to the user (i.e. vapour pressure, relative humidity, wind direction) or where the variable seemed to be of general interest (i.e. mean wind speed, PET). Potential evapotranspiration estimates for Daymet were derived using the Priestley-Taylor formula (Priestley and Taylor, 1972); PET estimates for RDRS were derived using the FOA-56 Penman–Monteith method (Allen et al., 1998). The equations used to derive data are provided in Sect. S2 in the Supplement. While the list of variables in Table 3 is unlikely to completely cover all models' data needs, it will provide a reasonable starting point for a large number of models.

We retained the original variable names used in each dataset so that users may easily refer to the existing documentation of RDRS, Daymet, ERA5 and EM-Earth if needed. For convenience and simplicity from a user perspective, we converted all hourly data to use a consistent set of units, although we kept the units of the daily data (Daymet) to be more directly applicable to the types of models more commonly run at daily time steps. Unit conversion of hourly data is mostly straightforward but required an assumption for the density of water, which we set at a constant value of 1000 kg m⁻³. Data are provided for the full time period covered by the observational record of each individual gauge when possible, including time steps for which streamflow data are missing (see also Sect. 4.2.2 and Table 4). For all variables, metadata (descriptions, units, derivations if applicable) are stored as variable attributes in the NetCDF files.

We provide the forcing data at three different spatial aggregation levels: (1) as gridded values at the original spatial resolution of each dataset, clipped to the basin outline; (2) aggregated at the sub-basin level; and (3) aggregated at the basin level (i.e. the level at which most of the datasets listed in Table 1 provide data). Averaging of the gridded data to (sub-)basin polygons was done with the EASYMORE toolbox (Gharari et al., 2023).

RDRS, ERA5 and EM-Earth provide data at an hourly resolution, in coordinated universal time (UTC). We process these time indices to be in each gauge's local standard time (LST) instead, so that the time indices in the forcing file align with those used for the flow observations. We make a slight adjustment for the 57 basins that are located in regions following Newfoundland standard time (NST [UTC-3 h 30]; National Research Council Canada, 2019). The time series of all forcing data products only provide values at the top of each hour (12:00, 01:00, etc.) and thus cannot easily be converted to NST without making assumptions about how

to interpolate the data between the times for which they are available. We treat these basins as following Atlantic standard time (AST [UTC-4h 00]) instead. Note that this leads to a 30 min offset between forcing data and streamflow observations for these basins. Daymet data are already provided as daily average values calculated in LST and require no further adjustment.

Variables in these forcing datasets are either instantaneous (i.e. representative of conditions at a specific point in time) or time averaged (i.e. representative of conditions over a given time window), and this means that the time stamps in each NetCDF file must be interpreted differently for different variables. For any instantaneous variable, a value is valid at the specific moment in time given by the time stamp (European Centre for Medium-range Weather Forecasting, 2023c). For any time-averaged variables, we need to distinguish between two cases. RDRS and ERA5 use period-ending or backwardlooking time stamps, meaning that, for example, the average precipitation rate at time 12:00 is the average rate over the interval 11:00-12:00 (ECCC, personal communication, 2024; European Centre for Medium-range Weather Forecasting, 2023b, Sect. "Mean rates/fluxes and accumulations"). EM-Earth's precipitation variable instead uses *period-beginning* or forward-looking time stamps, meaning that, for example, the average precipitation rate at time 12:00 is the average rate over the interval 12:00–13:00 (Guoqiang Tang, personal communication, 2024). Table 3 provides an overview of all forcing variables and summarizes this information.

2.5 Geospatial data

2.5.1 Context

Geospatial data in existing datasets cover four broad categories: (1) meteorology (as time series and derived summary statistics), (2) vegetation and land use, (3) topography and (4) soil and geology. In current large-sample datasets, geospatial data are typically not provided as maps in their original formats but tend to be presented as spatial statistics (mean, mode, etc.). These statistical summaries of the original data, commonly referred to as catchment attributes, can be helpful to succinctly characterize a location's hydroclimatic conditions and support classification efforts. For modelling purposes, geospatial data play a key role in defining model configurations and parameter values. For example, models such as Noah-LSM (Niu et al., 2011) and SUMMA (Clark et al., 2015a, b) rely on vegetation and soil classes to provide initial values for a number of land use and soil parameters. More generally, models might require the height of the vegetation canopy in the vertical direction or the fraction of the basin covered by open water in the horizontal direction as inputs. It is practically impossible to cover all possible use cases through statistical summaries of the data (i.e. through attributes) alone, and we therefore provide the geospatial data as maps clipped to the basin outlines. The

Table 3. CAMELS-SPAT meteorological variables. Variable names shown in bold indicate derived variables. "Flux validity" indicates how time-averaged variables must be interpreted.

	Dataset	RDRS	ERA5	EM-Earth	Dayme
	Resolution	Hourly	Hourly	Hourly	Daily
	Flux validity	Period-ending ^a	Period-ending ^b	Period-beginning ^c	n/a
Time-averaged variables	Units	Name in NetCDF files			
Precipitation rate	$[kg m^{-2} s^{-1}]$	RDRS_v2.1_A_PR0_SFC	mtpr	prcp	
Potential evapotranspiration rate	$[kg m^{-2} s^{-1}]$		mper ^d		
Precipitation rate	$[mmd^{-1}]$				prcp
Potential evapotranspiration rate	$[mmd^{-1}]$				pet
Downward shortwave radiation	$[{\rm W}{\rm m}^{-2}]$		msdwswrf		srad
Downward longwave radiation	$[{\rm W}{\rm m}^{-2}]$		msdwlwrf		
Net surface shortwave radiation	$[W m^{-2}]$		msnswrf ^e		
Net surface longwave radiation	$[{\rm W}{\rm m}^{-2}]$		msnlwrf ^e		
Instantaneous variables	Units	Name in NetCDF files			
Downward shortwave radiation	$[W m^{-2}]$	RDRS_v2.1_P_FB_SFC			
Downward longwave radiation	$[{\rm W}{\rm m}^{-2}]$	RDRS_v2.1_P_FI_SFC			
Potential evapotranspiration rate	$[kg m^{-2} s^{-1}]$	pet			
Air temperature	[K]	RDRS_v2.1_P_TT_1.5m	t	tmean	
Minimum daily air temperature	[°C]				tmin
Maximum daily air temperature	[°C]				tmax
Daylight length	$[sd^{-1}]$				day
Air pressure	[Pa]	RDRS_v2.1_P_P0_SFC	sp		
Specific humidity	$[kg kg^{-1}]$	RDRS_v2.1_P_HU_1.5m	q		
Relative humidity	$[kPakPa^{-1}]$	RDRS_v2.1_P_HR_1.5m	rh		
Vapour pressure	[kPa]	e	e		
Vapour pressure	[Pa]				vp
Wind speed (U direction)	$[m s^{-1}]$	RDRS_v2.1_P_UUC_10m	u		
Wind speed (V direction)	$[m s^{-1}]$	RDRS_v2.1_P_VVC_10m	V		
Wind speed (mean)	$[m s^{-1}]$	RDRS_v2.1_P_UVC_10m	W		
Wind direction	[degrees]	phi ^f	phi ^f		

^a ECCC, personal communication, 2024. ^b See https://confluence.ecmwf.int/pages/viewpage.action?pageId=82870405#ERA5:datadocumentation-Table4 (last access: 3 January 2024), https://confluence.ecmwf.int/pages/viewpage.action?pageId=82870405#ERA5:datadocumentation-Table9 (last access: 3 January 2024), https://confluence.ecmwf.int/pages/viewpage.action?pageId=82870405#ERA5:datadocumentation-Table2 (last access: 3 January 2024), communication, 2024. dassumptions underlying this variable are described here: https://codes.ecmwf.int/grib/param-db/?id=228251 (last access: 1 January 2024). Note that we provide the equivalent variable as a mean rate as part of the CAMELS-SPAT data, but the URL for that variable lacks a clear description: https://codes.ecmwf.int/grib/param-db/?id=235070 (last access: 1 January 2024). Note that these net radiation terms are based on interactions between the atmospheric and land surface components of the ERA5 modelling chain and should thus only be used carefully as a model input to prevent cases where the user's model duplicates processes already accounted for by the ERA5 models. ^f We derived most additional variables before averaging the gridded data onto (sub-)basins, but this is not easily possible for wind direction. Instead, we calculate wind direction separately for the gridded, semi-distributed and lumped cases from U and V components after (sub-)basin averages of these variables were created. We use the meteorological wind direction as defined by ECMWF (European Centre for Medium-range Weather Forecasting, 2023a): wind direction in this case indicates the direction that the wind comes from, not where it goes. n/a: not applicable.

maps will allow users to derive model parameters and further catchment delineations (such as elevation zones or land cover polygons) and to derive additional catchment attributes if our existing selection of attributes does not cover a particular study's needs (see Sect. 3). Figure 4 shows an overview of the 11 different datasets we selected for use in CAMELS-SPAT.

2.5.2 Methods and outcomes

For internal consistency of the CAMELS-SPAT data, we selected various geospatial datasets that cover at least the US

and Canada. The specific processing steps vary, but in general processing for each dataset involved downloading the data at continental or larger scales and clipping the data to the basin polygons (see Fig. 1). We also ensured that all geospatial maps are provided in a regular latitude/longitude coordinate system (EPSG:4326). Figure 4 provides an overview of the geospatial data layers, using a single basin as an example.

Climate. Long-term monthly means of several climate variables can be obtained from the WorldClim dataset (Fick and Hijmans, 2017). The advantage over calculating these means from gridded forcing data is WorldClim's much

higher spatial resolution. Available variables are the long-term means computed from 30 years each, showing minimum, mean and maximum monthly temperature, as well as the monthly precipitation, solar radiation, wind speed and water vapour pressure. WorldClim's data licence does not allow the redistribution of their raw data but does allow the data to be used to calculate derived statistics and to redistribute those. We primarily use the WorldClim data to calculate various attributes that quantify the spatial heterogeneity in climatic conditions and include various maps of derived variables as part of CAMELS-SPAT.

Vegetation. Process-based hydrological models typically include explicit representations of vegetation cover in a catchment. CAMELS-SPAT includes two datasets from which vegetation parameters may be derived. First, we included the time series of leaf area index (LAI) observations, derived from MODIS satellite observations (Myneni et al., 2021, MCD15A2H.061). These observations are available at an 8 d temporal resolution and cover the period 4 July 2002 to 8 October 2023. Certain models may be able to ingest these maps directly or typical seasonal LAI patterns may be derived from them. In addition, we included estimates of forest height in 2000 and 2020 (Potapov et al., 2021, part of the Global Land Cover and Land Use Change, 2000–2020 data).

Land cover and land use. To further assist parametrization and classification efforts, we included three different products related to land cover and land use. First, the Landsat-Derived Global Rainfed and Irrigated-Cropland Product (LGRIP30; Thenkabail et al., 2021; Teluguntla et al., 2023) can be used to estimate the magnitude and type of agriculture practised in each basin. Second, we include a map of International Geosphere-Biosphere Programme (IGBP) land classes in each basin, derived from MODIS satellite observations (Friedl and Sulla-Menashe, 2022). Third, we include high-resolution Global Land Cover and Land Use 2019 maps (Hansen et al., 2022). This is very high-resolution data derived from Landsat satellite observations, used to classify the landscape into several broad categories (inland water, permanent snow and ice, cropland, built-up, terra firma and wetlands), with several of these consisting of subclasses based on build-up area extent and vegetation extent and height.

Open water. We include cut-outs of the HydroLAKES data (Messager et al., 2016) to quantify the extent, type and volumes of open water bodies in each basin. These data can be used to estimate each catchment's open water area, retention volumes and parametrization of reservoir and lake modules in hydrologic and/or routing models.

Topography. The MERIT Hydro digital elevation model (DEM) used for basin delineation (Yamazaki et al., 2019) is also part of the maps provided for each catchment. We used the DEM to derive separate maps of slope and aspect because of their hydrologic relevance. For both, the DEM was first re-projected into ESRI:102009 (NAD 1983 Lambert North America) to ensure consistency between horizontal and vertical units. We then calculated slope maps expressed as angles

(i.e. degrees) and aspect maps in degrees indicating which direction a slope faces (with 0, 90, 180 and 270° being north, east-, south- and west-facing slopes, respectively). Additional variables such as elevation bands may be derived from the DEM map, but due to the subjectivity involved in deciding where the boundaries between the elevation bands are, we have not done so. The DEM data may also be useful in applying elevation-dependent lapse rates to meteorologic variables.

Soil and geology. We provide maps from three different datasets to characterize each catchment's subsurface. First, SoilGrids 2.0 (Poggio et al., 2021) provides estimates of various soil properties (bulk density; percentage coarse fragments; organic carbon content; and sand, silt and clay percentages) at six different depths (0-5, 5-15, 15-30, 30-60, 60-100 and 100-200 cm). These maps are given for mean values but also for 5th, 50th and 95th percentiles and an uncertainty estimate. To match the geological attributes described later in this paragraph, we also derive porosity and conductivity estimates from the mean sand and clay values for each layer using the regression equations described by Cosby et al. (1984). However, SoilGrids data are estimated for depths up to 2 m everywhere, without taking into account the actual depth to bedrock of any location. Thus, second, we included maps from the Pelletier soil database (Pelletier et al., 2016a, b). These distinguish between uplands, valley bottoms and lowlands and provide estimates of the depths of soil, intact regolith and sedimentary deposits above unweathered bedrock. These variables may be used to set more realistic soil depths in models compared to a spatially uniform depth. Third, we include cut-outs from the GLHYMPS data (Gleeson et al., 2014; Gleeson, 2018) as polygons. Contained as attributes are estimates of geologic permeability and porosity, which may be used to parametrize models.

3 Catchment attributes

Existing large-sample datasets do not provide the maps of geospatial data that we include as part of CAMELS-SPAT (see Sect. 2.5) and instead provide only statistical summaries of such maps, known as catchment attributes (for example, a dataset might include the mean catchment elevation but not the DEM from which this mean elevation is calculated). An informal analysis of some of the CAMELS datasets listed in Table 1 shows that these datasets together contain close to 300 different attributes, although any given individual dataset contains no more than 50 to slightly over 100 of those. Overlap between attributes provided by existing datasets is moderate at best, partly as a consequence of the differences in data products included in each individual dataset. This lack of uniformity is compounded by a lack of unified terminology, where different datasets may use the same terms to describe different calculations or different terms to describe the same attribute. This is in line with findings by Tarasova et al.

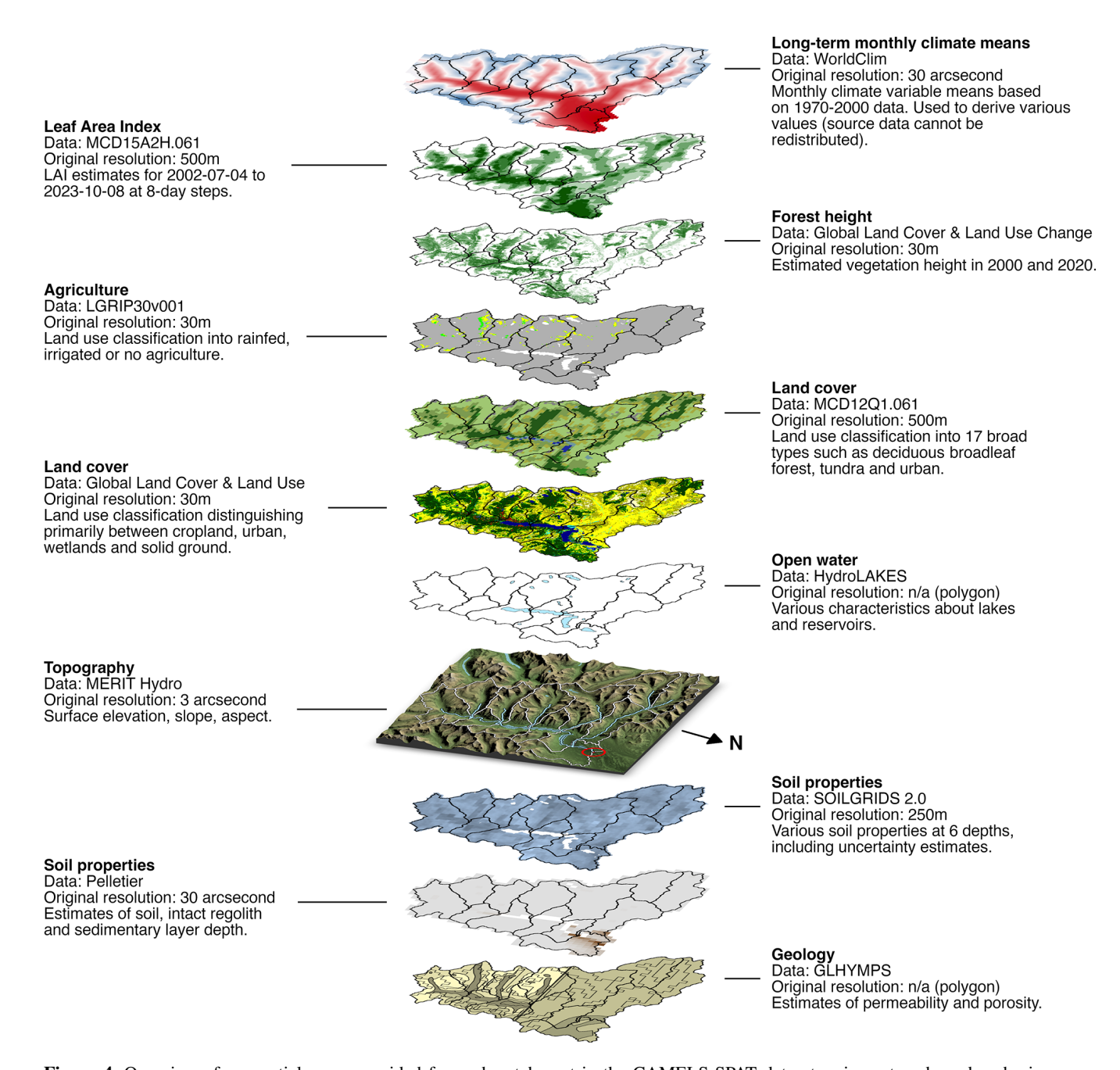


Figure 4. Overview of geospatial maps provided for each catchment in the CAMELS-SPAT dataset, using a transboundary basin as an example (Canadian gauge ID: 05AD003; sub-basin outlines given in black in all data layers apart from topography). The topography layer also shows the basin's gauge location as a red circle, the different sub-basins with white outlines and the river network and lakes in blue.

(2024), who analyse how 742 journal articles describe the hydroclimatic conditions of their study areas. They find that authors use a wide variety of attributes with only occasional verification of their attributes' usefulness. Relevant to our work, and in line with a cursory overview of attributes provided by the datasets listed in Table 1, they also find that the existing literature only rarely uses catchment descriptors that attempt to quantify the range a particular variable may cover

in a given catchment (the CAMELS-SE dataset, Teutschbein, 2024, is a notable exception).

We thus made a necessarily subjective choice of which attributes to calculate for the CAMELS-SPAT basins. We aimed for overlap with existing datasets when possible and to be mindful of the findings of Tarasova et al. (2024). In particular, in addition to the commonly provided mean attribute values, we also selected statistics that describe the range of an attribute's values. Examples include the minimum, maxi-

mum and standard deviation of vegetation height to give an impression of the spatial variability in the forest height data and the inclusion of monthly mean forcing variables to give an impression of the climatic seasonality that is only superficially captured by average seasonality attributes commonly found in other datasets. A list of all 1178 attributes can be found in Tables A1–A11, divided into five main categories: (1) climate, (2) topography and open water, (3) vegetation and land cover, (4) subsurface and (5) hydrology. We calculate the attribute values at both the basin and the sub-basin level (except for streamflow statistics, which are only available at the basin outlet). Further details are provided in the following subsections, although for obvious reasons we do not discuss every individual attribute. Instead, we focus in the following description of the CAMELS-SPAT attributes on providing various examples that highlight why the recommendations in Tarasova et al. (2024) are important.

3.1 Climate attributes

The climatic data used in the development of CAMELS-SPAT, i.e. the time series of meteorological forcing variables from RDRS and the monthly maps of mean climatic conditions from WorldClim, provide a unique opportunity to characterize each catchment's climatic conditions in time and space. From the RDRS data, we are able to determine seasonal variability and its variance over multiple years. From the WorldClim data, we are able to characterize the seasonal variability and its variance across space. This leads to a relatively large number of climatic attributes compared to other datasets and provides some insight into the variability in time and space of this driver of hydrologic behaviour.

Tables A1-A4 list the climatic attributes provided with CAMELS-SPAT. These cover annual mean values of variables of interest (such as precipitation, potential evapotranspiration and snow) commonly found in other datasets, as well as standard deviations for these values. We expand upon existing datasets by also providing monthly means and monthly standard deviations of all forcing variables, to allow more in-depth investigation of each catchment's seasonality. Figure 5 shows why going beyond annual mean values may be important. Figure 5a and b show long-term average aridity and the fraction of precipitation falling as snow (determined on a per-time-step basis using a 0 °C threshold; see also Sect. 4.2.8 for some further discussion about the PET estimates available in CAMELS-SPAT.). The broad geographical patterns seen here are not particularly surprising but are, importantly, not necessarily representative of climatic variability on a year-to-year basis (Fig. 5c, d) or of the range of conditions in each catchment (Fig. 5e, f). For example, across the Great Plains area and particularly in the southwestern US, the year-to-year variability in aridity (Fig. 5c) can be quite large, and certain catchments may fluctuate between arid and humid states on annual timescales. The fraction of precipitation falling as snow equally shows large inter-annual variability (Fig. 5d), with standard deviations close to 10% across a large part of the domain. Within-catchment variability of aridity (Fig. 5e) seems modest in most cases but is rather large for snowfall (Fig. 5f), highlighting why treating these catchments in a more spatially distributed fashion may be helpful.

3.2 Topography and open water attributes

Topography is a critical control on hydrologic behaviour at both the large and the small scale. For example, mountains influence precipitation patterns at the large scale, while at the small scale, slope angles affect lateral drainage and topographic features can lead to the formation of lakes. Tables A5 and A6 provide an overview of topographic and open water attributes, respectively. These cover various basic catchment descriptors, such as location and area, and various statistics about the topography and resulting drainage network. Figure 6a and b show the catchment elevation mean and standard deviation, respectively. As expected, elevation varies strongly throughout the domain, ranging from sea level to well over 3000 m above sea level (ma.s.l.). Elevation differences in catchments can be very high in mountainous regions, with prime examples being the northwestern US and southwestern Canada: the within-catchment standard deviations in elevation are close to 500 m here. Statistics that quantify basin slope (not shown for brevity) show similar patterns, showing that the topographic drivers of hydrologic behaviour can be highly variable in catchments. Topographic conditions lead to a certain amount of open water in the CAMELS-SPAT catchments, with lakes larger than 0.1 km² being more prevalent in the Canadian basins (Fig. 6c) than in basins in the US. Water storage in these can be considerable (Fig. 6d). Stream lengths (Fig. 6e and f) vary considerably based on the drainage area upstream of each gauge, emphasizing a need for within-catchment routing approaches. The examples in Fig. 6 are intended to highlight the variability of conditions in catchments and thus emphasize the need to go beyond treating basins as lumped entities. These examples (particularly Fig. 6a, b, e and f) also illustrate that attributes can show high correlations, suggesting that adding more attributes to an analysis will not necessarily increase the useful information by the same amount. Selecting which attribute to incorporate in any analysis must thus be done somewhat carefully (see also Sect. 4.2.7).

3.3 Land cover attributes

Table A7 provides an overview of vegetation and land cover attributes. Briefly, these cover various statistics on vegetation height during specific years, monthly leaf area index (LAI) catchment mean and standard deviation, as well as percatchment counts of three different land class products. We refer the reader to the original publications that describe each dataset for further information about the classes included.

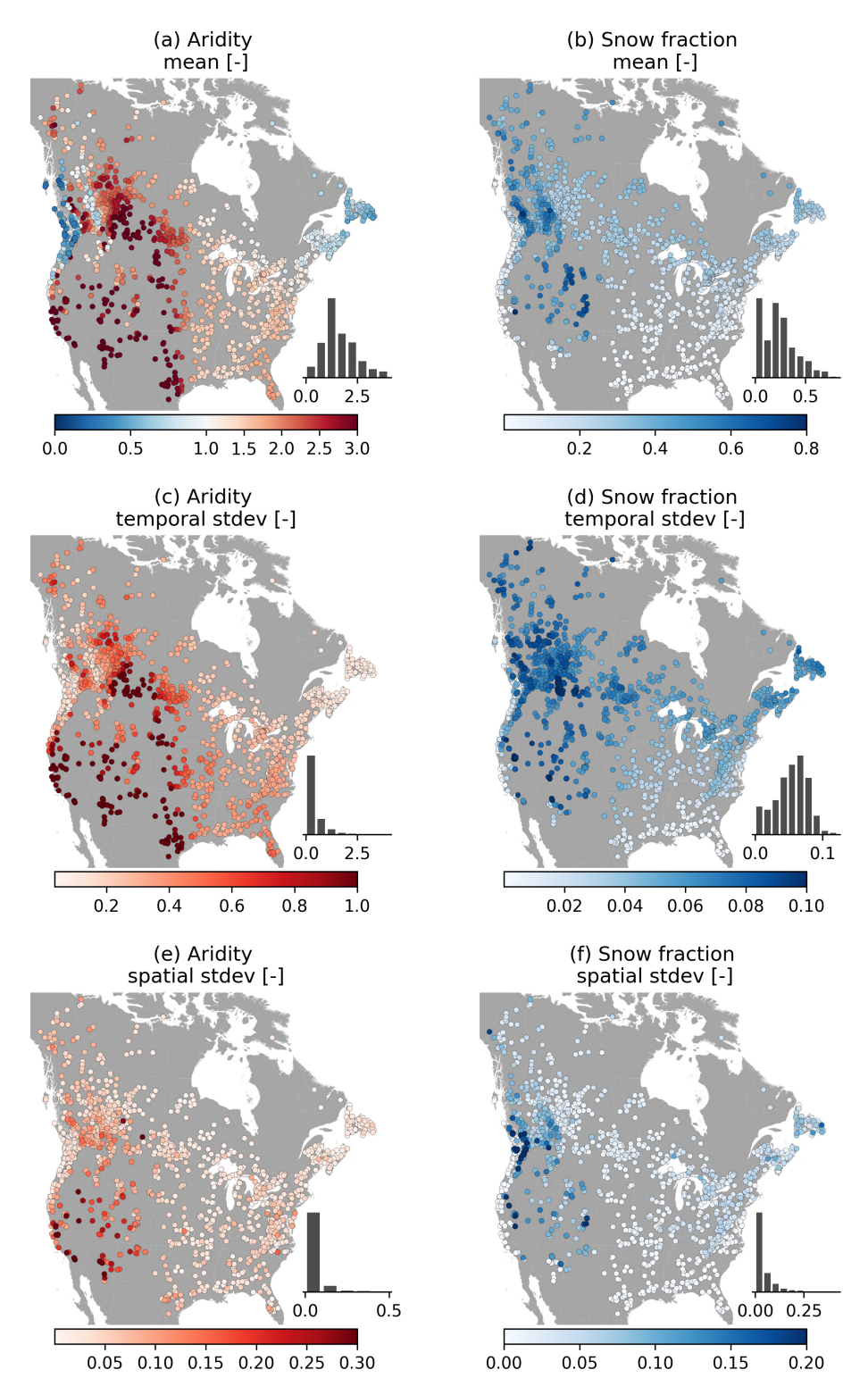


Figure 5. Selection of climate attributes. (a-d) Statistics derived from RDRS data, showing mean and variability in time. (e-f) Statistics derived from WorldClim data, showing variability in each catchment.

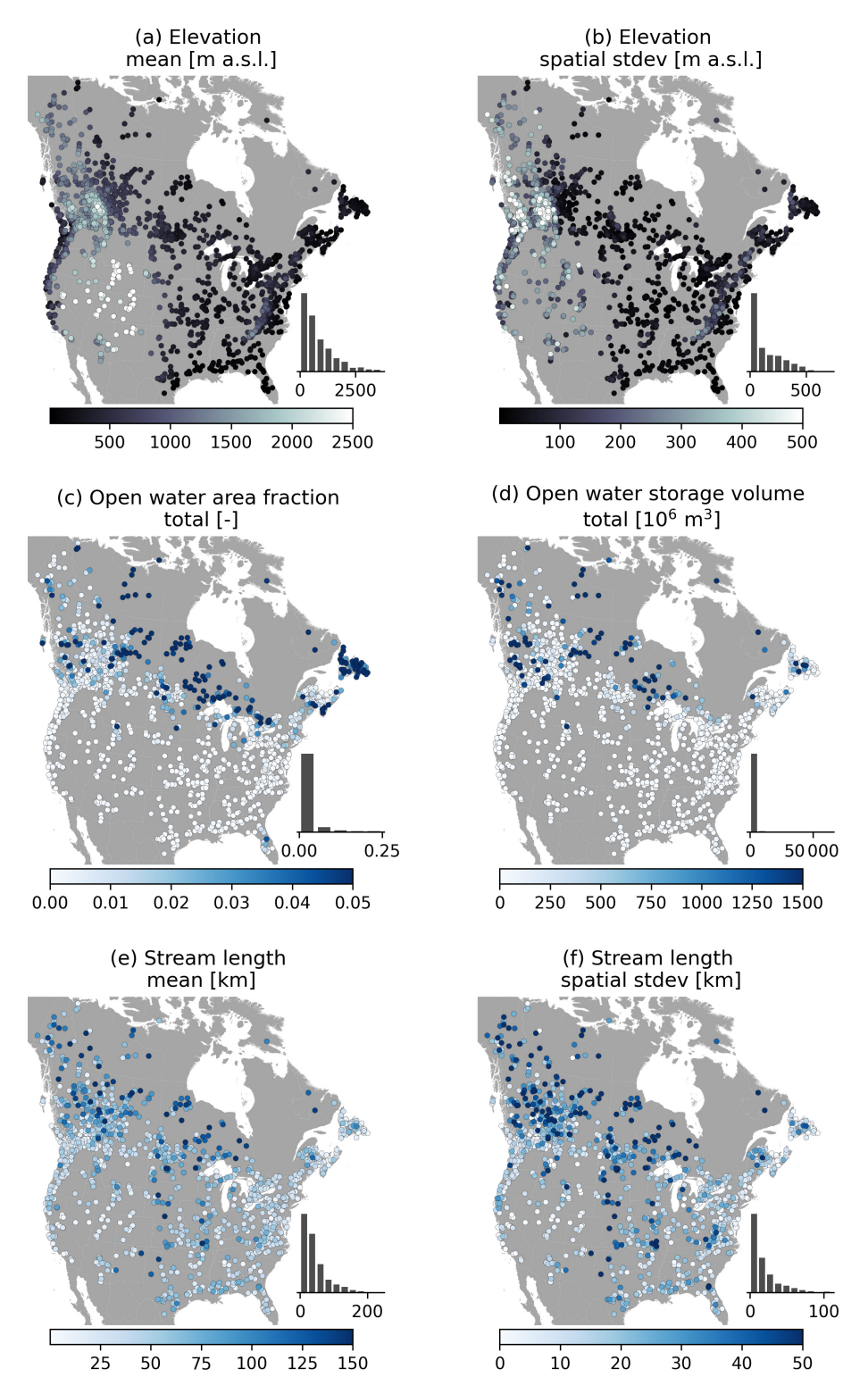


Figure 6. Selection of topographic attributes. Open water (**c**, **d**) estimates are obtained from the HydroLAKES database, which uses a threshold of 10 ha (0.1 km²) for lake and reservoir identification. (**e**, **f**) Stream length statistics are derived by starting at each headwater sub-basin upstream of a given gauge and tracing the flow path down until the gauge location is reached. From this ensemble of flow path lengths upstream of a given gauge, the mean and standard deviation of stream lengths are calculated.

Figure 7 provides an example of the spatial (Fig. 7a, b) and temporal (Fig. 7c, d) variability in vegetation characteristics. As may be expected, there is considerable variation in vegetation height in space, on both the continental and within-catchment scale. Forested areas in particular exhibit large standard deviations in vegetation height (see for example the Pacific Northwest and western Canada). On a seasonal scale, LAI exhibits large variability throughout the domain as a consequence of summer and winter patterns. Vegetation is a key control on hydrologic processes like interception and transpiration, and these images show that mean attribute values alone do not necessarily capture the complex vegetation patterns that may explain spatial and temporal variability in these processes.

3.4 Subsurface attributes

Attributes describing each catchment's subsurface characteristics are listed in Tables A8 and A9. Figure 8a and b show SoilGrids estimated sand content in the top layer of each catchment and the within-catchment standard deviation of this estimate, respectively. Sand content is often combined with clay and silt content estimates to derive soil parameters used in models, such as porosity and drainage rates. Withincatchment standard deviations tend to be around 20% of the estimated sand content, suggesting that within-catchment drainage properties can vary considerably. For a given depth, the SoilGrids property of interest (here, sand content) is estimated with a lower bound (Q0.05), median (Q0.50) and mean value, and upper bound (Q0.95). The prediction uncertainty is then calculated as the ratio of the 90 % prediction interval (Q0.95-Q0.05) and the median (Q0.50). Prediction uncertainty (Fig. 8c) adds more variability to the sand content estimates, although this is somewhat modest compared to the within-basin variability of sand content estimates (Fig. 8b). The spatial standard deviation of the uncertainty estimates is even smaller: a couple of percentage point difference at most (Fig. 8d). This suggests that the prediction intervals for sand content, in this layer at least, are relatively narrow. The main variability occurs in each catchment, further emphasizing that going beyond lumped representations of hydrologic behaviour may be useful. This is further supported by Fig. 8e and f, showing the estimated thickness of sedimentary deposits and their spatial standard deviation, respectively. There are clear large-scale patterns of the catchment mean values, where plains and flat areas show the thickest layers. Within-catchment variability is particularly large in catchments with sharp topographic relief (compare Fig. 6b), showing the difference in soil structure between high steep mountains and valley bottoms. However, soil properties are difficult to measure and as a result can be highly uncertain. We urge readers to consult the publications describing these datasets to understand how these values were derived and how they may feed into new work.

3.5 Hydrologic signatures

Statistics that describe flow regimes, commonly called signatures, are an active area of research (e.g. McMillan, 2021). As an initial start, we provide the same signatures as provided in the original CAMELS dataset and expand upon these in a number of ways: (1) in addition to mean values, we provide standard deviations when applicable; (2) we provide monthly runoff signatures to complement the monthly climate attributes; and (3) we expand the no-, low- and highflow duration signatures to include median, skewness and kurtosis values. For the signatures in Table A10, we calculate the signature per year of data first and then find the mean and standard deviation (if applicable) across years. For the statistics for the no-, low- and high-flow periods (Table A11), we instead use all years together and calculate the statistics from this single longer time series.

A subset of these hydrologic signatures is shown in Fig. 9. As expected, the signatures show strong relations to the climate attributes in Fig. 5a and b. Mean discharge (Fig. 9a) is particularly high in non-arid areas, and the standard deviation of annual mean discharge (Fig. 9b) suggests strong intraannual variability in the observed runoff at most gauges. The influence of snow processes can clearly be seen in the differences between the May and December mean runoff values (Fig. 9c, d). Low-flow duration (Fig. 9e; defined as days where discharge is below 20 % of the mean discharge for the basin) emphasizes the seasonality in runoff patterns in most of these basins. However, these mean values are likely not particularly representative of the duration of lowrunoff events. In the majority of basins, the distributions of low-flow durations (as well as no-flow and high-flow durations; not shown for brevity) are positively skewed (Fig. 9f). This indicates that these distributions have heavy tails and that the mean values may be heavily biased by a relatively small number of events. In many basins, the median duration may provide a more representative value of the typical no-, low- and high-flow durations. Almost all recent largesample datasets provide a mean duration of no-, low- and high-flow events, but the skewness and kurtosis of the underlying distributions are typically not accounted for. This leads to an overestimation of the typical duration of these events and may hinder classification efforts. We strongly suggest that the shape of the duration distributions is accounted for in future work.

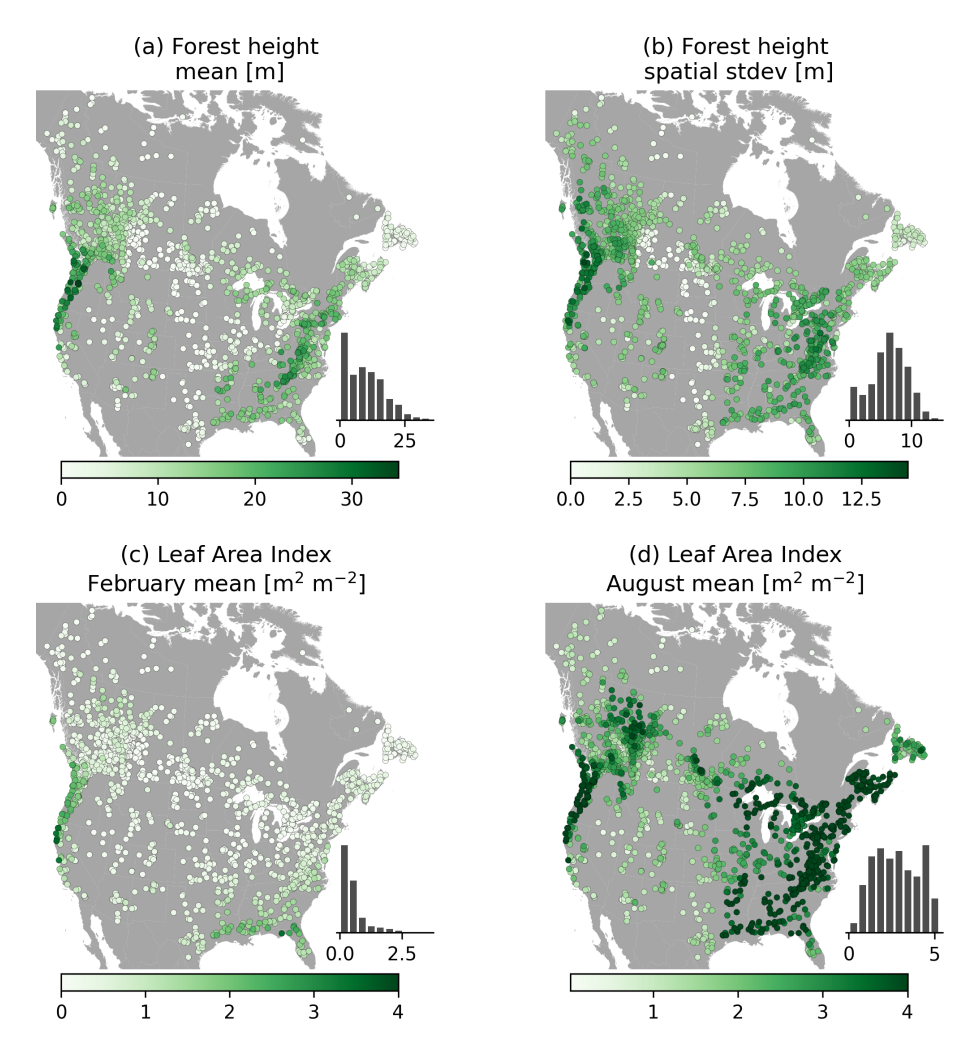


Figure 7. Selection of vegetation attributes. (**a, b**) The mean and standard deviation of forest height in each basin are derived from the Global Land Cover and Land Use Change dataset and are shown here for the year 2020. (**c, d**) Leaf area index values are derived from the MODIS MCD15A2H.061 dataset and are shown here as long-term averages values for February and August.

4 Discussion

4.1 Recommendations for data providers

4.1.1 Dimension boundary information in publicly available data

In Sect. 2.3 and 2.4, we describe the processing of stream-flow observations and meteorological data, respectively. One challenge here is determining the representativeness (or validity) of data values in time and space. Data can be instantaneous (i.e. valid at a specific point in time) or time averaged (i.e. valid over a specific time window), and treating one as the other leads to incorrect estimates of fluxes and thus state changes in the system (see also the derivation of hourly flow values in Sect. S1 in the Supplement). The same concern applies to space: values may be representative for a specific point or averaged over a given region. Accounting for these differences is not always straightforward, in particular be-

cause information about the spatial and temporal validity of publicly available data is not always easily available and may require informal inquiries to obtain. This hampers the correct application and interpretation of data and can lead to easily preventable biases in analyses and modelling efforts.

A simple solution is provided by the NetCDF Climate and Forecast (CF) metadata conventions (see Sect. 7 in Eaton et al., 2023). These conventions describe the specification of bounds for coordinate variables (i.e. dimensions such as latitude, longitude and time) that indicate between which coordinate values a given data value is considered valid. Specific examples for spatial gridded data can be found in Sect. 7.1 in Eaton et al. (2023), and time bounds are discussed in Example 7.5 and 7.6. The CF conventions are designed for NetCDF files, but the principle of specifying dimension bounds in time and space between which data values are valid is widely applicable. We strongly recommend

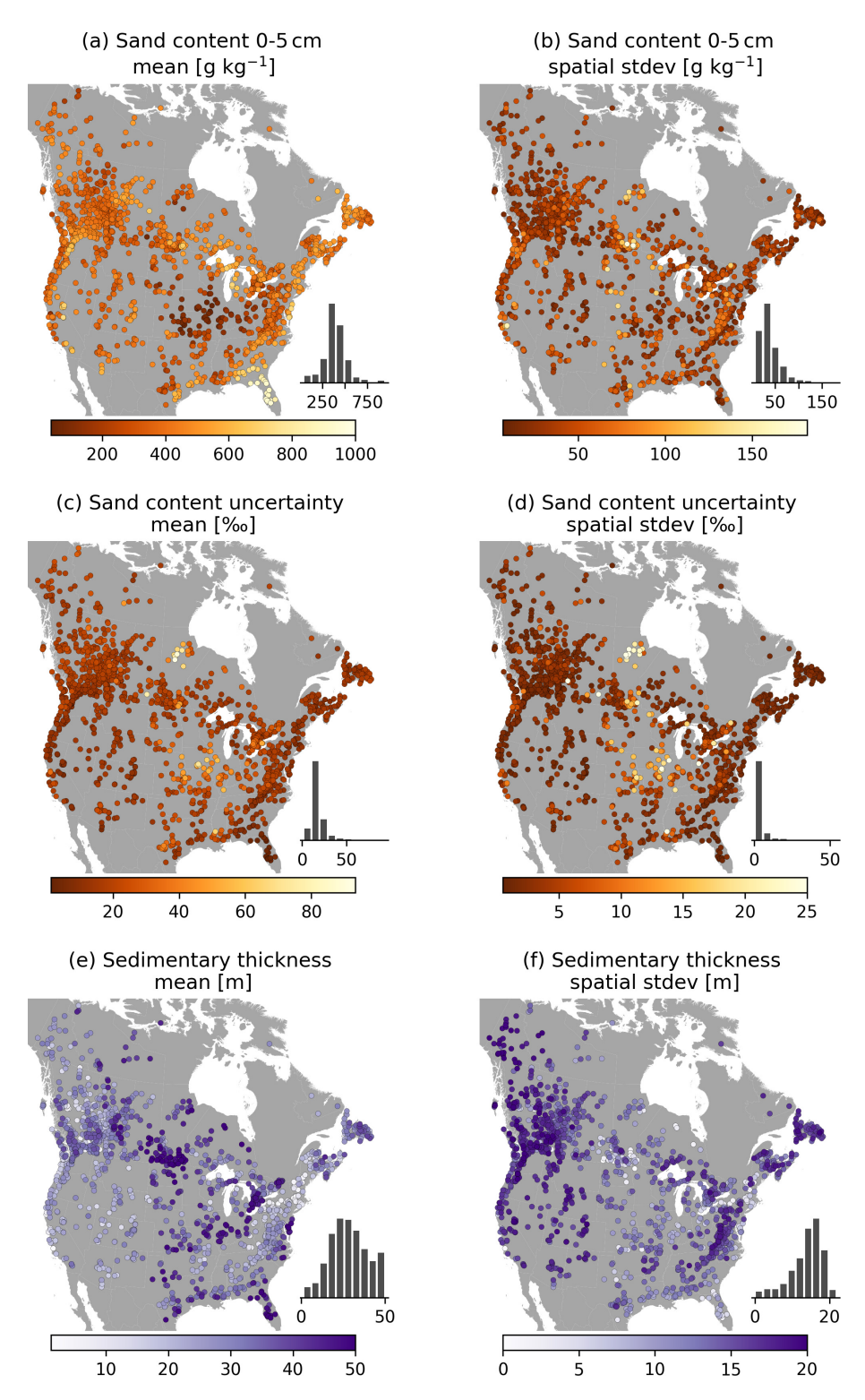


Figure 8. Selection of subsurface attributes. (**a-d**) Properties derived from the SoilGrids 2.0 dataset through spatial averaging for each catchment. (**a, b**) Mean and spatial standard deviation of sand content in the top SoilGrids layer. (**c, d**) Mean and spatial standard deviation of sand content uncertainty, defined as the ratio between the 90th-percentile prediction interval and the median prediction $\left(\frac{Q95-Q05}{Q50}\right)$. (**e, f**) Mean and spatial standard deviation of sedimentary deposit thickness estimates in the Pelletier dataset.

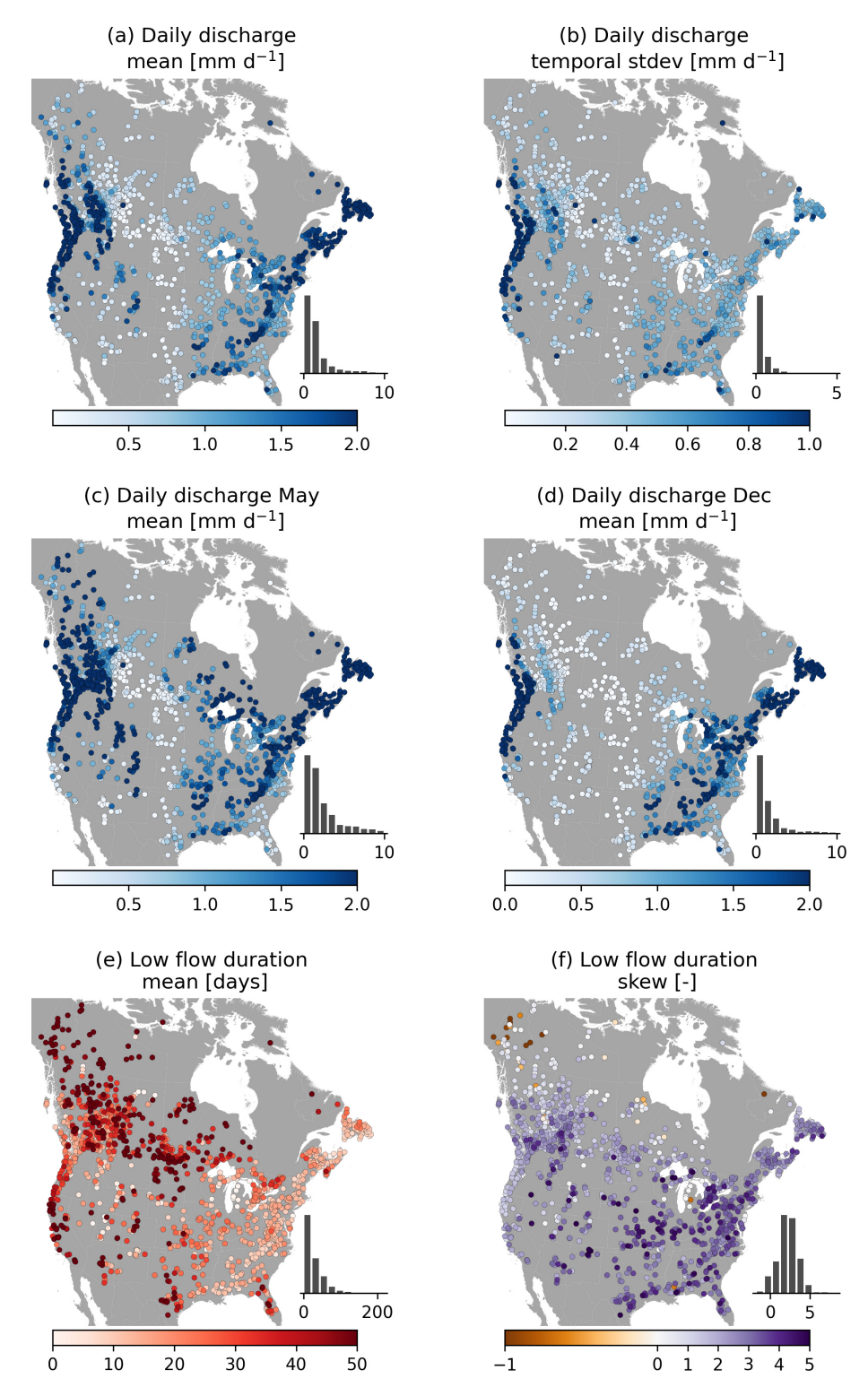


Figure 9. Selection of hydrologic signatures, derived from time series of daily data provided by USGS and WSC.

that including these bounds as part of data distributions becomes standard practice.

4.1.2 Sub-daily flow data derivations

Process-based models can be useful for long-term water assessments, provided that they are parameterized well and that the theoretical underpinnings of the model are valid (e.g. Kirchner, 2006; Clark et al., 2016). In the case of processbased models, assessing a model's physical realism requires observations at a sub-daily resolution. In CAMELS-SPAT, we therefore construct hourly streamflow series from time series of instantaneous streamflow observations that are publicly available. However, the phrase "streamflow observations" (although common) is somewhat misleading: in almost all cases, the observations are of water levels, and streamflow values are estimated for a given water level with rating curves. Especially at high observation frequencies, these water levels may be subject to random fluctuations unrelated to streamflow magnitude (e.g. due to wind or small eddies), which will translate into streamflow estimates affected by this noise. A cleaner approach would be to find the average hourly water level and estimate the average hourly flow from this through the station's rating curve. Development and maintenance of rating curves is complex, however, and rating curves tend to change through time (see for example the description of WSC's procedures in Gharari et al., 2024). Computing robust sub-daily streamflow estimates will be easier at the institutional level (not least because it requires access to the rating curves), and we express the hope that this may become standard practice.

4.2 Guidelines for practical use

Here, we outline various considerations that may be useful to readers. Our goal with these is to set expectations for dataset use and to highlight potential pitfalls that may not be immediately obvious.

4.2.1 Summary sheets of basin conditions

Following Delaigue et al. (2024), we created summary sheets of the conditions in each basin. These summaries are intended to aid quick assessments of each basin and cover the following elements: (1) identifier, location and long-term statistics (i.e. mean precipitation, streamflow, temperature, potential evapotranspiration, aridity and runoff ratio); (2) various graphics showing more detailed statistics (e.g. year-to-year variability in streamflow, mean monthly temperature ranges and elevation distribution); and (3) various maps showing the spatial variability of various key attributes (i.e. elevation, land cover, agriculture presence, forest height, soil class and soil depth). An example can be found in the Supplement, Sect. S5. The full collection of summary sheets is available on the data repository. Section S5 also contains an example that highlights the need to apply a basin mask

when working with the GeoTIFF maps provided as part of the CAMELS-SPAT data: in certain cases, pixel values outside the basin boundaries will contain values that are within the valid data range (for example, forest height values outside the basin are set to 0 m). Applying a basin mask ensures that only values within the basin boundaries are used in any analysis that relies on the GeoTIFF files.

4.2.2 Selection of time periods

Our aim with CAMELS-SPAT is to facilitate a wide range of studies, and we have therefore provided as much data for each gauge as seemed feasible. In particular, this meant that we only excluded station observations before 1950, because none of the forcing datasets covers this period, and we also accepted the fact that not all forcing products are available for the full period for a given gauge. For different purposes, it will thus be necessary to subset the data we provide to shorter time periods. Table 4 provides an overview of the time periods covered by the various data products that may assist in selecting appropriate periods for specific studies.

4.2.3 Utilization of streamflow data quality flags

We retained streamflow observation quality flags provided by the USGS and WSC during processing and stored these in the same NetCDF files as the streamflow observations themselves. These flags indicate conditions affecting the streamflow measurement, such as the presence of river ice, backwater effects, water levels below sensor level or equipment malfunction. These conditions suggest that streamflow data at these time steps may be inaccurate (even if the discharge data at such time steps are corrected by the data provider, large uncertainties may remain; see Gharari et al., 2024), and this may affect analyses that use these data. For example, it is known that differences between observed and simulated streamflow at individual time steps may have disproportionate effects on aggregated efficiency scores that are used in modelling (e.g. Newman et al., 2015; Clark et al., 2021), and, if one tries to match incorrect "observations", this may negatively impact the quality of the resulting model configuration. Excluding streamflow observations from efficiency score calculations based on data quality flags is a possible way to limit the impacts of potentially erroneous streamflow values.

4.2.4 Spatial validity of meteorological forcing data

CAMELS-SPAT contains meteorological data from four different datasets at their original gridded resolution, as well as averaged at the basin and sub-basin level. During this averaging process, we assumed that values provided at specific coordinates are valid for a grid cell around this point. This is a simplistic approach, but it is somewhat difficult to justify more elaborate assumptions (such as some form of interpolation), because in reality the change of meteorological variables in space would be dependent on local topography

Streamflow data Resolution Start (min) End (max) Notes **USGS** 7 Dec 1956 Hourly 3 Jan 2023 Varies per gauge, see Figs. 3 and A1 USGS Daily 1 Jan 1950 2 Jan 2023 Varies per gauge, see Figs. 3 and A1 WSC Hourly 1 Jun 2021 2 Jan 2023 Varies per gauge, see Figs. 3 and A1 Varies per gauge, see Figs. 3 and A1 WSC Daily 1 Jan 1950 31 Dec 2022 Forcing data Resolution Start End **RDRS** Hourly 1 Jan 1980 31 Dec 2018 1 Jan 1980 31 Dec 2023 Daymet Daily ERA5 Hourly 1 Jan 1950 3 Jan 2023 EM-Earth Hourly 1 Jan 1950 31 Dec 2019 Resolution Start End Geospatial data MODIS LAI 8-daily 4 Jul 2002 8 Oct 2023 1 Jan 2000 1 Jan 2020 Forest height 20-yearly

Table 4. Time periods covered by the different datasets included in CAMELS-SPAT. Geospatial data not listed are static products that have no time dimension.

at scales smaller than the typical forcing data grid cell. Interpolation methods may yield more realistic sub-basin and basin-averaged values, but it is beyond the scope of this paper to investigate these.

4.2.5 Combing soil depth and soil property estimates

CAMELS-SPAT contains both estimates of soil depth (derived from the Pelletier dataset; Pelletier et al., 2016a, b) and soil properties (derived from the SoilGrids 2.0 dataset; Poggio et al., 2021). Because the SoilGrids data assume a uniform depth of 2.0 m everywhere, soil properties will thus be unknown for actual soil depths greater than 2 m or incorrectly provided for actual soil depths less than 2 m. For estimated depths below 2 m, an appropriate approach may be to only use the SoilGrids layers that correspond to the estimated soil depth. For estimated soil depths greater than 2 m, recommendations are more difficult to provide. Appropriate approaches may be the derivation of pedotransfer functions or reliance on simple assumptions that extend the available layer information to deeper depths.

4.2.6 Modelling the Prairie Pothole Region

Model performance across the US is known to change regionally, where model performance is at its worst in the drier central regions (e.g. Newman et al., 2015; Towler et al., 2023). In CAMELS-SPAT, we compound this problem by including basins from the so-called Prairie Pothole Region. This area covers parts of southern Alberta, Saskatchewan, Manitoba, North Dakota, South Dakota, Minnesota and Iowa and is colloquially known as the "graveyard of hydrological models" (e.g. Muhammad et al., 2019; Budhathoki et al., 2020; Ahmed et al., 2023). The landscape in the Prairie Pothole Region is relatively young on a geological time scale, and large parts of it have not yet eroded into traditional

river networks. Surface depressions are common and typically not connected to the stream network, except through very slow groundwater drainage and the occasional fill-and-spill event (Hayashi et al., 2016; Clark and Shook, 2022). In the basins we provide as part of the CAMELS-SPAT data, all sub-basins are connected to the stream network. However, surface depressions below the resolution of the MERIT DEM are common and will affect hydrologic behaviour in these (sub-)basins. We recommend that users account for these potholes in their analyses and modelling efforts, possibly through the use of stand-alone models or post-processing tools (e.g. Clark and Shook, 2022), by adapting existing models with an appropriate landscape module (e.g. Ahmed et al., 2023), or by adjusting their expectations of model performance accordingly.

4.2.7 Selection and extension of catchment attributes

We derived various catchment attributes for the basins in CAMELS-SPAT for ease of use and comparison with existing datasets. However, the number of attributes included in CAMELS-SPAT is rather high, and we encourage others to make a careful selection of which attributes to use in their own work. Attribute values can show considerable correlations, and using a greater number of attributes will not necessarily add an equal amount of new information. Higher numbers of attributes will, however, increase computation and analysis times for applications such as regionalization, clustering and data-driven modelling. A more fruitful approach likely relies on defining hypotheses that can be tested with catchment attributes and deliberately selecting the right attributes for these tests. If our initial attribute calculations do not offer the right choices, new attributes can easily be derived from the data products included in CAMELS-SPAT. We refer the reader to Tarasova et al. (2024) for a deeper discussion and recommendations on the use of catchment descriptors. We particularly encourage investigations that evaluate the usefulness of our provided attributes for catchment characterization purposes, in line with those recommendations.

4.2.8 Potential evapotranspiration estimates

In order to facilitate a wide range of modelling studies, CAMELS-SPAT contains a variety of estimates of potential evapotranspiration (PET). These can be used as inputs to certain types of models and to calculate certain climatic attributes such as a basin's aridity. However, there are multiple ways to estimate PET depending on data availability and purpose (McMahon et al., 2013), and this results in a certain amount of uncertainty in these PET estimates and any values derived from them. Here we provide a brief overview of the various PET estimates available in CAMELS-SPAT, along with a brief assessment that may help users to decide which data to use. Table 5 summarizes this overview.

CAMELS-SPAT contains time series of PET (variable name mper) that are provided as an extra output of the ERA5 modelling chain (although note that this variable is not used directly in the production of ERA5 or the generation of forecasts). However, these values are known to be locally deficient in regions without low vegetation (see https: //confluence.ecmwf.int/display/CKB/ERA5%3A+data+ documentation#ERA5:datadocumentation-Knownissues, last access: 9 May 2025, Sect. "Known Issues", bullet point 15). This is also reported by Clerc-Schwarzenbach et al. (2024), who point out that PET data obtained from ERA5-Land must be treated carefully and may include unrealistic values. Section S4 in the Supplement contains a preliminary analysis that identifies where these issues are present in the mper data included in CAMELS-SPAT. We have kept the ERA5 PET estimates as a reference for users who wish to investigate this further but urge caution about

CAMELS-SPAT also contains time series of PET estimates obtained with the Penman-Monteith method and hourly RDRS data, as well as time series of PET estimates obtained with the Priestley-Taylor method and daily Daymet data. Finally, we included spatial PET estimates using the temperature-based method in Oudin et al. (2005), applied to monthly averaged WorldClim data. Equations for all three approaches can be found in Sect. S2.5 in the Supplement. We compared these to the PET estimates from Singer et al. (2021) and their overview of mean annual PET estimates from various products in their Fig. 1 and Table 2. Preliminary analysis (see Sect. S4 in the Supplement) suggests that our PET estimates from RDRS, Daymet and World-Clim all exhibit similar spatial patterns to the five datasets shown in Singer et al. (2021). Visual comparison also suggests that there is some spread in the magnitude of our estimates. Monthly estimates based on WorldClim data are low compared to the other methods and data sources and comparable to those in GLEAM. Daily estimates based on Daymet data are close to the middle of the range of estimates. Hourly estimates based RDRS data are within the ranges of estimates provided by the other methods and datasets, although somewhat high compared to most other products.

Due to the lack of uniformity in PET definitions and calculation methods (e.g. McMahon et al., 2013), it is difficult to say which estimates are the most accurate. For time series, any expected systematic biases could be corrected before using the time series as a model input. Derived statistics with clear physical interpretations, such as aridity, are more difficult. A basin may be classified as either water limited or energy limited solely as a consequence of the data and PET estimation method used, and this may hinder classification and interpretation efforts. Possible ways around this may involve the use of multiple estimates of PET-related attributes. We thus recommend caution when selecting and interpreting any PET estimates for further use.

4.3 Potential improvements

CAMELS-SPAT represents a substantial data-processing effort, but further enhancements are possible. We briefly list these here. First, approximately 15 % of our basin outlines have been assigned confidence ratings of medium or low. Future efforts can focus on refining these outlines through further manual intervention, higher resolution DEMs or both. Second, we necessarily needed to limit the extent of our geographical domain, and this means that there is a limit to the different types of landscapes our dataset covers. However, apart from Daymet and RDRS, all datasets used here have global coverage. Combination with local streamflow observations, and possibly high-quality local datasets, should allow for an extension of the dataset to other regions. The code available on our GitHub repository could provide a starting point for such efforts. Third, extending the dataset to include observations or estimates of variables of interest other than streamflow would help with multi-variate analysis and model evaluation. Examples include satellite observations of snow cover or estimates of evaporation fluxes or water storage in the soil.

4.4 Dataset structure and size

For convenience, we divided the collection of 1426 CAMELS-SPAT gauges into various subsets. At the highest level, we structured the dataset with different folders for attributes, forcing data, geospatial data, observations and shapefiles. At the next level, we divided the dataset into three categories of headwater and meso-scale and macroscale basins. Headwater basins are defined as catchments with only a single sub-basin in our delineation (note that for these basins, the lumped and distributed cases are identical). Meso-scale basins are basins that are not headwaters and below a total area of $10^3 \, \mathrm{km}^2$, and macro-scale basins are

Table 5. Overview of PET estimates in CAMELS-SPAT, how they are used in CAMELS-SPAT and a summary of how these values compare to each other as well as the estimates from five other PET estimates listed in Singer et al. (2021).

Source data	Temporal resolution	PET estimation method	Used for	Assessment
ERA5	Hourly	Energy balance assuming well-watered mixed crops*	_	Likely incorrect in locations with no or high vegetation
RDRS	Hourly	Penman-Monteith	Climate attributes	Plausible patterns; values somewhat high compared to most estimates
Daymet	Daily	Priestley-Taylor	-	Plausible patterns; values close to the middle of all estimates
WorldClim	Monthly	Eq. (3) in Oudin et al. (2005)	Climate attributes	Plausible patterns; values on the lower end of all estimates

^{*} PET variable mper is derived from variable pev. For more details about the calculation of pev, see https://codes.ecmwf.int/grib/param-db/228251 (last access: 9 May 2025).

those with areas between 10^3 and 10^4 km². Headwater basins account for 304 out of 1426 total (mean area of approximately $60 \, \mathrm{km}^2$), 727 basins fall into our meso-scale category (mean area $\approx 400 \, \mathrm{km}^2$, with on average nine sub-basins) and the remaining 446 basins are macro-scale basins (mean area $\approx 3000 \, \mathrm{km}^2$, on average 66 sub-basins). From here we divided the dataset into further subfolders when convenient.

The total size of the CAMELS-SPAT data is approximately 5.5 TB. Almost all of this is forcing data (5.4 TB) and specifically the gridded variants of the forcing data (4.3 TB). Basin-averaged data (summed for all four forcing datasets) sum up to 85 GB, while distributed forcing data (i.e. averaged at the sub-basin level) sum up to not quite 1.2 TB. A full overview of the size of various components of the dataset can be found on the data repository. This overview, combined with the overall folder structure, should allow users to finetune their downloads easily. Further instructions to include or exclude components from the download can be found on the data repository.

5 Conclusions

This paper describes the development of the CAMELS-SPAT dataset. Our goal is to enable a wide range of hydrologic studies, with a particular focus on hydrologic modelling, by performing a wide range of data-processing steps and sharing both the code and outcomes of these. We extend the original CAMELS data (Newman et al., 2015; Addor et al., 2017a) in five ways to achieve this goal. First, we extend the geographical domain of the dataset beyond the contiguous US by including Canadian basins. Second, we provide meteorological data specifically aimed at spatially distributed physics-based hydrologic models, in addition to the inputs needed to run lumped conceptual models. Third, we provide streamflow data at both daily and hourly time steps for each basin. Fourth, we provide maps of multiple geospatial datasets for each basin, rather than only a selection of summary statistics

derived from these maps. Fifth, we provide a variety of catchment attributes intended to describe the spatial and temporal range of our attributes, in addition to the more commonly provided mean attribute values.

CAMELS-SPAT thus consists of meteorological data, streamflow observations and geospatial data for 1426 basins across the US and Canada. The meteorological data include a number of variables typically associated with process-based models, as well as potential evapotranspiration estimates that can be used with the more conceptual model types, at hourly time steps (daily for the Daymet data). These forcing data are provided in a gridded format at their original resolution, as well as spatially averaged at the sub-basin and basin level. Streamflow observations are provided at daily time steps and complemented with hourly observations when these are available. Geospatial data, covering vegetation, land use, topography, soil and geology, are provided as georeferenced maps for each basin from which model inputs or summary statistics that go beyond our provided attributes can easily be derived. Finally, the information for each gauge (streamflow, meteorological, geospatial data) is summarized in an extensive number of catchment attributes, at both the basin and sub-basin level.

In developing CAMELS-SPAT, we focused on providing the necessary data for a wide variety of studies. We envision the data being helpful for studies aimed at improving our understanding of hydrologic processes and our ability to model those processes. By removing the need for a considerable amount of cumbersome data processing, we hope CAMELS-SPAT can support a wide range of hydrologic investigations at a fraction of the effort otherwise needed.

The dataset can be accessed through the Federated Research Data Repository (FRDR) at https://doi.org/10.20383/103.01306 (Knoben et al., 2025). When using CAMELS-SPAT, please note the attribution and licence requirements for dataset components outlined in the "Code and data availability" section.

Appendix A: Streamflow data availability

Figure A1 shows streamflow data availability at a more granular level than the aggregated data in Fig. 3.

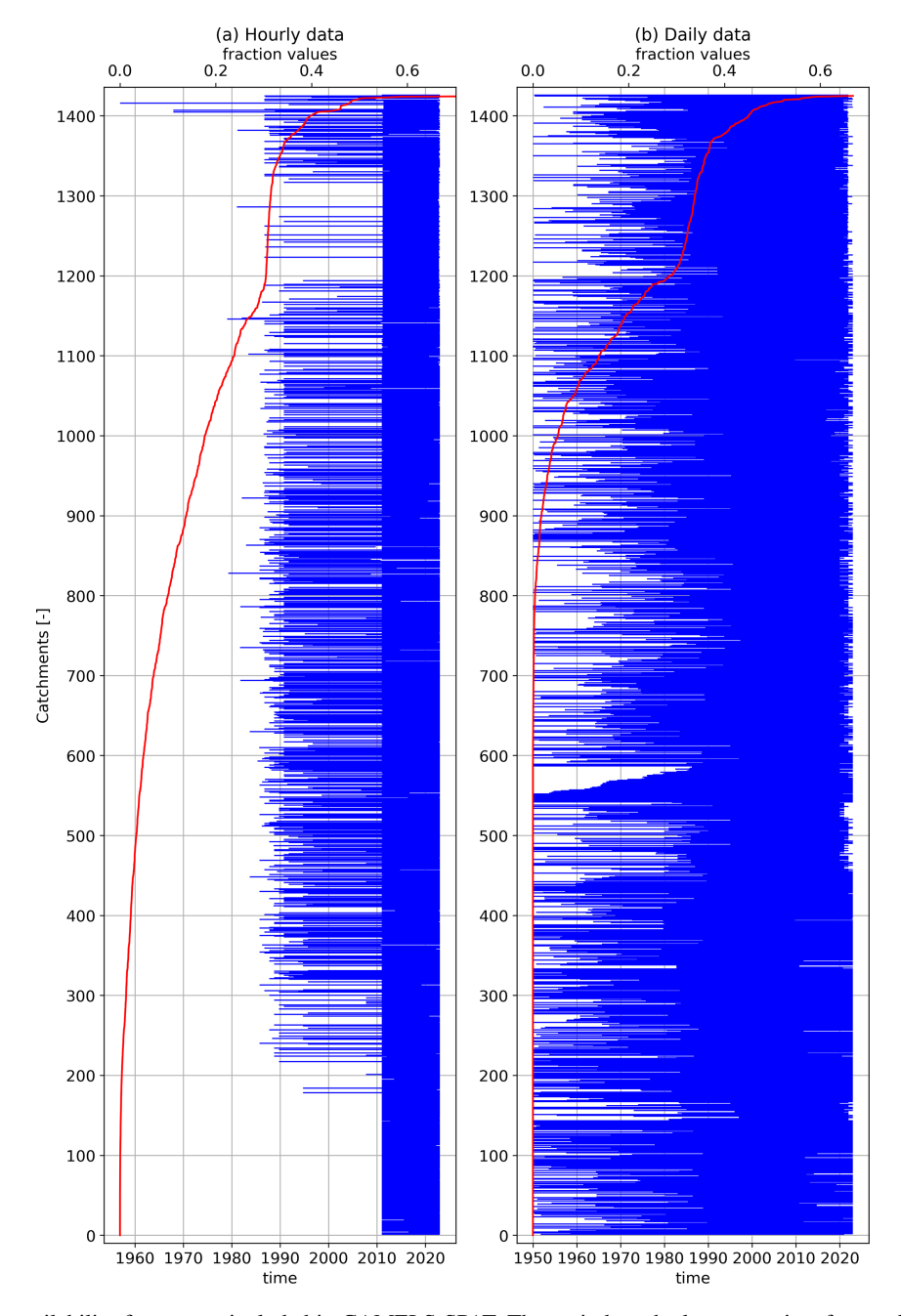


Figure A1. Flow data availability for gauges included in CAMELS-SPAT. The period on the lower x axis refers to the period between the first publicly available flow record for a given station and its last, with this record period given in blue for each gauge. Missing values occur in this record period and are given here in red as a fraction of the total record length on the top x axis.

Table A1. Climate attributes: annual statistics.

Attribute	Description	Units	Data source
num_years_rdrs	Number of years of RDRS data used to calculate attributes	years	RDRS
PR0_mean	Mean annual average precipitation total	$\mathrm{mm}\mathrm{yr}^{-1}$	RDRSa
PR0_std	Standard deviation of annual average precipitation total	${ m mmyr}^{-1}$	RDRS ^a
prec_mean	Mean annual average precipitation total	$\mathrm{mm}\mathrm{yr}^{-1}$	WorldClim
prec_std	Standard deviation of annual average precipitation total	${ m mmyr^{-1}}$	WorldClim
pet1_mean	Mean annual average potential evapotranspiration (PET) total	mm yr ⁻¹	RDRSa
pet1_std	Standard deviation of annual average PET total	${ m mmyr}^{-1}$	RDRS ^a
pet2_mean	Mean annual average potential evapotranspiration (PET) total	${ m mmyr}^{-1}$	WorldClim ^b
pet2_std	Standard deviation of annual average PET total	${ m mmyr^{-1}}$	WorldClim ^b
TT_mean	Mean of annual mean daily average temperature	°C	RDRSa
TT_std	Standard deviation of annual mean daily average temperature	°C	RDRS ^a
tavg_mean	Mean annual average temperature	°C	WorldClim
tavg_std	Spatial standard deviation of annual average temperature	°C	WorldClim
aridity1_mean	Mean annual aridity (PET/P)	_	RDRS
aridity1_std	Standard deviation of annual aridity (PET/P)	_	RDRS
aridity2_mean	Mean annual aridity (PET/P)	_	WorldClim
aridity2_std	Standard deviation of annual aridity (PET/P)	_	WorldClim
seasonality1_mean	Mean precipitation seasonality compared to temperature seasonality ^d	_	RDRS
seasonality1_std	Standard deviation of precipitation seasonality compared to temperature seasonality ^d	_	RDRS
seasonality2_mean	Mean precipitation seasonality compared to temperature seasonality ^e	_	WorldClim
seasonality2_std	Standard deviation of precipitation seasonality compared to temperature seasonality ^e	_	WorldClim
fracsnow1_mean	Mean annual snow fraction (0 °C degree threshold)	_	RDRS
fracsnow1_std	Standard deviation of annual snow fraction (0 °C degree threshold)	_	RDRS
fracsnow2_mean	Mean annual snow fraction (0 °C degree threshold)	_	WorldClim
fracsnow2_std	Standard deviation of annual snow fraction (0 °C degree threshold)	_	WorldClim

^a For consistency, we converted the RDRS units into those used in WorldClim. ^b Computed using WorldClim's *srad* and *tavg* variables and Eq. (3) in Oudin et al. (2005). ^c For consistency, we converted the WorldClim units into those used in RDRS. ^d Calculated using Eq. (14) in Woods (2009) for daily data from individual years, then finding the mean and standard deviation across years. ^e Calculated using Eq. (14) in Woods (2009) using monthly data, i.e. a much coarser temporal resolution than RDRS.

Table A2. Climate attributes – continued: frequency, duration and timing of high and low precipitation and of high and low temperature periods.

Attribute	Description	Units	Data source
low_temp_freq	Frequency of cold days (< 0 °C)	d yr ⁻¹	RDRS
low_temp_dur_mean	Mean duration of cold days (< 0 °C)	days	RDRS
low_temp_dur_median	Median duration of cold days (< 0 °C)	days	RDRS
low_temp_dur_skew	Skew of cold day durations (< 0 °C)	_	RDRS
low_temp_dur_kurtosis	Kurtosis of cold day durations (< 0 °C)	_	RDRS
low_temp_timing	Season during which most cold days occur (< 0 °C)	season	RDRS
high_temp_freq	Frequency of hot days (> mean daily max +5 °C) ^a	dyr ⁻¹	RDRS
high_temp_dur_mean	Mean duration of hot days ($>$ mean daily max $+5$ °C)	days	RDRS
high_temp_dur_median	Median duration of hot days (> mean daily max +5 °C)	days	RDRS
high_temp_dur_skew	Skew of hot day durations (> mean daily max +5 °C)	_	RDRS
high_temp_dur_kurtosis	Kurtosis of hot day durations (> mean daily max +5 °C)	_	RDRS
high_temp_timing	Season during which most hot days occur (> mean daily max $+5$ °C)	season	RDRS
low_prec_freq	Frequency of dry^b days ($< 1 \text{ mm d}^{-1}$)	d yr ⁻¹	RDRS
low_prec_dur_mean	Mean duration of dry days $(< 1 \text{ mm d}^{-1})$	days	RDRS
low_prec_dur_median	Median duration of dry days ($< 1 \text{ mm d}^{-1}$)	days	RDRS
low_prec_dur_skew	Skew of dry day durations $(< 1 \text{ mm d}^{-1})$	_	RDRS
low_prec_dur_kurtosis	Kurtosis of dry day durations ($< 1 \mathrm{mm}\mathrm{d}^{-1}$)	_	RDRS
low_prec_timing	Season during which most dry days occur ($< 1 \text{ mm d}^{-1}$)	season	RDRS
high_prec_freq	Frequency of wet ^b days (≥ 5 times mean daily precipitation)	d yr ⁻¹	RDRS
high_prec_dur_mean	Mean duration of wet days (≥ 5 times mean daily precipitation)	days	RDRS
high_prec_dur_median	Median duration of wet days (≥ 5 times mean daily precipitation)	days	RDRS
high_prec_dur_skew	Skew of wet day durations (≥ 5 times mean daily precipitation)	-	RDRS
high_prec_dur_kurtosis	Kurtosis of wet day durations (≥ 5 times mean daily precipitation)	_	RDRS
high_prec_timing	Season during which most wet days occur (≥ 5 times mean daily precipitation)	season	RDRS

 $[^]a$ Derived from the World Meteorological Organization's definition of heat waves: a 5 d or longer period with maximum daily temperatures 5 °C above the "standard" daily maximum temperature. "Standard" is defined as the mean daily max on each day, using the period 1961–1990 as a base. Here we define a hot day as a day where the maximum temperature is at least 5 °C over the long-term daily maximum temperature. We do not have data for the period 1961–1990 for all basins and therefore use all data available for a given basin to find the long-term daily maximum temperatures. b For consistency, we use the same definitions of dry and wet days as used in Addor et al. (2017a).

Table A3. Climate attributes – continued: spatial and temporal variability in climatic conditions. Attributes ending in $_{I}XI$ are calculated per month, with X ranging from 01 to 12. Statistics derived from RDRS are calculated over time; statistics derived from WorldClim are calculated across space.

Attribute	Description	Units	Data source
PR0_mean_month_{X}	Mean monthly average precipitation total	${\rm mmmonth}^{-1}$	RDRS ^a
$PR0_std_month_\{X\}$	Standard deviation of monthly average precipitation total	${ m mmmonth}^{-1}$	RDRS ^a
prec_mean_month_{X}	Mean monthly average precipitation total	$\mathrm{mm}\mathrm{month}^{-1}$	WorldClim
$prec_std_month_\{X\}$	Standard deviation of monthly average precipitation total	$\mathrm{mm}\mathrm{month}^{-1}$	WorldClim
pet1_mean_month_{X}	Mean monthly average potential evapotranspiration (PET) total	$\mathrm{mm}\mathrm{month}^{-1}$	RDRSa
pet1_std_time_month_{X}	Standard deviation of monthly average PET total	${ m mmmonth}^{-1}$	RDRS ^a
pet2_mean_month_{X}	Mean monthly average PET total	${\rm mmmonth}^{-1}$	WorldClim ^b
pet2_std_month_{X}	Standard deviation of monthly average PET total	${\rm mmmonth}^{-1}$	WorldClim ^b
tdavg_mean_month_{X}	Mean of monthly mean daily average temperature	°C	RDRSa
$tdavg_std_month_\{X\}$	Standard deviation of monthly mean daily average temperature	°C	RDRS ^a
$tavg_mean_month_\{X\}$	Mean monthly average temperature	°C	WorldClim
tavg_std_month_{X}	Spatial standard deviation of monthly average temperature	°C	WorldClim
$tdmin_mean_month_\{X\}$	Mean of monthly mean daily minimum temperature	°C	RDRS ^a
$tdmin_std_time_month_\{X\}$	Standard deviation of monthly mean daily minimum temperature	°C	RDRS ^a
tmin_mean_month_{X}	Mean monthly minimum temperature	°C	WorldClim
tmin_std_month_{X}	Standard deviation of monthly minimum temperature	°C	WorldClim
$tdmax_mean_month_\{X\}$	Mean of monthly mean daily maximum temperature	°C	RDRS ^a
$tdmax_std_month_\{X\}$	Standard deviation of monthly mean daily maximum temperature	°C	RDRS ^a
$tmax_mean_month_{X}$	Mean monthly maximum temperature	°C	WorldClim
tmax_std_month_{X}	Standard deviation of monthly maximum temperature	°C	WorldClim
FB_mean_month_{X}	Mean monthly downward shortwave radiation	$\mathrm{W}\mathrm{m}^{-2}$	RDRS
$FB_std_month_\{X\}$	Standard deviation of monthly downward shortwave radiation	$\mathrm{W}\mathrm{m}^{-2}$	RDRS
$srad_mean_month_\{X\}$	Mean monthly downward shortwave radiation	$\mathrm{W}\mathrm{m}^{-2}$	WorldClim ^c
$srad_std_month_\{X\}$	Standard deviation of monthly downward shortwave radiation	$\mathrm{W}\mathrm{m}^{-2}$	WorldClim ^c

^a For consistency, we converted the RDRS units into those used in WorldClim. ^b Computed using WorldClim's *srad* and *tavg* variables and Eq. (3) in Oudin et al. (2005).

Table A4. Climate attributes – continued: spatial and temporal variability in climatic conditions. Attributes ending in $_{I}X$ are calculated per month, with X ranging from 01 to 12. Statistics derived from ERA5 are calculated over time; statistics derived from WorldClim are calculated across space.

Attribute	Description	Units	Data source
FI_mean_month_{X}	Mean monthly downward longwave radiation	$\mathrm{W}\mathrm{m}^{-2}$	RDRS
$FI_std_month_{X}$	Standard deviation of monthly downward longwave radiation	$\mathrm{W}\mathrm{m}^{-2}$	RDRS
P0_mean_month_{X}	Mean monthly surface pressure	kPa	RDRS*
$P0_{std}_{month}\{X\}$	Standard deviation of monthly surface pressure	kPa	RDRS*
$vapr_mean_month_\{X\}$	Mean monthly vapour pressure	kPa	WorldClim
$vapr_std_month_\{X\}$	Standard deviation of monthly vapour pressure	kPa	WorldClim
HU_mean_month_{X}	Mean monthly specific humidity	kg kg ⁻¹	RDRS
$HU_std_month_{X}$	Standard deviation of monthly specific humidity	$kgkg^{-1}$	RDRS
HR_mean_month_{X}	Mean monthly relative humidity	$kPa kPa^{-1}$	RDRS
$HR_std_month_\{X\}$	Standard deviation of monthly relative humidity	$kPakPa^{-1}$	RDRS
UVC_mean_month_{X}	Mean monthly wind speed	$\mathrm{m}\mathrm{s}^{-1}$	RDRS
UVC_std_month_{X}	Standard deviation of monthly wind speed	$\mathrm{m}\mathrm{s}^{-1}$	RDRS
wind_mean_month_{X}	Mean monthly wind speed	$\mathrm{m}\mathrm{s}^{-1}$	WorldClim
$wind_std_month_{X}$	Standard deviation of monthly wind speed	$\mathrm{m}\mathrm{s}^{-1}$	WorldClim
phi_mean_month_{X}	Circular mean monthly wind direction	0	RDRS
phi_std_month_{X}	Circular standard deviation of monthly wind direction	0	RDRS
aridity1_mean_month_{X}	Mean monthly aridity (PET/P)	_	RDRS
aridity1_std_month_{X}	Standard deviation of monthly aridity	_	RDRS
aridity2_mean_month_{X}	Mean monthly aridity (PET/P)	_	WorldClim
$aridity2_std_month_\{X\}$	Standard deviation of monthly aridity	_	WorldClim
fracsnow1_mean_month_{X}	Mean monthly snow fraction (°C degree threshold)	_	RDRS
$fracsnow1_std_month_\{X\}$	Standard deviation of monthly snow fraction	_	RDRS
fracsnow2_mean_month_{X}	Mean monthly snow fraction (°C degree threshold)	_	WorldClim
fracsnow2_std_month_{X}	Standard deviation of monthly snow fraction	_	WorldClim

 $[\]ensuremath{^*}$ For consistency, we converted the RDRS units into those used in WorldClim.

 Table A5. Topographic attributes.

Attribute	Description	Units	Data source
centroid_lat	Basin centroid latitude	degrees	Varies
centroid_lon	Basin centroid longitude	degrees	Varies
gauge_lat	Station latitude	degrees	Varies
gauge_lon	Station longitude	degrees	Varies
basin_area	Basin area	km^2	MERIT Hydro
elev_min	Minimum elevation	ma.s.l.	MERIT Hydro
elev_mean	Mean elevation	ma.s.l.	MERIT Hydro
elev_max	Maximum elevation	ma.s.l.	MERIT Hydro
elev_std	Standard deviation of elevation	ma.s.l.	MERIT Hydro
slope_min	Minimum slope	degreesa	MERIT Hydro
slope_mean	Mean slope	degrees	MERIT Hydro
slope_max	Maximum slope	degrees	MERIT Hydro
slope_std	Standard deviation of slope	degrees	MERIT Hydro
aspect_min	Minimum aspect	degreesb	MERIT Hydro
aspect_mean	Mean aspect	degrees	MERIT Hydro
aspect_max	Maximum aspect	degrees	MERIT Hydro
aspect_std	Standard deviation of aspect	degrees	MERIT Hydro
stream_length_min	Minimum length from headwater to gauge	km	MERIT Hydro Basins
stream_length_mean	Mean length from headwaters to gauge	km	MERIT Hydro Basins
stream_length_max	Maximum length from headwater to gauge	km	MERIT Hydro Basins
stream_length_std	Standard deviation of length from headwaters to gauge	km	MERIT Hydro Basins
stream_length_total	Total stream length	km	MERIT Hydro Basins
stream_order_max	Stream order at gauge	_	MERIT Hydro Basins
stream_density	Ratio of total stream length and area	km ⁻¹	Derived
elongation_ratio	Ratio of diameter of circle with same size as basin and longest stream	_	Derived

^a Slope angle. ^b Azimuth that slopes are facing, with 0° indicating north-facing slopes, 90° east-facing, 180° south-facing and 270° west-facing.

Table A6. Open water attributes. For basins with no identified open water bodies or reservoirs, these attributes will be 0 and NaN.

Attribute	Description	Units	Data source
open_water_number	Number of open water bodies larger than 10 ha	_	HydroLAKES
known_reservoirs	Number of water bodies identified as reservoirs	_	HydroLAKES
open_water_area_min	Minimum open water area	km^2	HydroLAKES
open_water_area_mean	Mean open water area	km ²	HydroLAKES
open_water_area_max	Maximum open water area	km^2	HydroLAKES
open_water_area_std	Standard deviation of open water area	km^2	HydroLAKES
open_water_area_total	Total open water area	km^2	HydroLAKES
open_water_volume_min	Minimum open water volume	km ²	HydroLAKES
open_water_volume_mean	Mean open water volume	km^2	HydroLAKES
open_water_volume_max	Maximum open water volume	km^2	HydroLAKES
open_water_volume_std	Standard deviation of open water volume	km^2	HydroLAKES
open_water_volume_total	Total open water volume	km^2	HydroLAKES
reservoir_area_min	Minimum reservoir area	km ²	HydroLAKES
reservoir_area_mean	Mean reservoir area	km^2	HydroLAKES
reservoir_area_max	Maximum reservoir area	km^2	HydroLAKES
reservoir_area_std	Standard deviation of reservoir area	km^2	HydroLAKES
reservoir_area_total	Total reservoir area	km^2	HydroLAKES
reservoir_volume_min	Minimum reservoir volume	km ²	HydroLAKES
reservoir_volume_mean	Mean reservoir volume	km^2	HydroLAKES
reservoir_volume_max	Maximum reservoir volume	km^2	HydroLAKES
reservoir_volume_std	Standard deviation of reservoir volume	km^2	HydroLAKES
reservoir_volume_total	Total reservoir volume	km^2	HydroLAKES

Table A7. Vegetation and land cover attributes. Attributes ending in $_(X)$ are calculated per month, with X ranging from 01 to 12. Attributes ending in $_(Y)$ are calculated for specific years. Attributes ending in $_(Z)$ are categorical attributes, where Z varies between different datasets.

Attribute	Description	Units	Data source
lai_mean_month_{X} lai_std_month_{X}	Mean monthly leaf area index	$m^2 m^{-2}$	MCD15A2H.061
	Standard deviation of monthly leaf area index	$m^2 m^{-2}$	MCD15A2H.061
forest_height_{Y}_min	Minimum forest height in year 2000/2020	m	GLCLUC 2000–2020
forest_height_{Y}_mean	Mean forest height in year 2000/2020	m	GLCLUC 2000–2020
forest_height_{Y}_max	Maximum forest height in year 2000/2020	m	GLCLUC 2000–2020
forest_height_{Y}_std	Standard deviation of forest height in year 2000/2020	m	GLCLUC 2000–2020
lc1_{Z}_fraction	Fraction of land cover class present in the basin	_	GLCLU 2019
lc2_{Z}_fraction	Fraction of land cover class present in the basin	_	MCD12Q1.061
lc3_{Z}_fraction	Fraction of land cover class present in the basin	_	LGRIP30

 Table A8. Subsurface attributes.

Attribute	Description	Units	Data source
regolith_thickness_min	Minimum upland and hillslope regolith thickness	m	Pelletier ^a
regolith_thickness_mean	Mean upland and hillslope regolith thickness	m	Pelletier
regolith_thickness_max	Maximum upland and hillslope regolith thickness	m	Pelletier
regolith_thickness_std	Standard deviation of upland and hillslope regolith thickness	m	Pelletier
soil_thickness_min	Minimum upland and hillslope soil thickness	m	Pelletier
soil_thickness_mean	Mean upland and hillslope soil thickness	m	Pelletier
soil_thickness_max	Maximum upland and hillslope soil thickness	m	Pelletier
soil_thickness_std	Standard deviation of upland and soil regolith thickness	m	Pelletier
sedimentary_thickness_min	Minimum upland, valley bottom and lowland sedimentary deposit thickness	m	Pelletier
sedimentary_thickness_mean	Mean upland, valley bottom and lowland sedimentary deposit thickness	m	Pelletier
sedimentary_thickness_max	Maximum upland, valley bottom and lowland sedimentary deposit thickness	m	Pelletier
sedimentary_thickness_std	Standard deviation of upland, valley bottom and lowland sedimentary deposit thickness	m	Pelletier
average_thickness_min	Minimum average soil and sedimentary deposit thicknesses	m	Pelletier
average_thickness_mean	Mean average soil and sedimentary deposit thicknesses	m	Pelletier
average_thickness_max	Maximum average soil and sedimentary deposit thicknesses	m	Pelletier
average_thickness_std	Standard deviation of average soil and sedimentary deposit thicknesses	m	Pelletier
porosity_min	Minimum porosity	_	GLHYMPS
porosity_mean	Mean porosity	_	GLHYMPS
porosity_max	Maximum porosity	_	GLHYMPS
porosity_std	Standard deviation of porosity	-	GLHYMPS
log_permeability_min	Minimum permeability ^b	m^2	GLHYMPS
log_permeability_mean	Mean permeability	m^2	GLHYMPS
log_permeability_max	Maximum permeability	m^2	GLHYMPS
log_permeability_std	Standard deviation of permeability	m^2	GLHYMPS

a For definitions and user notes, see https://daac.ornl.gov/SOILS/guides/Global_Soil_Regolith_Sediment.html (last access: 6 March 2024). b Note that permeability *k* in the GLHYMPS database is given as log 10(*k*), due to the many decimal places otherwise needed.

Table A9. Subsurface attributes – continued: properties derived from the SoilGrids data. Attributes are provided at six depths $\{D\}$: 0–5, 5–15, 15–30, 30–60, 60–100 and 100–200 cm and for the SoilGrids *mean* (abbreviated in the table as $\{M\}$) and *uncertainty* ($\{U\}$ in the table) data fields. The mean values may be seen as expected values for a given grid cell, while the uncertainty is defined as the 90 % prediction interval divided by the median value for the cell^a.

Attribute	Description	Units	Data source
bdod_{M/U}_{D}_min bdod_{M/U}_{D}_mean bdod_{M/U}_{D}_max bdod_{M/U}_{D}_std	Minimum bulk density of fine earth Mean bulk density of fine earth Maximum bulk density of fine earth Standard deviation of bulk density of fine earth	cg cm ⁻³ cg cm ⁻³ cg cm ⁻³ cg cm ⁻³	SoilGrids SoilGrids SoilGrids SoilGrids
cfvo_{M/U}_{D}_min cfvo_{M/U}_{D}_mean cfvo_{M/U}_{D}_max cfvo_{M/U}_{D}_std	Minimum volumetric content of fragments > 2 mm Mean volumetric content of fragments > 2 mm Maximum volumetric content of fragments > 2 mm Standard deviation of volumetric content of fragments > 2 mm	cm ³ dm ⁻³ cm ³ dm ⁻³ cm ³ dm ⁻³ cm ³ dm ⁻³	SoilGrids SoilGrids SoilGrids SoilGrids
clay_{M/U}_{D}_min clay_{M/U}_{D}_mean clay_{M/U}_{D}_max clay_{M/U}_{D}_std	Minimum clay fraction Mean clay fraction Maximum clay fraction Standard deviation of clay fraction	g kg ⁻¹ g kg ⁻¹ g kg ⁻¹ g kg ⁻¹	SoilGrids SoilGrids SoilGrids SoilGrids
sand_{M/U}_{D}_min sand_{M/U}_{D}_mean sand_{M/U}_{D}_max sand_{M/U}_{D}_std	Minimum sand fraction Mean sand fraction Maximum sand fraction Standard deviation of sand fraction	gkg^{-1} gkg^{-1} gkg^{-1} gkg^{-1}	SoilGrids SoilGrids SoilGrids SoilGrids
silt_{M/U}_{D}_min silt_{M/U}_{D}_mean silt_{M/U}_{D}_max silt_{M/U}_{D}_std	Minimum silt fraction Mean silt fraction Maximum silt fraction Standard deviation of silt fraction	$g kg^{-1}$ $g kg^{-1}$ $g kg^{-1}$ $g kg^{-1}$	SoilGrids SoilGrids SoilGrids SoilGrids
soc_{M/U}_{D}_min soc_{M/U}_{D}_mean soc_{M/U}_{D}_max soc_{M/U}_{D}_std	Minimum organic carbon content Mean organic carbon content Maximum organic carbon content Standard deviation of organic carbon content	$dg kg^{-1}$ $dg kg^{-1}$ $dg kg^{-1}$ $dg kg^{-1}$	SoilGrids SoilGrids SoilGrids SoilGrids
porosity_{M}_{D}_min porosity_{M}_{D}_mean porosity_{M}_{D}_max porosity_{M}_{D}_std	Minimum soil porosity Mean soil porosity Maximum soil porosity Standard deviation of soil porosity	- - -	SoilGrids SoilGrids SoilGrids SoilGrids
conductivity_{M}_{D}_min conductivity_{M}_{D}_mean conductivity_{M}_{D}_max conductivity_{M}_{D}_std	Minimum soil conductivity Harmonic mean of soil conductivity ^b Maximum soil conductivity Standard deviation of soil conductivity ^{b,c}	$cm h^{-1}$ $cm h^{-1}$ $cm h^{-1}$ $cm h^{-1}$	SoilGrids SoilGrids SoilGrids SoilGrids

^a See https://www.isric.org/explore/soilgrids/faq-soilgrids (last access: 7 March 2024). ^b Following Addor et al. (2017a). ^c Note that no harmonic equivalent of a standard deviation exists, and this is a regular standard deviation.

Table A10. Hydrologic signatures. Note that streamflow observations have been converted from $m^3 s^{-1}$ to $mm d^{-1}$ using the basin areas of our newly delineated basin outlines. Please note the uncertainty in these area estimates (Fig. 2). For each signature, we calculated a sequence of yearly values and then found the mean and standard deviation across all years for which data were available.

Attribute	Description	Units	Data source
num_years_hyd	Years of daily data used to calculate signatures	years	-
daily_discharge_mean	Mean daily discharge	$\mathrm{mm}\mathrm{d}^{-1}$	USGS/WSC
daily_discharge_std	Standard deviation of daily discharge	$\mathrm{mm}\mathrm{d}^{-1}$	USGS/WSC
daily_discharge_mean_month_{X}	Mean daily discharge for month X	$\mathrm{mm}\mathrm{d}^{-1}$	USGS/WSC
$daily_discharge_std_month_\{X\}$	Standard deviation of average daily discharge in month X	$\mathrm{mm}\mathrm{d}^{-1}$	USGS/WSC
runoff_ratio_mean	Ratio of mean daily discharge to mean daily precipitation	_	USGS/WSC, RDRS
runoff_ratio_std	Ratio of mean daily discharge to mean daily precipitation	_	USGS/WSC, RDRS
streamflow_elasticity	Streamflow sensitivity to changes in precipitation ^a	-	USGS/WSC, RDRS
slope_fdc_mean	Slope of the log-transformed flow duration curve (33th to 66th percentile) ^e	-	USGS/WSC
slope_fdc_std	Standard deviation of the log-transformed flow duration curve ^e	-	USGS/WSC
bfi_mean	Mean baseflow index (ratio of mean daily baseflow ^b to mean daily discharge)	_	USGS/WSC
bfi_std	Standard deviation of baseflow index	-	USGS/WSC
hfd_mean	Circular mean half-flow date ^c	day of year	USGS/WSC
hfd_std	Circular standard deviation of half-flow dates	days	USGS/WSC
q{Y}_mean ^d	Mean Y % flow quantile, where q1 are low flows	${\rm mmd^{-1}}$	USGS/WSC
$q\{Y\}_{std}^d$	Standard deviation of Y % flow quantiles	$\mathrm{mm}\mathrm{d}^{-1}$	USGS/WSC

^a Calculated as described in Eq. (7) of Sankarasubramanian et al. (2001), with the modification described in Table 3 in Addor et al. (2017a). ^b Calculated from time series of baseflow derived using the Eckhardt (2005) digital filter method, as recommended and implemented by Xie et al. (2020). ^c Calculated as the day when cumulative flow in a water year passes half the total flow for that water year. ^d Y is one of [0.01, 0.05, 0.10, 0.25, 0.50, 0.75, 0.90. 0.95, 0.99]. ^e In cases with zero flows, 0.1 % of the mean flow is added to prevent issues with calculating the logarithm. Time steps with missing flow observations are removed from the calculation.

Table A11. Hydrologic signatures – continued: frequency, duration and timing of high- and low-flow events.

Attribute	Description	Units	Data source
no_flow_freq	Frequency of no-flow days	$\rm dyr^{-1}$	USGS/WSC
no_flow_dur_mean	Mean duration of no-flow days	days	USGS/WSC
no_flow_dur_median	Median duration of no-flow days	days	USGS/WSC
no_flow_dur_skew	Skew of no-flow day durations	_	USGS/WSC
no_flow_dur_kurtosis	Kurtosis of no-flow day durations	_	USGS/WSC
no_flow_timing	Season during which most no-flow days occur	season	USGS/WSC
low_flow_freq	Frequency of low-flow days (< 0.2 times the mean daily flow)*	dyr ⁻¹	USGS/WSC
low_flow_dur_mean	Mean duration of low-flow days (< 0.2 times the mean daily flow)	days	USGS/WSC
low_flow_dur_median	Median duration of low-flow days (< 0.2 times the mean daily flow)	days	USGS/WSC
low_flow_dur_skew	Skew of low-flow day durations (< 0.2 times the mean daily flow)	_	USGS/WSC
low_flow_dur_kurtosis	Kurtosis of low-flow day durations (< 0.2 times the mean daily flow)	_	USGS/WSC
low_flow_timing	Season during which most low-flow days occur (< 0.2 times the mean daily flow)	season	USGS/WSC
high_flow_freq	Frequency of high-flow days (> 9 times the median daily flow)*	d yr ⁻¹	USGS/WSC
high_flow_dur_mean	Mean duration of high-flow days (> 9 times the median daily flow)	days	USGS/WSC
high_flow_dur_median	Median duration of high-flow days (> 9 times the median daily flow)	days	USGS/WSC
high_flow_dur_skew	Skew of high-flow day durations (> 9 times the median daily flow)	_	USGS/WSC
high_flow_dur_kurtosis	Kurtosis of high-flow day durations (> 9 times the median daily flow)	_	USGS/WSC
high_flow_timing	Season during which most high-flow days occur (> 9 times the median daily flow)	season	USGS/WSC

^{*} For consistency, we use the same definitions of dry and wet days as used in Addor et al. (2017a).

Code and data availability. The complete CAMELS-SPAT dataset can be accessed through the Federated Research Data Repository (FRDR) at https://doi.org/10.20383/103.01306 (Knoben et al., 2025). Code needed to reproduce the CAMELS-SPAT data preparation is available on GitHub at https://github.com/ch-earth/camels_spat (Knoben, 2025). Data sources used in the preparation of this paper are listed below, separated into data used but not redistributed and data that are redistributed. These data products are provided under a variety of licences. Please see the individual licences for detail, and note that attribution is in almost all cases mandatory. We have provided a data_citation.bib file available on the CAMELS-SPAT data repository and ask users to cite each separate dataset that we redistribute in any publications that use CAMELS-SPAT. Elements in CAMELS-SPAT not covered below (processing code, attributes) are provided under a CC-BY-NC 4.0 licence.

Data (redistributed). Listed here are details of each of the datasets used in the creation of the CAMELS-SPAT data and partly reproduced in the CAMELS-SPAT data.

1. Meteorological data. Meteorological forcing fields were obtained from the Daymet v4.1 dataset (Thornton et al., 2021, 2022), which is openly shared, without restriction, in accordance with the NASA Earth Science Data and Information System (ESDIS) Project Data Use Policy. For licence terms, see https://www.earthdata.nasa.gov/learn/use-data/data-use-policy (last access: 24 May 2024).

Meteorological forcing fields were obtained from the ERA5 dataset (Hersbach et al., 2020, 2017, 2023) under the Copernicus data licence. For licence terms, see https://cds.climate.copernicus.eu/api/v2/terms/static/ licence-to-use-copernicus-products.pdf (last access: 18 December 2023; link since deprecated, see here for archived version: https://object-store.os-api.cci2.ecmwf.int/cci2-prodcatalogue/licences/). Redistributed ERA5 data were generated using Copernicus Climate Change Service information [2023] in the case of the gridded forcing files. CAMELS-SPAT also contains modified Copernicus Climate Change Service information [2023] in the case of the (sub-)basin-averaged forcing files. Neither the European Commission nor ECMWF is responsible for any use that may be made of the Copernicus information or data it contains.

Meteorological forcing fields were obtained from the Deterministic EM-Earth dataset (Tang et al., 2022a; Tang et al., 2022b) under a CC-BY 4.0 licence (https://doi.org/10.20383/102.0547; Tang et al., 2022a).

Meteorological forcing fields were obtained from the RDRS v2.1 dataset (Gasset et al., 2021, data source: Environment and Climate Change Canada) under the Environment and Climate Change Canada Data Server End-Use Licence version 2.1. For licence terms, see https://eccc-msc.github.io/open-data/licence/readme_en/ (last access: 7 February 2025).

2. Basin outlines. Sub-basin polygons were obtained from the MERIT Basins dataset (Lin et al., 2019, http://hydrology.princeton.edu/data/mpan/MERIT_Basins/, last access: 10 October 2025). No formal licence is stated in the paper, but data have since been moved elsewhere (https://www.reachhydro.org/home/params/merit-basins, last access: 7 February 2025) and are available there under a CC-BY-NC-SA 4.0 licence.

Reference shapefiles for the basins in the US were obtained from the CAMELS dataset (Newman et al., 2015; Addor et al., 2017a, https://doi.org/10.5065/D6MW2F4D). The source of these shapefiles is the U.S. Geological Survey HCDN-2009 dataset (Lins, 2012) and therefore is considered to be in the public domain (see https://www.usgs.gov/information-policies-and-instructions/copyrights-and-credits, last access: 21 March 2024).

The first set of reference shapefiles for the basins in Canada were obtained from the national hydrometric network basin polygons dataset (Environment and Climate Change Canada, 2020b, https://open.canada.ca/data/en/dataset/0c121878-ac23-46f5-95df-eb9960753375), available under the Open Government Licence – Canada (https://open.canada.ca/en/open-government-licence-canada, last access: 21 March 2024).

The second set of reference shapefiles for the basins in Canada were obtained from the Reference Hydrometric Basin Network (Government of Canada, 2022, https://www.canada.ca/en/environment-climate-change/services/water-overview/quantity/monitoring/survey/data-products-services/reference-hydrometric-basin-network.html, last access: 18 August 2022), available under an unknown licence.

3. Streamflow data. Daily flow data for the basins in the US were obtained from the Daily Values Service, courtesy of the U.S. Geological Survey (https://nwis.waterservices.usgs.gov/docs/dv-service/daily-values-service-details/, last access: 21 March 2024). Data are considered to be in the public domain (see https://www.usgs.gov/information-policies-and-instructions/copyrights-and-credits, last access: 21 March 2024)

Hourly flow data for the basins in the US were derived from the high-resolution Instantaneous Values Service (U.S. Geological Survey, https://nwis.waterservices.usgs.gov/docs/instantaneous-values/instantaneous-values-details/, last access: 21 March 2024). Data are considered to be in the public domain (see https://www.usgs.gov/information-policies-and-instructions/copyrights-and-credits, last access: 21 March 2024).

Daily flow data for the basins in Canada were obtained from the HYDAT database version 20230505, courtesy of the Water Survey of Canada (https://www.canada.ca/en/environment-climate-change/services/water-overview/quantity/monitoring/survey/data-products-services/national-archive-hydat.html, last access: 21 March 2024). Data are considered public information (see https://wateroffice.ec.gc.ca/disclaimer_info_e.html for full terms and details, last access: 21 March 2024). Note that the HYDAT database gets continuously updated and superseded versions are not publicly available.

Hourly flow data for the basins in Canada were derived from the high-resolution data available online from the Government of Canada (Water Survey of Canada, https://collaboration.cmc.ec.gc.ca/cmc/hydrometrics/www/UnitValueData/, last access: 31 March 2025). Data are considered public information (see https://wateroffice.ec.gc.ca/disclaimer_info_e. html for full terms and details, last access: 21 March 2024).

4. Geospatial data. Forest height grids were obtained from the Global Land Cover and Land Use Change, 2000–2020

dataset (Potapov et al., 2021) under a CC-BY licence (https://glad.umd.edu/dataset/GLCLUC2020/, last access: 16 October 2023).

Leaf area index grids were obtained from the MCD15A2H.061 dataset (Myneni et al., 2021, https://doi.org/10.5067/MODIS/MCD15A2H.061).

Data can be redistributed with no restriction. See https://lpdaac.usgs.gov/data/data-citation-and-policies/ (last access: 17 October 2023).

Agriculture grids were obtained from the LGRIP30 dataset (Thenkabail et al., 2021; Teluguntla et al., 2023, https://doi.org/10.5067/COMMUNITY/LGRIP/LGRIP30.001). Data can be redistributed with no restriction. See https://lpdaac.usgs.gov/data/data-citation-and-policies/ (last access: 17 October 2023).

Land cover and land use grids were obtained from the MCD12Q1.061 dataset (Friedl and Sulla-Menashe, 2022, https://doi.org/10.5067/MODIS/MCD12Q1.061). Data can be redistributed with no restriction. See https://lpdaac.usgs.gov/data/data-citation-and-policies/ (accessed: 17 October 2023).

Land cover and land use grids were obtained from the Global Land Cover and Land Use 2019 dataset (Hansen et al., 2022) under a CC-BY 4.0 licence (https://glad.umd.edu/dataset/global-land-cover-land-use-v1, last access: 16 October 2023). Lake polygons were obtained from the HydroLAKES dataset (Messager et al., 2016) under a CC-BY 4.0 licence (https://www.hydrosheds.org/products/hydrolakes, last access: 16 October 2023).

Digital elevation model grids were obtained from the MERIT Hydro Adjusted Elevations dataset (Yamazaki et al., 2019) under CC-BY-NC 4.0 or ODbL 1.0 licences (http://hydro.iis. u-tokyo.ac.jp/~yamadai/MERIT_Hydro/, last access: 10 October 2023).

Soil property grids were obtained from the SoilGrids 2.0 dataset (Poggio et al., 2021) under a CC-BY-NC 4.0 licence (https://soilgrids.org/, last access: 10 October 2023).

Soil property grids were obtained from the Pelletier dataset (Pelletier et al., 2016b, a, https://daac.ornl.gov/SOILS/guides/Global_Soil_Regolith_Sediment.html). Data can be redistributed with no restriction. See https://www.earthdata.nasa.gov/learn/use-data/data-use-policy (last access: 18 December 2023).

Geology polygons were obtained from the GLHYMPS dataset (Gleeson et al., 2014; Gleeson, 2018) under a CC-BY 4.0 licence (https://doi.org/10.5683/SP2/DLGXYO).

Data (not redistributed). Listed here are details of each of the datasets used in the creation of the CAMELS-SPAT data but not distributed as part of the CAMELS-SPAT data.

1. Basin delineation. Flow direction grids were obtained from the MERIT Hydro Adjusted Elevations dataset (Yamazaki et al., 2019) under CC-BY-NC 4.0 or ODbL 1.0 licences (http://hydro.iis.u-tokyo.ac.jp/~yamadai/MERIT_Hydro/, last access: 10 October 2023).

Flow accumulation grids were obtained from the MERIT Hydro Adjusted Elevations dataset (Yamazaki et al., 2019) under CC-BY-NC 4.0 or ODbL 1.0 licences (http://hydro.iis. u-tokyo.ac.jp/~yamadai/MERIT_Hydro/, last access: 10 October 2023).

 Geospatial data. Climate grids were obtained from the World-Clim dataset (Fick and Hijmans, 2017, https://www.worldclim. org/data/worldclim21.html, last access: 22 October 2023). WorldClim data were used to calculate high-resolution climate attributes and derive a number of maps. The source data cannot be redistributed.

Supplement. The supplement related to this article is available online at https://doi.org/10.5194/hess-29-5791-2025-supplement.

Author contributions. MPC developed the idea for this dataset, secured funding, and provided mentorship and support throughout the project. AP provided general guidance during the project and early feedback on paper drafts. NWC provided guidance on geospatial data products. LTR provided assistance with geospatial data-processing coding. CT tested multiple versions of the dataset, discovered various processing errors, created code to fix some of these and created the code needed to produce the summary sheets for each basin. KK provided assistance with forcing data subsetting. WJMK developed the methodology, created the code, performed the data processing and wrote the initial draft of this paper. The paper was finalized with contributions from all co-authors.

Competing interests. The contact author has declared that none of the authors has any competing interests.

Disclaimer. The dataset described in this paper is provided in the hopes that it will be useful but without any guarantee of correctness or fitness for purpose. See the licence terms for full details.

Publisher's note: Copernicus Publications remains neutral with regard to jurisdictional claims made in the text, published maps, institutional affiliations, or any other geographical representation in this paper. While Copernicus Publications makes every effort to include appropriate place names, the final responsibility lies with the authors.

Acknowledgements. We express our thanks to the U.S. Geological Survey and the Water Survey of Canada for their assistance in understanding how both agencies deal with time zones and timestamps in their data. We are grateful to Chris Marsh for pointing out some nuances about wind direction definitions, to Guoqiang Tang for providing details about the way timestamps in the EM-Earth data must be interpreted and to Frederik Kratzert for pointing out an issue with duplicated basin IDs. We also happily acknowledge the help of Louise Arnal, Chris Marsh and Gaby Gründemann for specific suggestions about our figures. We gratefully acknowledge the continued support with computational resources from the Global Institute for Water Security.

Financial support. This research was supported by the Cooperative Institute for Research to Operations in Hydrology (CIROH) with

funding under award NA22NWS4320003 from the NOAA Cooperative Institutes programme. The statements, findings, conclusions and recommendations are those of the author(s) and do not necessarily reflect the opinions of NOAA.

Review statement. This paper was edited by Nunzio Romano and reviewed by Brandi Gaertner and Yifan Cheng.

References

- Addor, N., Newman, A. J., Mizukami, N., and Clark, M. P.: The CAMELS data set: catchment attributes and meteorology for large-sample studies, Hydrol. Earth Syst. Sci., 21, 5293–5313, https://doi.org/10.5194/hess-21-5293-2017, 2017a.
- Addor, N., Newman, A. J., Mizukami, N., and Clark, M. P.: Catchment attributes for large-sample studies, https://ral.ucar.edu/solutions/products/camels (last access: 24 October 2025), 2017b (data set available at https://zenodo.org/records/15529996, last access: 24 October 2025).
- Addor, N., Do, H. X., Alvarez-Garreton, C., Coxon, G., Fowler, K., and Mendoza, P. A.: Large-sample hydrology: recent progress, guidelines for new datasets and grand challenges, Hydrol. Sci. J., 65, 712–725, https://doi.org/10.1080/02626667.2019.1683182, 2020.
- Ahmed, M. I., Shook, K., Pietroniro, A., Stadnyk, T., Pomeroy, J. W., Pers, C., and Gustafsson, D.: Implementing a parsimonious variable contributing area algorithm for the prairie pothole region in the HYPE modelling framework, Environ. Model. Softw., 167, 105769, https://doi.org/10.1016/j.envsoft.2023.105769, 2023.
- Allen, R. G., Pereira, L. S., Raes, D., and Smith, M.: Crop evapotranspiration: guidelines for computing crop water requirements, no. 56 in FAO irrigation and drainage paper, Food and Agriculture Organization of the United Nations, Rome, ISBN 978-92-5-104219-9, 1998.
- Almagro, A., Oliveira, P. T. S., Meira Neto, A. A., Roy, T., and Troch, P.: CABra: a novel large-sample dataset for Brazilian catchments, Hydrol. Earth Syst. Sci., 25, 3105–3135, https://doi.org/10.5194/hess-25-3105-2021, 2021.
- Alvarez-Garreton, C., Mendoza, P. A., Boisier, J. P., Addor, N., Galleguillos, M., Zambrano-Bigiarini, M., Lara, A., Puelma, C., Cortes, G., Garreaud, R., McPhee, J., and Ayala, A.: The CAMELS-CL dataset: catchment attributes and meteorology for large sample studies Chile dataset, Hydrol. Earth Syst. Sci., 22, 5817–5846, https://doi.org/10.5194/hess-22-5817-2018, 2018.
- Arsenault, R., Bazile, R., Ouellet Dallaire, C., and Brissette, F.: CANOPEX: A Canadian hydrometeorological watershed database: CANOPEX: A Canadian Hydrometeorological Watershed Database, Hydrol. Process., 30, 2734–2736, https://doi.org/10.1002/hyp.10880, 2016.
- Arsenault, R., Brissette, F., Martel, J.-L., Troin, M., Lévesque, G., Davidson-Chaput, J., Gonzalez, M. C., Ameli, A., and Poulin, A.: A comprehensive, multisource database for hydrometeorological modeling of 14,425 North American watersheds, Sci. Data, 7, 243, https://doi.org/10.1038/s41597-020-00583-2, 2020.
- Budhathoki, S., Rokaya, P., and Lindenschmidt, K.-E.: Improved modelling of a Prairie catchment using a progressive two-stage calibration strategy with in situ soil

- moisture and streamflow data, Hydrol. Res., 51, 505–520, https://doi.org/10.2166/nh.2020.109, 2020.
- Chagas, V. B. P., Chaffe, P. L. B., Addor, N., Fan, F. M., Fleischmann, A. S., Paiva, R. C. D., and Siqueira, V. A.: CAMELS-BR: hydrometeorological time series and landscape attributes for 897 catchments in Brazil, Earth Syst. Sci. Data, 12, 2075–2096, https://doi.org/10.5194/essd-12-2075-2020, 2020.
- Clark, M. P. and Shook, K. R.: The Numerical Formulation of Simple Hysteretic Models to Simulate the Large-Scale Hydrological Impacts of Prairie Depressions, Water Resour. Res., 58, e2022WR032694, https://doi.org/10.1029/2022WR032694, 2022.
- Clark, M. P., Nijssen, B., Lundquist, J. D., Kavetski, D., Rupp, D. E., Woods, R. A., Freer, J. E., Gutmann, E. D., Wood, A. W., Brekke, L. D., Arnold, J. R., Gochis, D. J., and Rasmussen, R. M.: A unified approach for process-based hydrologic modeling: 1. Modeling concept, Water Resour. Res., 51, 2498–2514, https://doi.org/10.1002/2015WR017198, 2015a.
- Clark, M. P., Nijssen, B., Lundquist, J. D., Kavetski, D., Rupp, D. E., Woods, R. A., Freer, J. E., Gutmann, E. D., Wood, A. W., Gochis, D. J., Rasmussen, R. M., Tarboton, D. G., Mahat, V., Flerchinger, G. N., and Marks, D. G.: A unified approach for process-based hydrologic modeling: 2. Model implementation and case studies, Water Resour. Res., 51, 2515–2542, https://doi.org/10.1002/2015WR017200, 2015b.
- Clark, M. P., Schaefli, B., Schymanski, S. J., Samaniego, L., Luce, C. H., Jackson, B. M., Freer, J. E., Arnold, J. R., Moore, R. D., Istanbulluoglu, E., and Ceola, S.: Improving the theoretical underpinnings of process-based hydrologic models, Water Resour. Res., 52, 2350–2365, https://doi.org/10.1002/2015WR017910, 2016.
- Clark, M. P., Vogel, R. M., Lamontagne, J. R., Mizukami, N., Knoben, W. J. M., Tang, G., Gharari, S., Freer, J. E., Whitfield, P. H., Shook, K. R., and Papalexiou, S. M.: The Abuse of Popular Performance Metrics in Hydrologic Modeling, Water Resour. Res., 57, e2020WR029001, https://doi.org/10.1029/2020WR029001, 2021.
- Clerc-Schwarzenbach, F., Selleri, G., Neri, M., Toth, E., van Meerveld, I., and Seibert, J.: Large-sample hydrology a few camels or a whole caravan?, Hydrol. Earth Syst. Sci., 28, 4219–4237, https://doi.org/10.5194/hess-28-4219-2024, 2024.
- Cloke, H. L. and Hannah, D. M.: Large-scale hydrology: advances in understanding processes, dynamics and models from beyond river basin to global scale, Hydrol. Process., 25, 991–995, https://doi.org/10.1002/hyp.8059, 2011.
- Commission for Environmental Cooperation: North American Atlas – Political Boundaries, statistics Canada, United States Census Bureau, Instituto Nacional de Estadística y Geografía (IN-EGI), http://www.cec.org/north-american-environmental-atlas/ political-boundaries-2021/ (last access: 20 December 2023), 2022.
- Cosby, B. J., Hornberger, G. M., Clapp, R. B., and Ginn, T. R.: A Statistical Exploration of the Relationships of Soil Moisture Characteristics to the Physical Properties of Soils, Water Resour. Res., 20, 682–690, https://doi.org/10.1029/WR020i006p00682, 1984.
- Coxon, G., Addor, N., Bloomfield, J. P., Freer, J., Fry, M., Hannaford, J., Howden, N. J. K., Lane, R., Lewis, M., Robinson, E. L., Wagener, T., and Woods, R.: CAMELS-GB: hydrome-

- teorological time series and landscape attributes for 671 catchments in Great Britain, Earth Syst. Sci. Data, 12, 2459–2483, https://doi.org/10.5194/essd-12-2459-2020, 2020.
- Delaigue, O., Guimarães, G. M., Brigode, P., Génot, B., Perrin, C., Soubeyroux, J.-M., Janet, B., Addor, N., and Andréassian, V.: CAMELS-FR dataset: a large-sample hydroclimatic dataset for France to explore hydrological diversity and support model benchmarking, Earth Syst. Sci. Data, 17, 1461–1479, https://doi.org/10.5194/essd-17-1461-2025, 2025.
- Duan, Q., Schaake, J., Andréassian, V., Franks, S., Goteti, G., Gupta, H. V., Gusev, Y. M., Habets, F., Hall, A., Hay, L., Hogue, T., Huang, M., Leavesley, G., Liang, X., Nasonova, O. N., Noilhan, J., Oudin, L., Sorooshian, S., Wagener, T., and Wood, E. F.: Model Parameter Estimation Experiment (MOPEX): An overview of science strategy and major results from the second and third workshops, Journal of Hydrology, 320, 31117, https://doi.org/10.1016/j.jhydrol.2005.07.031, 2006.
- Eaton, B., Gregory, J., Drach, B., Taylor, K., Hankin, S., Blower, J., Caron, J., Signell, R., Bentley, P., Rappa, G., Höck, H., Pamment, A., Juckes, M., Raspaud, M., Horne, R., Whiteaker, T., Blodgett, D., Zender, C., Lee, D., Hassell, D., Snow, A. D., Kölling, T., Allured, D., Jelenak, A., Meier Soerensen, A., Gaultier, L., Herlédan, S., Manzano, F., Bärring, L., Barker, C., and Bartholomew, S.: NetCDF Climate and Forecast (CF) Metadata Conventions v1.11, http://cfconventions.org/Data/cf-conventions/cf-conventions-1.11/cf-conventions.html, last access: 11 January 2024, 2023.
- Eckhardt, K.: How to construct recursive digital filters for baseflow separation, Hydrol. Process., 19, 507–515, https://doi.org/10.1002/hyp.5675, 2005.
- Environment and Climate Change Canada: National Water Data Archive: HYDAT, https://www.canada.ca/en/environment-climate-change/services/water-overview/quantity/monitoring/survey/data-products-services/national-archive-hydat.html (last access: 5 July 2018), 2010.
- Environment and Climate Change Canada: Reference Hydrometric Basin Network, https://www.canada.ca/en/environment-climate-change/services/water-overview/quantity/monitoring/survey/data-products-services/reference-hydrometric-basin-network.html (last access: 26 February 2021), 2020a.
- Environment and Climate Change Canada: National hydrometric network basin polygons Open Government Portal, Government of Canada [data set], https://open.canada.ca/data/en/dataset/0c121878-ac23-46f5-95df-eb9960753375 (last access: 23 August 2022), 2020b.
- European Centre for Medium-range Weather Forecasting: ERA5: How to calculate wind speed and wind direction from u and v components of the wind? Copernicus Knowledge Base ECMWF Confluence Wiki, https://confluence.ecmwf.int/pages/viewpage.action?pageId=133262398 (last access: 2 January 2024), 2023a.
- European Centre for Medium-range Weather Forecasting: ERA5: data documentation Copernicus Knowledge Base ECMWF Confluence Wiki, https://confluence.ecmwf.int/display/CKB/ERA5%3A+data+documentation#ERA5: datadocumentation-Howtoacknowledge,citeandrefertoERA5 (last access: 3 January 2024), 2023b.

- European Centre for Medium-range Weather Forecasting: ERA5 terminology: analysis and forecast; time and steps; instantaneous and accumulated and mean rates and min/max parameters Copernicus Knowledge Base ECMWF Confluence Wiki, https://confluence.ecmwf.int/pages/viewpage.action?pageId=85402030# ERA5terminology:analysisandforecast;timeandsteps; instantaneousandaccumulatedandmeanratesandmin/maxparameters-Instantaneous,accumulated,meanrateandmin/maxparameters (last access: 3 January 2024), 2023c.
- Färber, C., Plessow, H., Mischel, S., Kratzert, F., Addor, N., Shalev, G., and Looser, U.: GRDC-Caravan: extending Caravan with data from the Global Runoff Data Centre, Earth Syst. Sci. Data Discuss. [preprint], https://doi.org/10.5194/essd-2024-427, in review, 2024.
- Fick, S. E. and Hijmans, R. J.: WorldClim 2: new 1-km spatial resolution climate surfaces for global land areas, Int. J. Climatol., 37, 4302–4315, https://doi.org/10.1002/joc.5086, 2017.
- Fowler, K. J. A., Acharya, S. C., Addor, N., Chou, C., and Peel, M. C.: CAMELS-AUS: hydrometeorological time series and land-scape attributes for 222 catchments in Australia, Earth Syst. Sci. Data, 13, 3847–3867, https://doi.org/10.5194/essd-13-3847-2021, 2021.
- Fowler, K. J. A., Zhang, Z., and Hou, X.: CAMELS-AUS v2: updated hydrometeorological time series and landscape attributes for an enlarged set of catchments in Australia, Earth Syst. Sci. Data, 17, 4079–4095, https://doi.org/10.5194/essd-17-4079-2025, 2025.
- Friedl, M. and Sulla-Menashe, D.: MODIS/Terra+Aqua Land Cover Type Yearly L3 Global 500m SIN Grid V061, NASA Land Processes Distributed Active Archive Center [data set], https://doi.org/10.5067/MODIS/MCD12Q1.061, 2022.
- Gasset, N., Fortin, V., Dimitrijevic, M., Carrera, M., Bilodeau, B., Muncaster, R., Gaborit, É., Roy, G., Pentcheva, N., Bulat, M., Wang, X., Pavlovic, R., Lespinas, F., Khedhaouiria, D., and Mai, J.: A 10 km North American precipitation and land-surface reanalysis based on the GEM atmospheric model, Hydrol. Earth Syst. Sci., 25, 4917–4945, https://doi.org/10.5194/hess-25-4917-2021, 2021.
- Gharari, S., Keshavarz, K., Knoben, W. J., Tang, G., and Clark, M. P.: EASYMORE: A Python package to streamline the remapping of variables for Earth System models, SoftwareX, 24, 101547, https://doi.org/10.1016/j.softx.2023.101547, 2023.
- Gharari, S., Whitfield, P. H., Pietroniro, A., Freer, J., Liu, H., and Clark, M. P.: Exploring the provenance of information across Canadian hydrometric stations: implications for discharge estimation and uncertainty quantification, Hydrol. Earth Syst. Sci., 28, 4383–4405, https://doi.org/10.5194/hess-28-4383-2024, 2024.
- Gleeson, T.: GLobal HYdrogeology MaPS (GLHYMPS) of permeability and porosity, Borealis [data set], https://doi.org/10.5683/SP2/DLGXYO, 2018.
- Gleeson, T., Moosdorf, N., Hartmann, J., and Van Beek, L. P. H.: A glimpse beneath earth's surface: GLobal HYdrogeology MaPS (GLHYMPS) of permeability and porosity, Geophys. Res. Lett., 41, 3891–3898, https://doi.org/10.1002/2014GL059856, 2014.
- Government of Canada: Web Service Links Interface Water Level and Flow Environment Canada, https://wateroffice.ec.gc.ca/services/links_e.html, last access: 22 December 2023.

- Government of Canada: Index of /cmc/hydrometrics/www/HydrometricNetworkBasinPolygons, https://collaboration.cmc.ec.gc.ca/cmc/hydrometrics/www/ (last access: 18 August 2022), 2022.
- Hamman, J. J., Nijssen, B., Bohn, T. J., Gergel, D. R., and Mao, Y.: The Variable Infiltration Capacity model version 5 (VIC-5): infrastructure improvements for new applications and reproducibility, Geosci. Model Dev., 11, 3481–3496, https://doi.org/10.5194/gmd-11-3481-2018, 2018.
- Hansen, M. C., Potapov, P. V., Pickens, A. H., Tyukavina, A., Hernandez-Serna, A., Zalles, V., Turubanova, S., Kommareddy, I., Stehman, S. V., Song, X.-P., and Kommareddy, A.: Global land use extent and dispersion within natural land cover using Landsat data, Environ. Res. Lett., 17, 034050, https://doi.org/10.1088/1748-9326/ac46ec, 2022.
- Hao, Z., Jin, J., Xia, R., Tian, S., Yang, W., Liu, Q., Zhu, M., Ma, T., Jing, C., and Zhang, Y.: CCAM: China Catchment Attributes and Meteorology dataset, Earth Syst. Sci. Data, 13, 5591–5616, https://doi.org/10.5194/essd-13-5591-2021, 2021.
- Hayashi, M., Van Der Kamp, G., and Rosenberry, D. O.: Hydrology of Prairie Wetlands: Understanding the Integrated Surface-Water and Groundwater Processes, Wetlands, 36, 237–254, https://doi.org/10.1007/s13157-016-0797-9, 2016.
- Helgason, H. B. and Nijssen, B.: LamaH-Ice: LArge-SaMple DAta for Hydrology and Environmental Sciences for Iceland, Earth Syst. Sci. Data, 16, 2741–2771, https://doi.org/10.5194/essd-16-2741-2024, 2024.
- Hersbach, H., Bell, B., Berrisford, P., Hirahara, S., Horányi, A., Muñoz-Sabater, J., Nicolas, J., Peubey, C., Radu, R., Schepers, D., Simmons, A., Soci, C., Abdalla, S., Abellan, X., Balsamo, G., Bechtold, P., Biavati, G., Bidlot, J., Bonavita, M., De Chiara, G., Dahlgren, P., Dee, D., Diamantakis, M., Dragani, R., Flemming, J., Forbes, R., Fuentes, M., Geer, A., Haimberger, L., Healy, S., Hogan, R. J., Hólm, E., Janisková, M., Keeley, S., Laloyaux, P., Lopez, P., Lupu, C., Radnoti, G., de Rosnay, P., Rozum, I., Vamborg, F., Villaume, S., and Thépaut, J.-N.: Complete ERA5 from 1940: Fifth generation of ECMWF atmospheric reanalyses of the global climate, Copernicus Climate Change Service (C3S) Climate Data Store (CDS) [data set], https://doi.org/10.24381/cds.143582cf, 2017.
- Hersbach, H., Bell, B., Berrisford, P., Hirahara, S., Horányi, A., Muñoz-Sabater, J., Nicolas, J., Peubey, C., Radu, R., Schepers, D., Simmons, A., Soci, C., Abdalla, S., Abellan, X., Balsamo, G., Bechtold, P., Biavati, G., Bidlot, J., Bonavita, M., De Chiara, G., Dahlgren, P., Dee, D., Diamantakis, M., Dragani, R., Flemming, J., Forbes, R., Fuentes, M., Geer, A., Haimberger, L., Healy, S., Hogan, R. J., Hólm, E., Janisková, M., Keeley, S., Laloyaux, P., Lopez, P., Lupu, C., Radnoti, G., De Rosnay, P., Rozum, I., Vamborg, F., Villaume, S., and Thépaut, J.: The ERA5 global reanalysis, Q. J. Roy. Meteor. Soc., 146, 1999–2049, https://doi.org/10.1002/qj.3803, 2020.
- Hersbach, H., Bell, B., Berrisford, P., Biavati, G., Horányi, A., Muñoz Sabater, J., Nicolas, J., Peubey, C., Radu, R., Rozum, I., Schepers, D., Simmons, A., Soci, C., Dee, D., and Thépaut, J.-N.: ERA5 hourly data on single levels from 1940 to present, Copernicus Climate Change Service (C3S) Climate Data Store (CDS) [data set], https://doi.org/10.24381/cds.adbb2d47, 2023.
- Hogan, R.: Radiation Quantities in the ECMWF model and MARS, Tech. rep., European Centre for Medium-range Weather

- Forecasting, https://www.ecmwf.int/sites/default/files/elibrary/2015/18490-radiation-quantities-ecmwf-model-and-mars.pdf (last access: 1 January 2024), 2015.
- Höge, M., Kauzlaric, M., Siber, R., Schönenberger, U., Horton, P., Schwanbeck, J., Floriancic, M. G., Viviroli, D., Wilhelm, S., Sikorska-Senoner, A. E., Addor, N., Brunner, M., Pool, S., Zappa, M., and Fenicia, F.: CAMELS-CH: hydro-meteorological time series and landscape attributes for 331 catchments in hydrologic Switzerland, Earth Syst. Sci. Data, 15, 5755–5784, https://doi.org/10.5194/essd-15-5755-2023, 2023.
- Hrachowitz, M. and Clark, M. P.: HESS Opinions: The complementary merits of competing modelling philosophies in hydrology, Hydrol. Earth Syst. Sci., 21, 3953–3973, https://doi.org/10.5194/hess-21-3953-2017, 2017.
- Kirchner, J. W.: Getting the right answers for the right reasons: Linking measurements, analyses, and models to advance the science of hydrology, Water Resour. Res., 42, 2005WR004362, https://doi.org/10.1029/2005WR004362, 2006.
- Klingler, C., Schulz, K., and Herrnegger, M.: LamaH-CE: LArge-SaMple DAta for Hydrology and Environmental Sciences for Central Europe, Earth Syst. Sci. Data, 13, 4529–4565, https://doi.org/10.5194/essd-13-4529-2021, 2021.
- Knoben, W. J. M.: Catchment Attributes and MEteorology for Large-sample Studies for SPATially distributed modeling (CAMELS-SPAT) – code (v1.0.0), Zenodo [code], https://doi.org/10.5281/zenodo.16751492, 2025.
- Knoben, W. J. M., Freer, J. E., Fowler, K. J. A., Peel, M. C., and Woods, R. A.: Modular Assessment of Rainfall–Runoff Models Toolbox (MARRMoT) v1.2: an open-source, extendable framework providing implementations of 46 conceptual hydrologic models as continuous state-space formulations, Geosci. Model Dev., 12, 2463–2480, https://doi.org/10.5194/gmd-12-2463-2019, 2019.
- Knoben, W. J. M., Freer, J. E., Peel, M. C., Fowler, K. J. A., and Woods, R. A.: A Brief Analysis of Conceptual Model Structure Uncertainty Using 36 Models and 559 Catchments, Water Resour. Res., 56, e2019WR025975, https://doi.org/10.1029/2019WR025975, 2020.
- Knoben, W., Thébault, C., Keshavarz, K., Torres-Rojas, L., Chaney, N., Pietroniro, A., and Clark, M.: Catchment Attributes and MEteorology for Large-Sample SPATially distributed analysis (CAMELS-SPAT): Streamflow observations, forcing data and geospatial data for hydrologic studies across North America, Federated Research Data Repository [data set], https://doi.org/10.20383/103.01306, 2025.
- Kratzert, F., Klotz, D., Shalev, G., Klambauer, G., Hochreiter, S., and Nearing, G.: Towards learning universal, regional, and local hydrological behaviors via machine learning applied to large-sample datasets, Hydrol. Earth Syst. Sci., 23, 5089–5110, https://doi.org/10.5194/hess-23-5089-2019, 2019.
- Kratzert, F., Nearing, G., Addor, N., Erickson, T., Gauch, M., Gilon, O., Gudmundsson, L., Hassidim, A., Klotz, D., Nevo, S., Shalev, G., and Matias, Y.: Caravan - A global community dataset for large-sample hydrology, Sci. Data, 10, 61, https://doi.org/10.1038/s41597-023-01975-w, 2023.
- Lafaysse, M., Cluzet, B., Dumont, M., Lejeune, Y., Vionnet, V., and Morin, S.: A multiphysical ensemble system of numerical snow modelling, The Cryosphere, 11, 1173–1198, https://doi.org/10.5194/tc-11-1173-2017, 2017.

- Liang, X., Lettenmaier, D. P., Wood, E. F., and Burges, S. J.: A simple hydrologically based model of land surface water and energy fluxes for general circulation models, J. Geophys. Res., 99, 14415, https://doi.org/10.1029/94JD00483, 1994.
- Lin, P., Pan, M., Beck, H. E., Yang, Y., Yamazaki, D., Frasson, R., David, C. H., Durand, M., Pavelsky, T. M., Allen, G. H., Gleason, C. J., and Wood, E. F.: Global Reconstruction of Naturalized River Flows at 2.94 Million Reaches, Water Resour. Res., 55, 6499–6516, https://doi.org/10.1029/2019WR025287, 2019.
- Lindström, G., Johansson, B., Persson, M., Gardelin, M., and Bergström, S.: Development and test of the distributed HBV-96 hydrological model, J. Hydrol., 201, 272–288, https://doi.org/10.1016/S0022-1694(97)00041-3, 1997.
- Lins, H. F.: USGS Hydro-Climatic Data Network 2009 (HCDN–2009), Tech. Rep. U.S. Geological Survey Fact Sheet 2012–3047, United States Geological Survey, https://pubs.usgs.gov/fs/2012/3047/ (last access: 21 March 2024), 2012.
- Liu, J., Koch, J., Stisen, S., Troldborg, L., Højberg, A. L., Thodsen, H., Hansen, M. F. T., and Schneider, R. J. M.: CAMELS-DK: hydrometeorological time series and landscape attributes for 3330 Danish catchments with streamflow observations from 304 gauged stations, Earth Syst. Sci. Data, 17, 1551–1572, https://doi.org/10.5194/essd-17-1551-2025, 2025.
- Loritz, R., Dolich, A., Acuña Espinoza, E., Ebeling, P., Guse, B., Götte, J., Hassler, S. K., Hauffe, C., Heidbüchel, I., Kiesel, J., Mälicke, M., Müller-Thomy, H., Stölzle, M., and Tarasova, L.: CAMELS-DE: hydro-meteorological time series and attributes for 1582 catchments in Germany, Earth Syst. Sci. Data, 16, 5625–5642, https://doi.org/10.5194/essd-16-5625-2024, 2024.
- Mangukiya, N. K., Kumar, K. B., Dey, P., Sharma, S., Bejagam, V., Mujumdar, P. P., and Sharma, A.: CAMELS-IND: hydrometeorological time series and catchment attributes for 228 catchments in Peninsular India, Earth Syst. Sci. Data, 17, 461–491, https://doi.org/10.5194/essd-17-461-2025, 2025.
- Marsh, C. B., Pomeroy, J. W., and Wheater, H. S.: The Canadian Hydrological Model (CHM) v1.0: a multi-scale, multi-extent, variable-complexity hydrological model design and overview, Geosci. Model Dev., 13, 225–247, https://doi.org/10.5194/gmd-13-225-2020, 2020.
- Maurer, T. and Zehe, E.: CATFLOW: A Physically Based and Distributed Hydrological Model for Continuous Simulation of Catchment Water- and Solute Dynamics User Guide and Program Documentation (Version CATSTAT), Tech. rep., INSTITUTE FOR WATER RESOURCES PLANNING, HYDRAULICS AND RURAL ENGINEERING (IWK), University of Karlsruhe (TH), 2007.
- Maxwell, R. M., Kollet, S. J., Condon, L. E., Smith, S. G., Woodward, C. S., Falgout, R. D., Ferguson, I. M., Engdahl, N., Hector, B., Lopez, S. R., Gilbert, J., Bearup, L., Jefferson, J., Collins, C., De Graaf, I., Prubilick, C., Baldwin, C., Bosl, W. J., Hornung, R., and Ashby, S.: PARFLOW User's Manual, Tech. rep., Integrated GroundWater Modeling Center, 2019.
- McMahon, T. A., Peel, M. C., Lowe, L., Srikanthan, R., and McVicar, T. R.: Estimating actual, potential, reference crop and pan evaporation using standard meteorological data: a pragmatic synthesis, Hydrol. Earth Syst. Sci., 17, 1331–1363, https://doi.org/10.5194/hess-17-1331-2013, 2013.
- McMillan, H., Coxon, G., Araki, R., Salwey, S., Kelleher, C., Zheng, Y., Knoben, W., Gnann, S., Seibert, J., and Bolotin,

- L.: When good signatures go bad: Applying hydrologic signatures in large sample studies, Hydrol. Process., 37, e14987, https://doi.org/10.1002/hyp.14987, 2023.
- McMillan, H. K.: A review of hydrologic signatures and their applications, WIREs Water, 8, e1499, https://doi.org/10.1002/wat2.1499, 2021.
- Mekonnen, M. and Brauner, H.: MESH A Community Hydrology-Land Surface Model: Meteorological Input, https://wiki.usask.ca/display/MESH/Meteorological+Input (last access: 27 January 2022), 2020.
- Messager, M. L., Lehner, B., Grill, G., Nedeva, I., and Schmitt, O.: Estimating the volume and age of water stored in global lakes using a geo-statistical approach, Nat. Commun., 7, 13603, https://doi.org/10.1038/ncomms13603, 2016.
- Mitchell, K., Ek, M., Wong, V., Lohmann, D., Koren, V., Schaake, J., Duan, Q., Gayno, G., Moore, B., Grunmann, P., Tarpley, D., Ramsay, B., Chen, F., Kim, J., Pan, H.-L., Lin, Y., Marshall, C., Mahrt, L., Meyers, T., and Ruscher, P.: THE COMMUNITY Noah LAND-SURFACE MODEL (LSM) User's guide Public Release Version 2.7.1, Tech. rep., ftp://ftp.emc.ncep.noaa.gov/mmb/gcp/ldas/noahlsm/ver_2.7.1 (last access: 28 January 2022), 2005.
- Muhammad, A., Evenson, G. R., Stadnyk, T. A., Boluwade, A., Jha, S. K., and Coulibaly, P.: Impact of model structure on the accuracy of hydrological modeling of a Canadian Prairie watershed, J. Hydrol.: Regional Studies, 21, 40–56, https://doi.org/10.1016/j.ejrh.2018.11.005, 2019.
- Myneni, R., Knyazikhin, Y., and Park, T.: MODIS/Terra+Aqua Leaf Area Index/FPAR 8-Day L4 Global 500m SIN Grid V061, NASA Land Processes Distributed Active Archive Center [data set], https://doi.org/10.5067/MODIS/MCD15A2H.061, 2021.
- National Research Council Canada: Time zones and daylight saving time, https://nrc.canada.ca/en/certifications-evaluations-standards/canadas-official-time/time-zones-daylight-saving-time (last access: 25 October 2022),
- National Weather Service: II.3-SAC-SMA: Conceptualization of the Sacramento Soil Moisture Accounting model, in: National Weather Service River Forecast System (NWSRFS) User Manual, 1–13, http://www.nws.noaa.gov/ohd/hrl/nwsrfs/users_ manual/htm/xrfsdocpdf.php (last access: 8 April 2020), 2005.
- Newman, A., Sampson, K., Clark, M., Bock, A., Viger, R., and Blodgett, D.: A large-sample watershed-scale hydrometeorological dataset for the contiguous USA, artwork Size: approximately 2.5 GB Medium: text/plain, text/tab-separated-values, png, shp Pages: approximately 2.5 GB, Zenodo [data set], https://doi.org/10.5065/D6MW2F4D, 2014.
- Newman, A. J., Clark, M. P., Sampson, K., Wood, A., Hay, L. E., Bock, A., Viger, R. J., Blodgett, D., Brekke, L., Arnold, J. R., Hopson, T., and Duan, Q.: Development of a large-sample watershed-scale hydrometeorological data set for the contiguous USA: data set characteristics and assessment of regional variability in hydrologic model performance, Hydrol. Earth Syst. Sci., 19, 209–223, https://doi.org/10.5194/hess-19-209-2015, 2015.
- Newman, A. J., Mizukami, N., Clark, M. P., Wood, A. W., Nijssen, B., and Nearing, G.: Benchmarking of a physically based hydrologic model, J. Hydrometeorol., 18, 2215–2225, 2017.
- Nijssen, B.: SUMMA Input SUMMA Meteorological Forcing Files, https://summa.readthedocs.io/en/latest/input_output/

- SUMMA_input/#meteorological-forcing-files (last access: 30 December 2023), 2017.
- Niu, G.-Y., Yang, Z.-L., Mitchell, K. E., Chen, F., Ek, M. B., Barlage, M., Kumar, A., Manning, K., Niyogi, D., Rosero, E., Tewari, M., and Xia, Y.: The community Noah land surface model with multiparameterization options (Noah-MP): 1. Model description and evaluation with local-scale measurements, J. Geophys. Res., 116, D12109, https://doi.org/10.1029/2010JD015139, 2011.
- Oudin, L., Hervieu, F., Michel, C., Perrin, C., Andréassian, V., Anctil, F., and Loumagne, C.: Which potential evapotranspiration input for a lumped rainfall–runoff model?, J. Hydrol., 303, 290–306, https://doi.org/10.1016/j.jhydrol.2004.08.026, 2005.
- Pellerin, J. and Nzokou Tanekou, F.: Reference Hydrometric Basin Network Update, Tech. rep., Environment and Climate Change Canada, Gatineau, QC, https://collaboration.cmc.ec.gc.ca/cmc/ hydrometrics/www/RHBN/RHBN_EN.pdf (last access: 18 December 2023), 2020.
- Pelletier, J., Broxton, P., Hazenberg, P., Zeng, X., Troch, P., Niu, G., Williams, Z., Brunke, M., and Gochis, D.: Global 1-km Gridded Thickness of Soil, Regolith, and Sedimentary Deposit Layers, p. 1032.940581 MB, ORNL Distributed Active Archive Center [data set], https://doi.org/10.3334/ORNLDAAC/1304, 2016a.
- Pelletier, J. D., Broxton, P. D., Hazenberg, P., Zeng, X., Troch, P. A., Niu, G., Williams, Z., Brunke, M. A., and Gochis, D.: A gridded global data set of soil, intact regolith, and sedimentary deposit thicknesses for regional and global land surface modeling, J. Adv. Model. Earth Sy., 8, 41–65, https://doi.org/10.1002/2015MS000526, 2016b.
- Perrin, C., Michel, C., and Andréassian, V.: Improvement of a parsimonious model for streamflow simulation, J. Hydrol., 279, 275–289, https://doi.org/10.1016/S0022-1694(03)00225-7, 2003.
- PIHM team: PennState Integrated Hydrologic Model (PIHM) Version 2.0 Input File Formats, Tech. rep., Hydrology Group, Civil & Environmental Engineering, Pennsylvania State University, http://www.pihm.psu.edu/Downloads/Doc/pihm2.0_input_file_format.pdf (last access: 28 January 2022), 2007.
- Poggio, L., de Sousa, L. M., Batjes, N. H., Heuvelink, G. B. M., Kempen, B., Ribeiro, E., and Rossiter, D.: SoilGrids 2.0: producing soil information for the globe with quantified spatial uncertainty, SOIL, 7, 217–240, https://doi.org/10.5194/soil-7-217-2021, 2021.
- Pomeroy, J. W., Gray, D. M., Brown, T., Hedstrom, N. R., Quinton, W. L., Granger, R. J., and Carey, S. K.: The cold regions hydrological model: a platform for basing process representation and model structure on physical evidence, Hydrol. Process., 21, 2650–2667, https://doi.org/10.1002/hyp.6787, 2007.
- Potapov, P., Li, X., Hernandez-Serna, A., Tyukavina, A., Hansen, M. C., Kommareddy, A., Pickens, A., Turubanova, S., Tang, H., Silva, C. E., Armston, J., Dubayah, R., Blair, J. B., and Hofton, M.: Mapping global forest canopy height through integration of GEDI and Landsat data, Remote Sens. Environ., 253, 112165, https://doi.org/10.1016/j.rse.2020.112165, 2021.
- Priestley, C. H. B. and Taylor, R. J.: On the Assessment of Surface Heat Flux and Evaporation Using Large-Scale Parameters, Mon. Weather Rev., 100, 81–92, https://doi.org/10.1175/1520-0493(1972)100<0081:OTAOSH>2.3.CO;2, 1972.
- Rakovec, O., Kumar, R., Shrestha, P. K., and Samaniego, L.: Global assessment of hydrological components using a seam-

- less multiscale modelling system, EGU General Assembly 2023, Vienna, Austria, 24–28 April 2023, EGU23-11945, https://doi.org/10.5194/egusphere-egu23-11945, 2023.
- Sankarasubramanian, A., Vogel, R. M., and Limbrunner, J. F.: Climate elasticity of streamflow in the United States, Water Resour. Res., 37, 1771–1781, https://doi.org/10.1029/2000WR900330, 2001.
- Schaake, J., Cong, S. Z., and Duan, Q. Y.: The US MOPEX data set, Large sample basin experiments for hydrological model parameterization: results of the model parameter experiment–MOPEX, edited by: Andreassian, V., Hall, A., Chahinian, N., and Schaake, J., IAHS Press, 307, 9–28, 2006.
- Schulla, J.: Model Description WaSIM (Water balance Simulation Model), Tech. rep., Hydrology Software Consulting J. Schulla, http://www.wasim.ch/en/products/wasim_description.htm (last access: 30 December 2023), 2021.
- Singer, M. B., Asfaw, D. T., Rosolem, R., Cuthbert, M. O., Miralles, D. G., MacLeod, D., Quichimbo, E. A., and Michaelides, K.: Hourly potential evapotranspiration at 0.1° resolution for the global land surface from 1981–present, Sci. Data, 8, 224, https://doi.org/10.1038/s41597-021-01003-9, 2021.
- SMHI: HYPE file reference [HYPE Model Documentation], http://www.smhi.net/hype/wiki/doku.php?id=start: hype_file_reference#observation_data_files (last access: 27 January 2022), 2022.
- Stein, L., Clark, M. P., Knoben, W. J. M., Pianosi, F., and Woods, R. A.: How Do Climate and Catchment Attributes Influence Flood Generating Processes? A Large-Sample Study for 671 Catchments Across the Contiguous USA, Water Resour. Res., 57, e2020WR028300, https://doi.org/10.1029/2020WR028300, 2021.
- Tang, G., Clark, M., and Papalexiou, S.: EM-Earth: The Ensemble Meteorological Dataset for Planet Earth, Federated Research Data Repository [data set], https://doi.org/10.20383/102.0547, 2022a.
- Tang, G., Clark, M. P., and Papalexiou, S. M.: EM-Earth: The Ensemble Meteorological Dataset for Planet Earth, B. Am. Meteorol. Soc., 103, E996–E1018, https://doi.org/10.1175/BAMS-D-21-0106.1, 2022b.
- Tarasova, L., Gnann, S., Yang, S., Hartmann, A., and Wagener, T.: Catchment characterization: current descriptors, knowledge gaps and future opportunities, Earth Sciences Reviews, 252, 104739, ISSN 0012-8252, https://doi.org/10.1016/j.earscirev.2024.104739, 2024.
- Teluguntla, P., Thenkabail, P., Oliphant, A., Gumma, M., Aneece, I., Foley, D., and McCormick, R.: Landsat-Derived Global Rainfed and Irrigated-Cropland Product 30 m V001, NASA Land Processes Distributed Active Archive Center [data set], https://doi.org/10.5067/COMMUNITY/LGRIP/LGRIP30.001, 2023.
- Teutschbein, C.: CAMELS-SE: Long-termhydroclimatic observations (1961–2020) across 50 catchments in Sweden as a resource for modelling, education, and collaboration, Geoscience Data Journal, 11, 655–668, https://doi.org/10.1002/gdj3.239, 2024.
- Thenkabail, P. S., Teluguntla, P. G., Xiong, J., Oliphant, A., Congalton, R. G., Ozdogan, M., Gumma, M. K., Tilton, J. C., Giri, C., Milesi, C., Phalke, A., Massey, R., Yadav, K., Sankey, T., Zhong, Y., Aneece, I., and Foley, D.: Global Cropland-Extent Product at 30-m Resolution (GCEP30) Derived from Landsat

- Satellite Time-Series Data for the Year 2015 Using Multiple Machine-Learning Algorithms on Google Earth Engine Cloud, USGS Numbered Series, U.S. Geological Survey, series: Professional Paper, https://doi.org/10.3133/pp1868, 2021.
- Thornton, M., Shrestha, R., Wei, Y., Thornton, P., and Kao, S.-C.: Daymet: Daily Surface Weather Data on a 1-km Grid for North America, Version 4 R1, ORNL Distributed Active Archive Center [data set], https://doi.org/10.3334/ORNLDAAC/2129, 2022.
- Thornton, P. E., Shrestha, R., Thornton, M., Kao, S.-C., Wei, Y., and Wilson, B. E.: Gridded daily weather data for North America with comprehensive uncertainty quantification, Sci. Data, 8, 190, https://doi.org/10.1038/s41597-021-00973-0, 2021.
- Towler, E., Foks, S. S., Dugger, A. L., Dickinson, J. E., Essaid, H. I., Gochis, D., Viger, R. J., and Zhang, Y.: Benchmarking high-resolution hydrologic model performance of long-term retrospective streamflow simulations in the contiguous United States, Hydrol. Earth Syst. Sci., 27, 1809–1825, https://doi.org/10.5194/hess-27-1809-2023, 2023.
- Trotter, L., Knoben, W. J. M., Fowler, K. J. A., Saft, M., and Peel, M. C.: Modular Assessment of Rainfall–Runoff Models Toolbox (MARRMoT) v2.1: an object-oriented implementation of 47 established hydrological models for improved speed and readability, Geosci. Model Dev., 15, 6359–6369, https://doi.org/10.5194/gmd-15-6359-2022, 2022.

- Water Survey of Canada: Sub-daily data download location, https://collaboration.cmc.ec.gc.ca/cmc/hydrometrics/www/UnitValueData/ (last access: 2 June 2025), 2025.
- Wood, A. W., Hopson, T., Newman, A., Brekke, L., Arnold, J., and Clark, M.: Quantifying streamflow forecast skill elasticity to initial condition and climate prediction skill, J. Hydrometeorol., 17, 651–668, 2016.
- Woods, R. model A.: Analytical of seasonal mate impacts on snow hydrology: Continuous snowpacks, Adv. Water Resour., 32 1465-1481, https://doi.org/10.1016/j.advwatres.2009.06.011, 2009.
- Xie, J., Liu, X., Wang, K., Yang, T., Liang, K., and Liu, C.: Evaluation of typical methods for baseflow separation in the contiguous United States, J. Hydrol., 583, 124628, https://doi.org/10.1016/j.jhydrol.2020.124628, 2020.
- Yamazaki, D., Ikeshima, D., Sosa, J., Bates, P. D., Allen, G. H., and Pavelsky, T. M.: MERIT Hydro: A High-Resolution Global Hydrography Map Based on Latest Topography Dataset, Water Resour. Res., 55, 5053–5073, https://doi.org/10.1029/2019WR024873, 2019.
- Yuning Shi: MM-PIHM, v. 0.10.10, Zenodo [code], https://doi.org/10.5281/ZENODO.4533260, 2018.